IN-SITU MONITORING OF THE LEGACY PONDS AND SILOS AT SELLAFIELD

A thesis submitted to The University of Manchester for the degree of

Doctor of Philosophy

in the Faculty of Science and Engineering

2018

OLUSOLA S. AYOOLA

SCHOOL OF ELECTRICAL AND ELECTRONIC ENGINEERING

TABLE OF CONTENT

Contents

LIST OF FIGURES

9

LIST OF TABLES

ABSTRACT

This research is aimed at identifying and evaluating experimental factors which influence variations in results from sludge sampling and analysis, and investigating the feasibility of an *in-situ* solution for sludge characterisation. Due to the challenges present in removing sludge from wet nuclear storage facilities for laboratory-based analysis, it is difficult to generate characterization maps with high confidence as typically only very limited measurements can be made.

This research presents a method of estimating the percentage confidence in sludge characterization results, specifically focusing on the Particle Size Distribution (PSD) as a representation of other sludge properties relevant to UK's nuclear decommissioning programme. Also introduced is a novel algorithm, referred to as Recursive Relative Accuracy (RRA), which is shown to provide an indication of the benefits of taking more samples. Access to real nuclear site data is restricted; hence the chapter adopts the use of a real-life non-radioactive corroded magnesium sludge simulant tank.

Sludge samples were collected from computer modelled and real-life simulant sludge beds under varying experimental conditions such as: the number of sampled locations, sampling strategy, the penetration depth and the selective bias of the sampling device used. These samples were in some cases, analysed for their PSD under varying experimental conditions such as: type of instrument model used, the concentration of samples and the dispersion medium used. Using PSD data measured at sampled positions and inferring data at non-sampled positions, three-dimensional sludge characterisation maps were obtained and analysed.

It was observed that the factor "depth of penetration of the sampling device" contributes about 48 % to result variability, while the instrument model used and the sample concentration chosen each contribute about 40 % and 7 %, respectively, to variations in the PSD laboratory analysis results. The feasibility study conducted on ultrasonic spectroscopy failed to confirm the existence of an analytical model for interpreting PSD data *in-situ*. The average error margin in the inference of PSD mean values was over 600 μm.

DECLARATION

I hereby make a declaration that no portion of the work referred to in this report has been submitted in support of an application for another degree or qualification of this or any other university or other institute of learning.

COPYRIGHT STATEMENT

i.   The author of this report (including any appendices and/or schedules to this thesis) owns certain copyright or related rights in it (the "Copyright") and s/he has given The University of Manchester certain rights to use such Copyright, including for administrative purposes.

ii.   Copies of this report, either in full or in extracts and whether in hard or electronic copy, may be made only in accordance with the Copyright, Designs and Patents Act 1988 (as amended) and regulations issued under it or, where appropriate, in accordance with licensing agreements which the University has from time to time. This page must form part of any such copies made.

iii.   The ownership of certain Copyright, patents, designs, trademarks and other intellectual property (the "Intellectual Property") and any reproductions of copyright works in the thesis, for example graphs and tables ("Reproductions"), which may be described in this report , may not be owned by the author and may be owned by third parties. Such Intellectual Property and Reproductions cannot and must not be made available for use without the prior written permission of the owner(s) of the relevant Intellectual Property and/or Reproductions.

iv.   Further information on the conditions under which disclosure, publication and commercialisation of this thesis, the Copyright and any Intellectual Property and/or Reproductions described in it may take place is available in the University IP Policy (see http://documents.manchester.ac.uk/DocuInfo.aspx?DocID=487), in any relevant Thesis restriction declarations deposited in the University Library, The University Library's regulations (see http://www.manchester.ac.uk/library/aboutus/regulations) and in The University's policy on Presentation of Theses.

ACKNOWLEDGEMENT

GLOSSARY

LIST OF ABBREVIATIONS

- 3D – Three Dimensional

- ANOVA – Analysis Of Variance

- CLD – Chord Length Distribution

- CM – Confusion Matrix

- FBRM – Focused Beam Reflectance Method

- FGMSP – First Generation Magnox Storage Pond

- HLW – High Level Waste

- HSAC – Horizontal Spatial Autocorrelation

- ILW – Intermediate Level Waste

- LDM – Laser Diffraction Method

- LLW – Low Level Waste•

- MSSS – Magnox Swarf Storage Silo

- NNL – National Nuclear Laboratory

- OKA – Ordinary Kriging Algorithm

- PFCS – Pile Fuel Cladding Silo

- PFSP – Pile Fuel Storage Pond

- PSD – Particle Size Distribution•

- ROV – Remote Operated Vehicle

- RRA – Recursive Relative Accuracy

- SOP – Standard of Procedure

- TDA – Triangular Delaunay Algorithm

- UAS – Ultrasonic Attenuation Spectrum

- UVS – Ultrasonic Velocity Spectrum

- VSAC – Vertical Spatial Autocorrelation

DEFINITION OF TERMS

- Active Samples – also known as "Radioactive Samples" refers to substances which may spontaneously emit ionizing rays or contain one or more components of nuclear fuels or are contaminated with such substances. [1]

- Particle Size Distribution – is described [2] as a representative indication of the array of sizes of particles present in a given medium, and their respective proportions in the particulate sample group measured.

- Data Quality – this refers to the degree to which the data integrity, accuracy and data completeness of a data resource satisfies the implied information need. [3]

- Sampling Intensity – as used in this report refers to the average number of samples collected per unit area in a given population.

- Sludge – refers to a settling or precipitated solid matter commonly formed underwater by activities of treatment processes. [4]

- Tomography – refers to a technique for developing a graphical representation of the cross section through a solid object, by detecting changes made in the properties of the incident signal, for example using X-rays or ultrasound. [5]

- D10 – refers to "the particle diameter corresponding to 10 % of the cumulative undersize distribution by volume" [6].

- D90 – refers to "the particle diameter corresponding to 90 % of the cumulative undersize distribution by volume" [6].

- Obscuration – refers to "the fraction of incident light that is attenuated due to scattering or absorption by particles" [6].

- Sampling Intensity – as used in this thesis refers to the average number of samples collected per unit area in a given population.

- Sampling Uncertainty – refers to "the part of the total measurement uncertainty attributable to sampling" [7].

- Sludge – refers to a settling or precipitated solid matter commonly formed underwater by activities of treatment processes. [4]

- Spatial Autocorrelation – refers to "the correlation among values of a single variable strictly attributable to their relatively close locational positions on a two-dimensional (2-D) surface" [8]

- Spatial Extrapolation – refers to "the estimation of the values of a variable at non-sampled locations from observations at surrounding points" [7].

- Sludge characterization – refers to the quantitative measurement of the behaviour of sludge in the treatment and disposal processes [9].

- Variogram – refers to a plot of covariance between all possible pairs of sampled data against their respective proximities.

- Voxel – refers to "each of an array of elements of volume that constitute a notional three-dimensional space, especially each of an array of discrete elements into which a representation of a three-dimensional object is divided". [5]

1 Chapter 1 – Introduction

1.1 Research Background

In the 1940s, two Windscale Pile nuclear reactors were commissioned in the United Kingdom for military purposes [10]. Another facility known as the Calder Hall facility was later commissioned in the '50s to meet civil energy demands. During this period, there was no clear programme for the permanent disposal of the resulting nuclear radioactive waste such as spent fuel rods, magnesium and aluminium claddings and environmental debris [10].

For the purpose of temporary waste storage, wet nuclear storage facilities were commissioned at the Sellafield sites. These now legacy storage facilities are the First Generation Magnox Storage Pond (FGMSP), Pile Fuel Storage Pond (PFSP), Pile Fuel Cladding Silo (PFCS) and the Magnox Swarf Storage Silos (MSSS) [11].

For several decades, these storage facilities have provided steel-concrete reinforced containment and underwater storage of radioactive waste. However, underwater storage can cause material corrosion and the settlement of fine suspended materials. This results in a solid-like slurry formation of considerable volume at the bottom of the legacy storage facility. This formation is known as sludge.

1.2 Sludge

Sludge refers to precipitated solid matter commonly formed underwater by activities of treatment processes [4]. Sludge is typically formed as a result of corrosion of metallic waste stored underwater. However, dirt and debris also contribute to sludge formation [12]. In the case of the nuclear storage ponds, radioactive sludge is formed mainly by the product of nuclear waste corrosion such as corroded fuel rod claddings.

An example of sludge is shown in Figure 1. This is the picture of radioactive sludge formed at the bottom of a storage pond at the NPP A1 Jaslovske-Bohunice Reactor in Slovakia [13].

Figure 1: Example of radioactive sludge from the Nuclear Power Plant (NPP) A1 Jaslovske Bohunice Reactor [13]. This plant was completed in 1972 and was operational until 1977 when an accident (International Nuclear Event Scale Level 4) led to its closure. [13]

The safe and efficient removal of such sludge formation is a major concern in the clean-up of early nuclear facilities in the UK. The decommissioning process requires the transportation, treatment and permanent disposal of radioactive waste using appropriately designed mechanisms.

Unlike with regular sludge, the retrieval and transportation of radioactive sludge requires adequate analysis of the risks and implementation of appropriate control measures [12]. Hence, a comprehensive understanding of the properties and behaviour of the radioactive waste content, especially the sludge is critical. This can be achieved through a process known as sludge characterisation [9].

The application of 3-dimensonal (3D) sludge characterisation can provide a map of the sludge bed, showing the spatial distribution of chemical, physical and/or radiological properties. Properties of interest include: rheology, morphology, viscosity, density, temperature, and particle size distribution. For example, prior to decommissioning, a legacy nuclear storage tank in Hanford, United States was characterised in order to assess the suitability of pump transportation and to determine suitable control measures [14].

1.3 Waste Classification, Treatment and Disposal

Radioactive waste may be in itself radioactive or may be so contaminated. In managing radioactive waste, there exists a classification which enables efficient management, treatment, storage and disposal.

1.3.1 Classification of Radioactive Waste in the UK

1. High Level Waste (HLW):

   This refers to waste which have an activity high enough to generate significant heat, thereby increasing its temperature and that of the surrounding. This activity is usually higher than 4 GBq/te (giga-becquerels per tonne) of alpha activity or 12 GBq/te beta-gamma activity. Therefore, when designing the storage and disposal plan for HLW, concerns about heat generation during storage must be considered. This class of waste is currently stored on site temporarily. A typical example of HLW is the liquid waste resulting from the treatment of spent nuclear fuel. [15]

2. Intermediate Level Waste (ILW):

   This refers to waste which have an activity higher than 4 GBq/te of alpha activity and 12 GBq/te beta-gamma activity but does produce significant heat (unlike HLW) and therefore does not require concerns about heat generation during storage. This class of waste is currently stored on site temporarily. This is because there is still a need to prevent exposure of its radiation to the environment. A major source of ILW is also the treatment of spent nuclear fuel as well as from maintenance operations within a nuclear site. Common examples of ILW include graphite and radioactive sludge from wet storage facilities. [15]

3. Low Level Waste (LLW):

   This refers to waste which have an activity higher than 4 Bq/g but not exceeding 4 GBq/te of alpha activity or higher than 400 kBq beta-gamma activity but not exceeding 12 GBq/te beta-gamma activity. LLW is usually light contaminated waste produced during maintenance

and monitoring routines as part of the operations of a nuclear site. Typical examples include daily wastes such as papers, plastic containers and disposable personal protective equipment (PPE). [15]

4. Very Low Level Waste (VLLW):

This refers to any waste which has an activity less than that of LLW such as disposable plates and utensils used in the kitchen area as well as other regular kitchen and office waste. These types of waste do not need any special treatment. They are disposed as parts of the general refuse.

1.3.2 Treatment of Radioactive Waste

Radioactive waste must be retrieved and separated based on the waste classification. The waste must then be decontaminated. The treatment of waste could be thermal, chemical or physical. [15] [16]

An example of the thermal treatment can be observed in the treatment of the highly active aqueous effluent known as Highly Active Liquor (HAL) resulting from the treatment of spent fuels. HAL is treated using the method of evaporation. One purpose of this is to reduce the total volume of waste. With the aid of low pressure steam heating for up to 15 days, the concentrate can then be collected and stored for disposal, while the vapour is collected via a cooling tower tube exchanger and stored. [15] [16]

Another treatment method is the radionuclide decontamination of sludge waste streams. To achieve this treatment, either of two methods are applicable, the site-ion exchange or the enhanced actinide removal. The method of site-ion exchange is particularly useful for decontaminating pond waters prior to discharge into the environment. Similarly, the method of enhanced actinide removal is commonly applied for decontaminating aqueous effluents resulting from treatment operations. [15] [16]

1.3.3   Long-term Disposal of Waste

Ahead of disposal, waste must be conditioned into a wasteform that ensures the retention of radionuclides when disposed. This is because in this wasteform, the radionuclides become immobilised as they are dissolved in the solid structural network at an atomic level. In this state, the wasteform can then be encapsulated for long-term storage. [15] [16]

While ILW is encapsulated by solidification in cement, HLW is encapsulated by vitrification in a glass matrix. Vitrification converts highly active liquors into dense solid glass blocks further reducing their volume. After immobilisation and encapsulation, the waste can then be packaged into steel reinforced drums for storage. [15]

The appropriate long-term repository for encapsulated ILW and HLW is the Geological Disposal Facility (GDF). There are a number of considerations to be given before a suitable GDF site is chosen. Such sites should not have mineral resources, and should not be permeable to water or viscous fluid. It should also be able to provide thermal insulation where necessary. It may therefore be a challenge to find a suitable GDF site and obtain the support of the community. However, until there becomes a conclusive disposal route, encapsulated waste must remain safely stored on site.   [16] [17]

LLW is suitable for long-term disposal after containment in near surface engineered facilities. The authorised disposal site for this class of waste is at the Low Level Waste Repository (LLWR) near Drigg, Cumbria, UK.

1.4   The Legacy Storage Facilities

The legacy storage facilities at Sellafield are the pioneering storage ponds and silos used in the early days of nuclear activities in the United Kingdom. They date back to the early '50s and are located in Sellafield sites. They are listed as follows:

1.	Magnox Swarf Storage Silo (MSSS).

2.	Pile Fuel Cladding Silo (PFCS).

3.	Pile Fuel Storage Pond (PFSP).

4.	First Generation Magnox Storage Pond (FGMSP).

Records of the original designs of these facilities and the inventories of their waste content may no longer represent the current situation at these legacy sites. This is as a result of over 50 years of physical and chemical changes which the waste may have undergone. A clear understanding of what these storage facilities now contain is beneficial to the planning of a suitable approach for nuclear decommissioning. This section therefore discusses the history of these legacy storage facilities, the complexities in their design, and the challenge involved in adequate monitoring.

1.4.1   Magnox Swarf Storage Silo (MSSS)

The Magnox Swarf Storage Silo (MSSS) as shown in Figure 2 comprises 22 water filled concrete silos. Each silo has a depth of about 16 metres [18]. They contain waste which is predominantly the product of magnox treatment. This waste has over time degraded into sludge and is therefore expected to be mainly corroded magnox alloy.
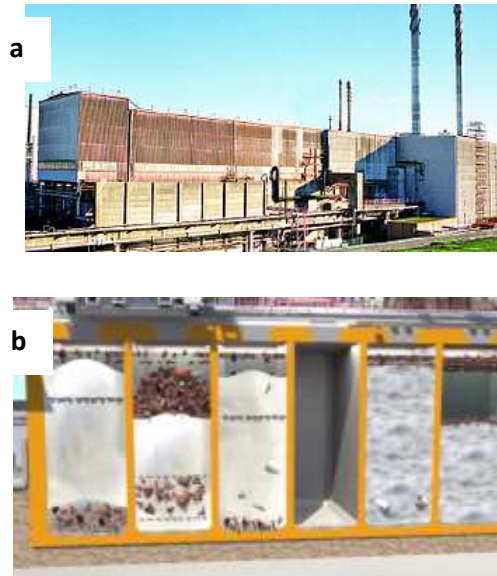
Figure 2: (a) Magnox Swarf Storage Silo (MSSS) (b) Some of the 22 silos inside the MSSS. The top picture shows the external view of one of UK's legacy nuclear storage facilities. A schematic of the composition of these silos is shown in the bottom picture.

A product of sludge corrosion is hydrogen gas which is flammable [18]. For safety reasons therefore, this gas should not be allowed to get trapped anywhere within the silo. The heat produced from any such corrosion must also be controlled by convectional cooling [18]. Hence, it is important to consistently monitor changes in the physical properties of the sludge as large porosity within sludge could be an indication of gas entrapment. Similarly, uneven temperatures may sometimes be an indication of various degrees of on-going chemical or radiological reactions within the sludge.

1.4.2   Pile Fuel Cladding Silo (PFCS)

Another storage silo is the PFCS shown in Figure 3. This was designed in the '50s to be a locked vault never to be opened again [19] [20]. In March 2017 however, the first of six large holes was cut into the side of the PFCS in order to reach inside the silo for waste retrieval. Although these holes are known as the "waste retrieval access penetration" [20], they do provide an opportunity for waste inspection and characterisation ahead of decommissioning.

Figure 3: Pile Fuel Cladding Silos (PFCS). This picture shows the external view of one of UK's legacy nuclear storage facilities commissioned in the '50s. The silos house intermediate level waste at the Sellafield sites.

1.4.3 Pile Fuel Storage Pond (PFSP)

There are two legacy storage ponds at Sellafield. One of them is the PFSP. The 100 m × 25 m × 7 m pond containing skips of irradiated fuel and waste (algae, corrosion products and wind-blown material) facility is an outdoor storage pond [21] [22]. This pond, as shown in Figure 4 was constructed in 1948 and became operational in 1952. The pond served as a facility for storing, cooling and decanning fuel from the Windscale Piles in preparation for treatment. In mid '50s, this facility was modified to allow for the receipt of another high level waste, spent Magnox fuel from the Calder hall reactors [11] [23].

Figure 4: Pile Fuel Storage Pond (PFSP).This picture shows the top view of one of UK's legacy nuclear storage ponds. The PFSP is a 100 m by 25 m by 7 m pond comprising radioactive sludge formed from nuclear fuels and debris .

In 1962, when decanning operations of spent fuel were stopped, the pond remained in use as a storage facility for fuel contaminated items and operational waste. The pond remained in active use until the '70s when all operations in the pond ceased. During its active regime, the pond is estimated to have received about 2100 tonnes of pile fuel and 300 tonnes of Magnox fuel. It is noted that the pond therefore contains water, Magnox cladding, aluminium, steel and uranium. [11] [23] [24]

1.4.4   First Generation Magnox Storage Pond (FGMSP)

In view of the expanding UK nuclear programme, the construction of the FGMSP also began in the '50s and ended in the 1960s. During this period, the pond, shown in Figure 5, served as a facility for receiving, storing and cooling irradiated fuel from the Magnox reactors and to remove the Magnox cladding in preparation for treatment. [11] [23]
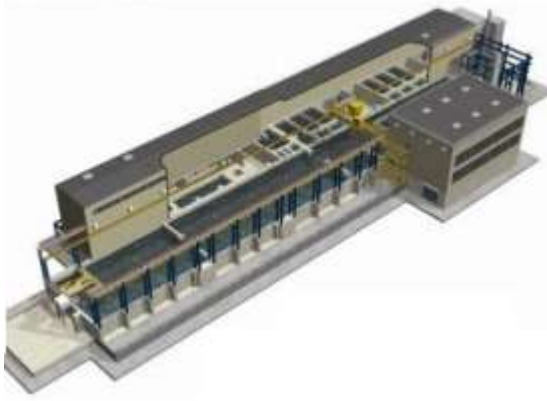
Figure 5: First Generation Magnox Storage Pond (FGMSP) [18]. This picture shows a schematic drawing of the external view of one of UK's legacy nuclear storage ponds, the FGMSP used until the '90s.

In 1974 however, due to a long shutdown of the treatment facility at Sellafield, the FGMSP ended up storing fuel underwater for a period longer than required. This resulted in Magnox fuel corrosion and increased radiation levels [11] [23]. Visibility through the pond waters also became obscured and this slowed down the rate of decanning, further compounding the problem. The FGMSP remained in active use up until 1992 when it received the last fuel. The waste content of this pond is similar to that of the PFSP except that it was not used for Pile fuel. There is the need for a safe removal and processing of these various levels of wastes through separate routes. [11] [23]

1.4.5   Remarks

The construction of these legacy storage facilities was for the purpose of improved operational safety and hazard reduction. The use of water was deliberate. Water serves as a radiological barrier and also serves as heat sink for any on-going reactions. However, the use of water introduced additional challenges to the decommissioning of these facilities. For example, magnox cladding material was deemed fit as a barrier between a fuel rod and the environment due to its neutron transparency. The problem with the alloy however, is that it offers weak resistance to underwater corrosion. Hence, it

should not be left underwater for longer than a set time; otherwise it corrodes, forming a toxic and radioactive sludge. [25]

Unfortunately, corrosion is aided by acidity and as a control measure; low pH values of water should therefore be avoided. It is for this reason that alkaline liquor is regularly pumped into the storage ponds with the aim of maintaining the pH at 11.5. [25] The challenge with this is that these ponds are in the open. With rainwater pouring in, lowering the pH through the process of carbonation, the corrosion may be minimised but may not be halted.

Other sources of sludge in these ponds include bird droppings, and other organic waste in the environment. These could lead to an imbalance or variation in chemical properties of the pond water. Unless the chemical parameters of the water are carefully maintained, there could be corrosion. Attempts at controlling the chemical properties of legacy storage ponds may be a challenge, especially as they were not designed to serve as long-term waste storage facilities.

1.5   Problem Definition

Due to the inherent complexities in the design and logistics within and around the legacy nuclear storage facilities, the decommissioning of each of these four facilities could take over two decades [18]. The inadequate knowledge about the content of these facilities also poses a challenge to the decommissioning process [22] [25]. The possibility of having trapped gasses, ongoing exothermic reactions and significant radioactivity within the sludge makes it necessary for the industry to develop a means of monitoring the physical, chemical and radiological state of the sludge before and during decommissioning.

The sludge will need to be pumped out of the pond for treatment and packaging before it is disposed in a permanent geological facility. The logistics and design of an adequate transportation system needs to be supported by a thorough understanding of the rheological properties and the

sizes of particles found within the sludge. The method of waste treatment and eventual permanent disposal also requires a detailed understanding of the chemical and physical behaviour of sludge during all stages of nuclear decommissioning through to permanent disposal. [18]

Presently, this understanding of the physical properties of sludge is carried out by analysing (in a laboratory) sludge samples retrieved from accessible locations within temporary storage ponds [25]. This can be referred to as an ex-situ approach because of the onward transportation of retrieved sludge samples to the laboratory. Figure 6 shows a summary of this procedure.
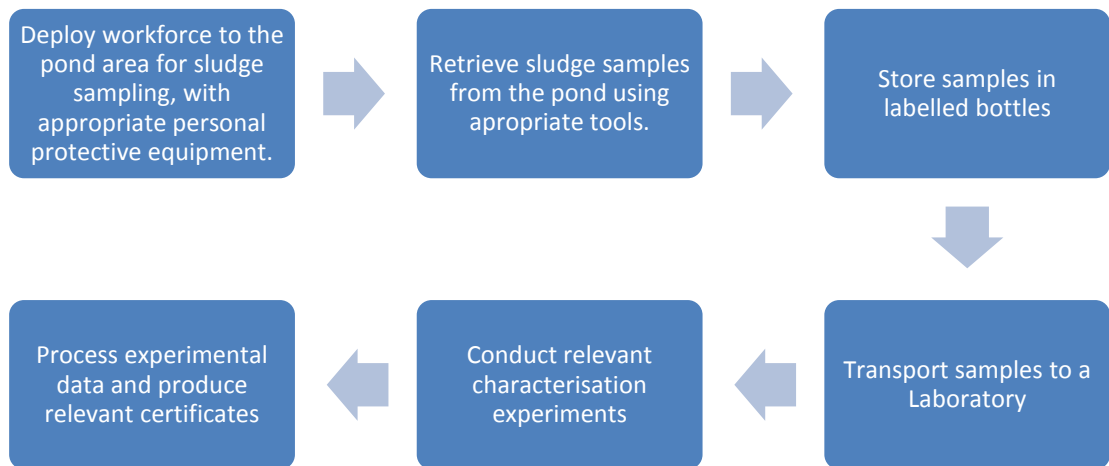
Figure 6: A typical *ex-situ* procedure for sludge characterisation involving the safe retrieval and transportation of sludge samples to a laboratory.

A useful example of where such procedure is outlined in detail is the technical report [26] by the United States Department of Energy. The report was produced in the year 2000 to support the management of characterisation campaigns ahead of the nuclear decommissioning of Hanford K Basin, United States. In that report, emphasis was placed on the need for quality controls relating to the characterisation activities. Following this, a remotely operated method of sludge retrieval was carried out in 2010 [27]. In this exercise, 99.7 % of the radioactive sludge was successfully

evacuated from ten submerged tanks and transported 45 m away for treatment.

There is a limit to the depth and position from which sludge samples can be retrieved in a nuclear pond given the internal design of the ponds and silos which has not made certain areas of the facilities readily accessible. Furthermore, as the sampling procedure in use requires some level of direct human involvement [28], there is a legal limit to radiation dose exposure of UK radiation workers (20 mSv). The impact of this is the inevitable delay in the time required for adequate monitoring of sludge properties.

Thus, comprehensive and precise real-time monitoring at these sites has proven to be very difficult. This is because in order to produce a spatial map representation of the physical properties of sludge within any facility, an adequate number and spread of collected samples is required for data processing [29].

In order to appreciate the present challenge, it is essential to analyse the uncertainties that may have been introduced to historical sludge characterisation data as a result of the method shown in Figure 6. In so doing, there is need to identify and evaluate technical and environmental factors (such as sample size, position of samples and method of sample collection and analysis) which may contribute to the result uncertainty or confidence [30].

Adequate knowledge of the confidence is useful in assessing the quality of decisions which can be taken based on any available sludge characterisation result. Such knowledge is also useful in supporting the development of more reliable techniques for sludge characterisation [24].

For example, concerns about validity of laboratory results obtained ex-situ arise due to uncertainties introduced when sludge samples are exposed to varying transportation and handling conditions [29]. However, with the growing confidence in the use of Remote Operated Vehicles (ROVs) to support nuclear decommissioning [25], it is now vital to assess the obtainable benefits (such as reduction in uncertainty, cost effectiveness and

general safety). This is because ROVs can be used to support sludge characterisation underwater by an *in-situ* approach which eliminates the need for sludge transportation out of the ponds.

By taking *in-situ* measurements, sludge samples may become retrievable from areas within the pond which may have been inaccessible to humans and with even less disturbance to the sludge conditions. The development of an *in-situ* approach requires adequate investigation into a suitable mechanism for collecting samples and conducting relevant analysis under the water at varying depths and spread within the pond.

1.6 Scope of Research

Real particulate systems are known to comprise particles of various shapes and sizes, with diameters ranging from nanometres to millimetres. Measuring the geometric properties of these particles provides a means of characterising the system. Characterisation is useful for quality control, process planning and research purposes [31]. Particle Size distribution (PSD), one of such properties, characterises a system based on the array of individual particle sizes contained therein. Aside variation in size, particles within a given sample may also vary in shape, colour, rheology, chemistry and density. All of which are of interest to the nuclear industry.

In this research however, Particle Size Distribution (PSD) is chosen as the sludge property of interest. It characterises sludge based on the array of particle sizes within any given sample. PSD is a key aspect of quality monitoring in nuclear storage facilities as well as drug, food and detergent manufacturing and water purification. It is expected that the findings contained in this research will be applicable to other physical properties for which sludge may be characterised.

1.7 Research Aim and Objectives

1.7.1 Aim of Research

The aim of this research is to identify, evaluate, and optimise experimental factors which influence confidence in the results obtained from sludge characterisation mapping, and using Particle Size Distribution (PSD) as a case study.

1.7.2 Key Research Objectives

1. To understand the available techniques for measuring particle size distribution.

   i.   To identify what parameters should be evaluated in order to assess the quality of results.

   ii. To review literature on existing techniques for particle size measurement.

   iii. To understand their limitations and applicability to radioactive sludge samples.

   iv. To conduct simulation and experimental validation of preferred solutions.

   v.   To determine whether there are techniques available that could be used to determine particle size distribution *in-situ*.

2. To understand how sampling and analytical procedures affect the overall result confidence.

   i.   To set up a simulant sludge bed which can be used to analyse the effects of sampling and instrumentation on measurements of particle size distribution.

   ii. To obtain particle size distribution measurements from existing sludge samples that have been collected from the storage

ponds, using different sampling procedures and measurement techniques.

    iii.   To employ statistical tools to analyse the measurements and draw conclusions.

    iv.   To ascertain the appropriate sampling strategy and procedure required in order to satisfactorily improve the repeatability and reproducibility of sludge characterisation results.

    v.   To ascertain the number of sampled locations required in order to satisfactorily improve the repeatability and reproducibility of sludge characterisation results.

3. To investigate, using bench-top experiments, the feasibility of an *in-situ* analysis technique.

    i.   To understand the particle size measurement techniques available for in situ application.

    ii.   To understand the design amendments required on an existing Remote Operation Vehicle (ROV) that has been developed at the University of Manchester.

1.8 Deliverables, Benefits, Contributions and Challenges

1.8.1 Key Deliverables

1. Following from objectives 1 and 2 above, a statistical evaluation of how the various sampling and analytical factor settings relate to the overall confidence level and uncertainty of observed results will be conducted.

2. With the findings in the deliverable (1) above, a recommendation for how Sellafield should therefore undertake sludge sampling and PSD analysis campaign towards obtaining optimal representation of the PSD characteristics of the sludge will be made and how overall data confidence should be evaluated.

3. In line with objective 3, a demonstration will be made of how an *in-situ* particle size distribution analysis can be conducted using ultrasonic spectroscopy.

1.8.2 Benefits of this Research

A thorough understanding of the characteristics of the sludge bed will provide insight into the physical changes that may have occurred in the storage facilities over time.

Secondly, optimizing confidence in PSD measurements is not only useful in the design of appropriate transportation facilities [32] but is of general importance to other fields such as water treatment, detergent manufacturing, food and drug quality monitoring [33] [34] [35] [36].

Thirdly, an improved quality in sludge characterisation is beneficial to the design of appropriate simulant sludge and other test materials, thus supporting further research works.

Furthermore, an investigation into the feasibility of *in-situ* sludge characterisation techniques seeks to promote data quality for efficient nuclear decommissioning.

1.8.3 Contribution to Knowledge

At the end of this research and for any sludge characterisation exercises, it will become possible to estimate an overall uncertainty and confidence that account for the effect of varying experimental factors across sludge characterisation campaigns. This will also be retrospectively applicable to old data from previous campaigns. There has not been sufficient research focus on the evaluation of measurement uncertainties that account for differences in experimental procedures occasioned by having different operators.

This research also seeks to contribute to the list of viable techniques for *in-situ* particle size analysis with particular consideration of ultrasonic spectroscopy. The main challenge in the wide adoption of ultrasonic

spectroscopy has been that the widely employed theoretical models require a number of thermo-mechanical properties of materials which are majorly unavailable for unknown samples. If an analytical model is proffered, this will be another major contribution to knowledge.

1.8.4   Technical Challenges Involved

For the outcome of a sludge sampling and PSD analysis campaign to be useful for decision making, the characterisation results must be proven to be consistent and reproducible. It must also be ensured that the samples provide representative information regarding the properties of the sludge across the ponds. To achieve this theoretically, a significantly high number of samples are required for high confidence levels. Working within practical restrictions in a radioactive environment therefore represents a challenge if the same confidence must be realised.

In using non-active samples for the experimental phase of this research, the analysis technique adopted must be validated and confirmed to be reliable. Also, the samples to be used must be stable and non-reactive. These factors if not well designed, may introduce systematic errors in the experimental results of this research. Similarly, the simulation results derivable will depend on the suitability of the treatment models used. Hence, ensuring that the models fairly represent the actual behaviour of the field situation is a challenge that will need to be addressed.

While the sludge PSD spatial distribution and spatial autocorrelation in the legacy ponds remain largely uncertain, the research will need to develop a design solution that is robust enough against such unpredictable disturbances. Another factor that the design will need to be robust against is the inaccessibility of certain areas in the pond for sampling. The ability to model the sludge bed and other crucial factors appropriately will go a long way in ensuring reliable simulation test results.

1.9 Thesis Layout

Chapter 1 introduces the theme of the research with details of the aim and objectives.

Chapter 2 describes the fulfilment of objective 1 of the research (see Section 1.7.2). It provides theoretical backgrounds in the process of sludge sampling, sludge analysis and the statistical analysis involved in sludge characterisation.

Chapter 3 details the fulfilment of objectives 2(ii), 2(iii) and 2(v) of the research. It provides a discussion on the experimental factors (relating to sludge sampling only) that affect the quality of sludge characterisation and their percentage contribution to the overall confidence.

Chapter 4 fulfils the objectives 2 (i) and 2(iv) of the research. This includes relevant theory in sludge sampling, spatial extrapolation, result confidence and statistical evaluation tools. It also includes a discussion of results from simulated and experimental sludge sampling exercises.

Chapter 5 is in fulfilment of objectives 1, 2(ii), 2(iii) and 2(v) of the research. This includes theoretical backgrounds in PSD analysis techniques and results from laboratory experiments on PSD measurements. This chapter focuses on the aspect of laboratory analysis of sludge samples. It discusses the contribution of relevant experimental factors (relating to the laboratory analysis of sludge only) on the confidence obtainable.

Chapter 6 is in fulfilment of objective 2. This chapter brings together the findings in Chapters 3 and 5 (comprising experimental factors relating to both sludge sampling and laboratory analysis of sludge) to develop a useful parameter known as the "cross-campaign confidence".

Chapter 7 is in fulfilment of objective 3 of the research. This includes discussions on the theory, simulations and experiments conducted on ultrasonic spectroscopy as a method for *in-situ* PSD analysis.

Chapter 8 gives a summary of the overall research findings, general conclusions and future recommendations.

All relevant records in support of the research findings can be found in the DCF robotics shared folder.

2 Chapter 2 – Theoretical background

2.1 Motivation

The removal of sludge as part of the UK's nuclear decommissioning programme involves decision making. Making the right decisions is necessary to improve safety, reduce cost and reduce the duration of the programme. It is therefore important that decision makers have adequate knowledge of any sludge population before deciding on a technique for sludge removal. This is because there are a number of techniques by which sludge may be transported, reprocessed and stored. The choice of any technique is dependent on a number of properties of sludge such viscosity, settling time, particle sizes, chemistry and radiology.

Experimental data can be obtained by retrieving sludge samples, and analysing such samples in a laboratory. The level of accuracy of any such experimental data obtained would impact on the effectiveness of decisions made concerning the method of sludge retrieval, transportation, treatment and disposal. Unfortunately, the accuracy of any such experimental data cannot be evaluated when the true values are unknown. The accuracy however depends on the adequacy of both the sludge samples and analysis procedure involved. In seeking to improve this quality, there is the need to be able to measure quality.

In a definition of the term "quality", Montgomery [37] refers to it as being inversely proportional to variability. The author also suggests that by reducing such variability, quality is improved. By adopting this definition, this research considers the variation of results from a number of repeated sludge characterisation exercises as a useful measure of the quality of the sampling and analysis procedure involved.

With knowledge of the existing quality, it would be useful to have an understanding of the mitigating factors that seek to affect such quality. This involves the application of relevant statistical tools.

The essence of such learning is the need to re-engineer the overall data collection and analysis procedure. One aspect of procedure re-engineering is the possible introduction of an *in-situ* monitoring and characterisation system. With such a system in place, and by incorporating the desired safety protocols, time and cost reduction can be achieved.

This research derives further motivation from a 1999 study on ecology by Hansen *et al*. [38]. In the study, a two-dimensional (2D) map characterising the ecosystem of a place called Greater Yellowstone was generated. The characterisation of that ecosystem was based on an ecological parameter known as Aboveground Net Primary Productivity (ANPP) which indicates the presence of life in the give area. While it was only possible to take ANPP measurements at only selected locations in Greater Yellowstone, statistical tools were used to infer the spatial distribution of ANPP across the ecosystem as can be seen in Figure 7(a).

In addition to the characterisation map of Figure 7(a), the study went further to develop a counterpart map known as a variance map showing the coefficient of variation of the inferences made on the characterisation map of Figure 7(a). This map can be seen in Figure 7(b).
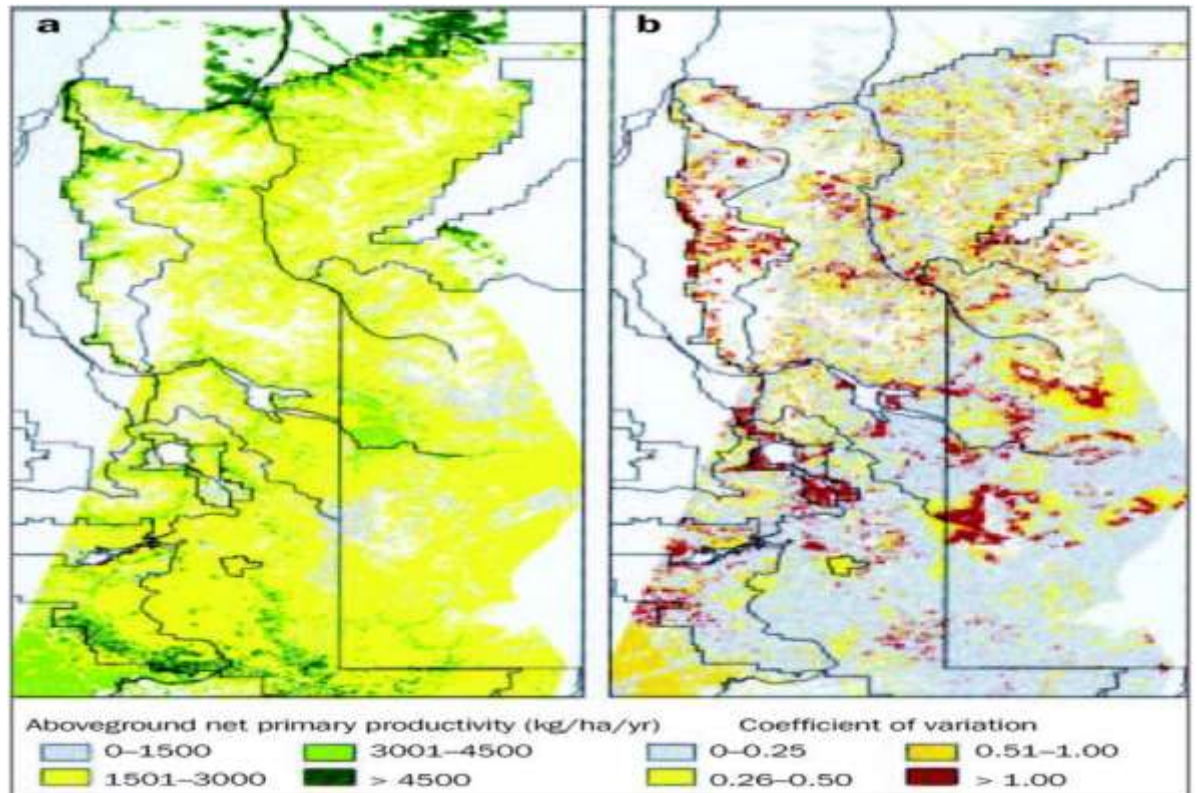
Figure 7: (a) Inferred distribution of Average Net Primary Production (ANPP) over the study area (b) Coefficient of variation in the ANPP inferred in (a) [38]. This figure is taken from an ecological research on the ANPP characteristics of a region called Yellowstone.

Highlighting the relevance of the variance map, it was shown in Figure 8b that the northern part of the ecosystem had higher variance values compared to the southern part, thus implying that the results in the southern part were of higher precision and confidence. The resulting variance map of Figure 7(b) therefore provided an indication that the confidence in the characterisation map of Figure 7(a) could have been improved if further sampling had been conducted in the northern part.

The study [38] is evidence that the characterisation map of a given area can be statistically inferred using an adequate number of sampled data. It is also evidence that a variance map is a useful tool for evaluating the confidence in any characterisation map and for indicating whether the number of sampled data had been adequate or not.

This research is motivated by the evidence in Figure 7(a) and Figure 7(b), and seeks to develop similar maps for the radioactive sludge bed in the legacy nuclear storage ponds at Sellafield. A three-dimensional map (3D) is however of interest to this research as against the 2D maps of Figure 7(a) and Figure 7(b). The similarity between this research and the ecological study [38] is that the nuclear industry also requires a thorough understanding of the physical, chemical and radiological properties of nuclear waste in storage facilities.

There are however site restrictions which limit the amount of sampled data and map accuracy obtainable. Therefore, the concept of a confidence or variance map as seen in Figure 7(b) which indicates the quality of inferred results will aid decision making. Especially decisions on how to improve the sampling, analyses and data processing standards.

2.2   Sludge Characterisation

To facilitate the decommissioning of wet nuclear storage facilities, all of the sludge contained therein need to be retrieved and transported, either to a permanent repository or to a re-processing facility. However, a thorough understanding of the composition of sludge is a prerequisite [39]. Haugan and Mininni [9] describe sludge characterization as the quantitative measurement of sludge behaviour during treatment and disposal processes. The outcome of sludge characterization provides an understanding of the cost of treatment and disposal, and their potential hazards to the environment [9]. Sludge characterization involves the analyses of particulate sludge samples for a number of properties such as chemical composition, rheology, radioactivity and particle size distribution.

Particle Size Distribution (PSD) is a key aspect of quality monitoring in nuclear storage facilities. Simpson *et al*., [40] points out the possible effect of fine sludge particles on visibility and airborne contamination during clean-up induced agitations. A number of techniques for the analysis of particle sizes

have been developed over the years including laser diffraction method, sieve analysis and microscopy [41].

Whilst concerted efforts have been made towards the improvement of analytical techniques [42] [43], the influence of limited sampled data and extrapolation techniques on the overall quality of maps requires further investigation. This research seeks to understand how field operators can practically estimate the number of samples required for adequate sludge characterisation and to investigate how this number may be reduced with minimal effect on confidence in results. This research also seeks to identify the various experimental factors which affect confidence in maps generated.

2.3   Particle Size Distribution

Real particulate systems comprise particles of various shapes and sizes, with diameters ranging from nanometres to several millimetres. Measuring the geometric properties of particles in the system provides a means of characterising the system's behaviour during transportation and permanent disposal. Besides variation in particles sizes, variations may also exist in particle shapes, colour, rheology, chemistry, and density. Ignoring any of these variations while measuring PSD could introduce errors in PSD results. This is why the various techniques for measuring PSD potentially give different results and have varying degrees of reliability [44]. With each technique being uniquely dependent on and influenced by certain physical properties of the sample, it is important to carefully consider the applicability of an analysis technique to sludge characterisation in order to improve repeatability and reproducibility of PSD results.

It is also noteworthy that irregular shapes tend to have different diameter readings depending on the location of the observer. In determining a PSD however, the diameter size of particles are represented regardless of shape, in terms of the 'equivalent diameter size' of a spherical particle which is

expected to behave similarly to the irregular shaped particle, under the exact same condition of analysis used for the measurement.

In general, particle size measuring techniques can be categorised into counters, fractionation methods and macroscopic fitting method [45]. These methods involve measuring certain properties of the particulate medium and deriving a PSD graph therefrom using appropriate mathematical theories. Relevant theories are known and defined in the ISO Standards [46]. The counters and fractionation methods are quantitative and direct measurement techniques while the macroscopic fitting method is qualitative and indirect.

Common techniques for particle size analysis are: sieve and hydrolysis analysis, microscopic image analysis, laser diffraction, dynamic light scattering principle and ultrasonic spectroscopy [47] [48] [49]. Before carrying out a particle size analysis, it must be ensured that the analysis technique has an appropriate size detectability range. Also, the size of the particulate sample taken must be understood to be a satisfactory representation of the bulk medium and adequate for the derivation of a normal distribution. Sampling factors must also be given due attention so as to allow for a collection and retention of qualitative information contained in the samples.

2.3.1 Representation of Particle Size Distribution

The result of a particle size distribution may be represented graphically in a number of ways. These include: density histogram, cumulative distribution curve and a density distribution curve as shown in Figure 8 (a), (b) and (c) respectively. The cumulative distribution allows for visual interpretation of the percentile regions, while the density distribution allows for a visual interpretation of the mean and spread.

The x-axis is usually the equivalent size diameter x_i while the y-axis is the frequency density q_i of the particles that belong to the respective size diameter class. This frequency density may be measured in terms of volume, mass, length, surface or number. It is very important to clearly state what the frequency density represents.
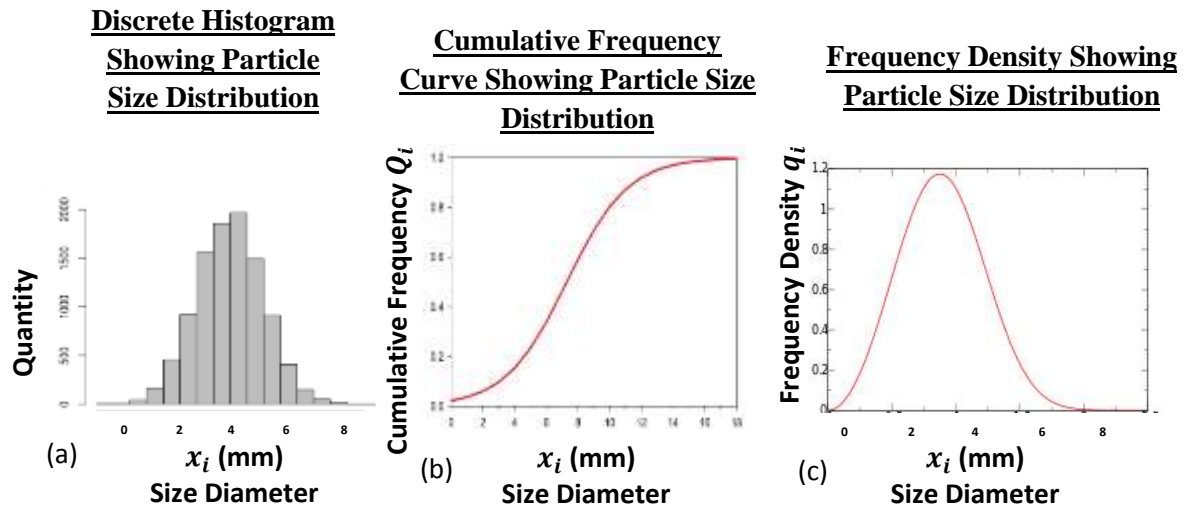
Figure 8: (a) A discrete histogram   (b) A cumulative frequency curve   (c) A frequency density curve. These figures show three methods of representing the result of the particle size distribution measurement of a given sample.

This is because a change in the frequency quantity parameter may lead to a totally different distribution graph for the same particulate sample. The cumulative frequency curve offers a measure of the particle diameters which correspond to 10 % and 90 % of the cumulative undersize distribution by volume [6]. Similarly, the density function curve offers an understanding of the nature of the spread, the mean and mean deviation of the distribution.

2.4   Sludge Sampling in Extreme Environment

In order to generate a three-dimensional map of the sludge characteristics in a nuclear storage pond, an important criterion is the collection of an adequate quantity of sludge samples for analysis. Unfortunately, this is constrained by radiation exposure and access limitations within and around the sludge bed. In a practical sense, it could require several years of regular sludge sampling and analysis in order to retrieve representative samples. This is because of the limited dose of radiation to which field operators may be exposed to within any given period, as well as the cost involved in such campaigns. In doing this, it is necessary to keep an adequate record of relevant experimental factors, settings and conditions.

Such records should include the exact position coordinates from which each sample has been retrieved, the sludge property observed for each sample, details of the sampling and laboratory analysis method and relevant procedure documentations [50] and environmental conditions.

At any point in time, the sludge property in areas of a sludge bed yet to be sampled can be statistically inferred using a variety of methods. With observed and inferred data, a 3D map of sludge characteristics can be generated at any point in time.

The procedure of inferring data at non-sampled positions, by efficiently analysing data at sampled positions is referred to as spatial extrapolation. The resulting 3D characterisation map, being a collation of sampled and inferred data, is therefore regarded as an inferred map. The accuracy and reliability of such an inferred map is dependent on that of the sampling, analysis and spatial extrapolation procedures.

Therefore, in relying on the data contained on an inferred map, there needs to be a measure of the level of confidence. It is expected that the evaluation of confidence should require a statistical analysis of the data as well as the experimental factors, settings and conditions involved. This therefore underscores the relevance of keeping records of inventory and experimental logs. Knowledge of the following would also be relevant:

- The identification of relevant sampling and analysis factors.
- The influence of sampling and analytical factors on result confidence.
- The adequacy of the quantity of sludge samples used.
- The appropriateness of sludge sampling and laboratory analysis techniques used.
- The adequacy of the method of spatial extrapolation used

Although historical data exists from various attempts at sludge characterisation in the past, the non-recording of any relevant experimental factor could affect the evaluation of confidence of such data. This may therefore diminish its relevance for decision making. However, an

investigation of all major experimental factors, to quantify their influence on confidence will be of essence going forward.

2.4.1 Experimental Factors Involved in Sludge Sampling

a)   The Number of Sampled Locations

A sampled location refers to any sub-division of the top surface area of a sludge bed. The top surface of a sludge bed can be sub-divided into pixels (as shown in Figure 9). The total number of sampled locations per total number of pixels is referred to as the 'sampling intensity'.
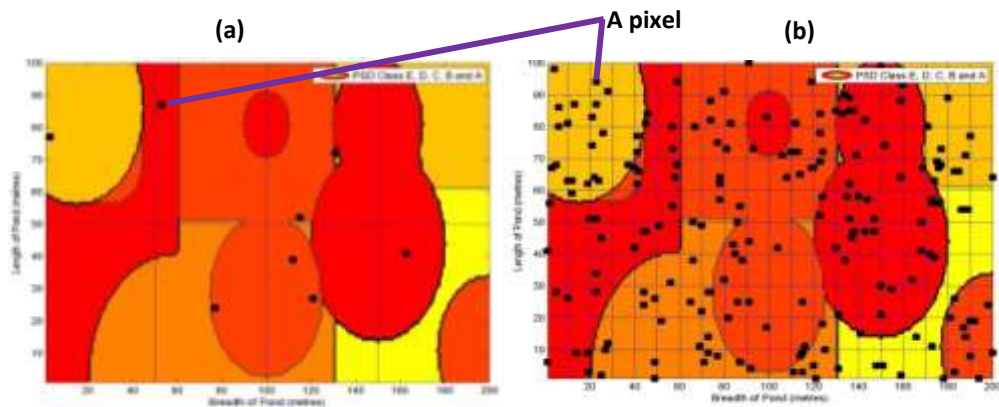
Figure 9: (a) 8 sampled locations (0.04 % Sampling Intensity)   (b) 200 sampled locations (1 % sampling Intensity). These pictures illustrate a two dimensional plan view of a sludge bed. The different colours indicate the class to which the average particle size found in the different regions belong.

The desirable size of a pixel is the surface area of the sludge which the particular sampling device being used can retrieve from any given position. However, this high resolution may not be feasible as it could lead to challenges in data processing. However, compared to the relative size of a sludge bed, the number of pixels can be increased considerably. For example, in a 100 m × 50 m sludge bed, to restrict the number of sampled and non-sampled locations to 20,000, a pixel size of 0.5 m × 0.5 m is required. Although this pixel size is significantly large compared to the size of a sludge sample surface area, it improves the manageability of the data being processed.

The ideal number of sampled locations that is required in order to achieve sample representativeness is typically calculated using Equation (1) [32].

$$n = \frac{\left(z_{\frac{\alpha}{2}}^2\right)(s^2)}{(R^2)(\bar{x}^2)}$$

(1)

This calculation relies on the following parameters: the desired level of risk R, the desired level of significance α, the estimated standard deviation s and mean value $\bar{x}$ of the data across the population. Where z is the z-score.

In a study [51] to determine the effect of sampling intensity on the overall accuracy of landscape classification mapping, it was observed that an increase in sampling intensity from 10 % to 90 % resulted in an improvement in map accuracy from 59% to 67 %. It is important to note that increasing sampling intensity does not proportionally lead to an increase in the accuracy of results. While an early increase in sampling intensity may cause accuracy to increase significantly, depending on the heterogeneity of a population, there is a critical value (of sampling intensity) above which further increase would only cause accuracy to steadily approach 100 %.

In hazardous environments however, achieving a sampling intensity above 0.04 % as seen in Figure 9(a) may pose significant challenges. By implication, the recommended value of n in Equation (1) may not always be realisable without some form of automation. It is therefore important to determine the influence of the number of sampled locations (or sampling intensity) on the confidence in characterisation maps generated.

b) **The Sampling Strategy**

The strategy for selecting the locations that are to be sampled is referred to as the sampling strategy. The three major sampling strategies often considered are: simple random sampling, systematic random sampling and

stratified random sampling [52]. The merits and demerits of these strategies have been discussed by a number of authors [53, 54].

For example, simple random sampling is considered a less challenging approach compared to the systematic and stratified random sampling methods. This is because unlike simple random sampling, the stratified random and systematic sampling methods require a predetermination of the specific locations to be sampled. Simple random sampling could in some cases lead to under-sampling in instances where the heterogeneity of the population is significantly high.

For this reason, the systematic sampling method may be introduced. This method requires that sampling locations are predetermined and are evenly spread out and with precisely equal spacing. This method is expected to enable a more representative sampling, the disadvantage in this however, is that it may consistently miss out on sludge properties that occur at regular intervals.

Hence, a combination of the simple random and systematic sampling methods is the stratified sampling method. This allows a predetermination of grids within which samples will be collected. Such grids are uniform and evenly spread-out. However, the choice of a sampling location within each grid is completely random.

The number of the grids and their dimension may be determined based on the number of locations to be sampled and the dimension of the sludge bed. The aim is to achieve grids of equal dimensions and shapes, unless where for historical reasons the grid distribution has to be biased to allow for a more detailed investigation.

For a sludge bed of dimensions 100 m $\times$ 50 m, in order to achieve a square grid, the number of grids must only be to the powers of 2. Hence, the number of grids required is 2^{Φ}. Where Φ is any integer which belongs to the set $\{0, 1, 2, 3 \ldots, \log_2 n\}$ and 'n' is the number of locations to be sampled. The basic implication of this method is that a number of grids can be any integer from 1 to n but in squares of 2.

The dimension of the chosen grid is given by $\left(\frac{a}{r}, \frac{b}{s}\right)$ where (a, b) is the dimension of the sludge bed. r and s are any two numbers which multiply to give the number of grids to be produced.

Regardless of the sampling strategy adopted, it is important to ensure a high precision underwater positioning system for the sampling devices used. A global positioning system (GPS) is recommended [55] for reliability and improved data quality.

In hazardous environments however, the implementation of the theoretical sampling strategies discussed is usually affected by access limitations. In most cases, it is only possible to collect sludge samples from the surrounding areas of the sludge bed. It is therefore important to fully understand the impact of variations in sampling strategies on result variability.

c)   **The Bias of the Sampling Device**

The objective of sludge characterisation will be defeated if the device used in collecting samples alters the physical or chemical state of the collected samples. The type of sampling device used may be considered to be the most critical factor [56].

A sampling device is used in penetrating the sludge bed, entrapping and retaining an adequate volume of representative sludge samples for analysis. This requires understanding the limitations and peculiarities of different sampling devices.

A sampling device may introduce bias into the sampling process if it filters the samples based on properties such as particle size, rheological properties or morphology [57]. For instance, it was reported [32] that the use of a grab sampler as in the case of Figure 10 may fail if large particles attempt to prevent the grab from closing, leading to loss of some amount of smaller particles during transit.

Figure 10: A Grab Sampler [22]

The grab sampler is a type of sampling device which can be used to collect sludge samples from the surface of a sludge bed.

Hence, the collection bias is an important factor to be considered when choosing a suitable sampling device [58]. Consideration may also be given to the resistance to breakage and the holding capacity [59] of the device. The minimisation of sludge disturbance to the entire sludge population is also an important consideration [60].

Due to the heterogeneity of a typical sludge population analysis [57], there cannot be any one sampling device that satisfies all sludge conditions. There is therefore the possibility of a chosen sampler to exhibit bias towards certain elements of the population. In a 2014 report on sampling device validation, the National Nuclear Laboratory (NNL), UK determined the applicability of a number of sampling devices to depth and particle size types. Due to the confidentiality of that report, reference will not be made to it. However, a 1991 document [61] by the New York State Department of Environmental Conservation provides guidelines for choosing sampling devices. Table 1 is a summary of the guideline.

Table 1: Sampling devices and their applicability to sludge

Sampling Device	Applicability
Scoop/Spade/Trowel	Surface or near surface sampling.
Trier	Sampling of sticky or moist samples. Could reach depths below 15 feet.
Thief Sampler	Sampling of dry powdered material.
Hand Auger	Sampling at different depths.
Sludge Getter Grab Sampler	Penetration into a desired depth of a viscous sludge material.
Ponar Grab	Suitable for most types of sludge but cannot penetrate below several centimetres.
Dipper or Pond Sampler	Sampling surface water.

d)   Penetration Depth of the Sampling Device (in 3D Characterisation Mapping)

The syringe sampler and scoop sampler are examples of sampling devices that can be used for shallow sludge bed sampling. A sludge core sampler is however appropriate for sampling at different depths below surface.

The depth from which a sampling device can collect sludge samples is very important in 3D characterisation mapping. For this reason, a multi-level adaptation of the bottle-on-pole sludge sampler was designed [62] with a capacity to collect samples at two or more vertical levels. Similarly, the use of a core sampler was proffered [63] for a study that sought to understand the vertical distribution of a particular biological organism.

Unless the data being monitored is known to be a function of depth, in which case a 2D data acquisition and processing is appropriate, a 3D sampling should be implemented [64, 65]. This involves the labelling of sludge samples with reference to their sourced positions (x-, y- and z-coordinates). The vertical resolution should be given due consideration [66]. It is however dependent on the design of the sampling device used.

2.5 Particle Size Analysis: The Influence of Experimental Factors

The PSD property of the sludge provides a measure of what the expected behaviour of sludge will be during transportation, treatment and disposal processes [9]. This information has been identified [40] as an important decision making factor in the planning and execution of the clean-up project.

For example, in research [67] to assess the stabilisation process within a sewage sludge landfill, the authors observed an over 400% increase in the median particle size from 37 micrometres on the first day to 143 micrometres after the 300 days. This suggested the rate of stabilisation which had taken place. Similar examples that have identified the importance of PSD to sludge management and disposal exist in the study of the effect of anaerobic digestion [68] and water treatment systems [36]. With regards to the design of efficient transportation systems for radioactive sludge, Luckham and Ukeje [69] have observed that the viscosity in a given dispersion medium is influenced by the PSD. In that study, it was observed that the narrower the particle size distribution, the higher is the relative viscosity.

There are a number of techniques for measuring PSD ranging from the coulter-counter method and sieve analysis method to more technologically advanced methods like the Laser Diffraction Method (LDM) [68] and Ultrasonic Spectroscopy [70], each having its merits and limitations.

Other PSD measurement techniques include: microscopy and image analysis, electrozone sensing and light scattering [71]. Most techniques operate by taking direct measurement [45] of a certain property of the sample, and then use such measurements to mathematically deduce the PSD data. Accordingly, each technique could yield a different PSD result from any other technique [72]. Similarly, adopting different experimental procedures and laboratory conditions could give a different result. Hence, Kane [72] and Jones [73] recommend the elimination of variable operator discretion. They propose the

introduction of an adequate standard of procedure (SOP) and the use of consistent and correct parameters for data interpretation.

2.5.1 The Principle of Laser Diffraction Method

Laser Diffraction Method (LDM) is an indirect technique for particle size characterisation. It is based on the principle of light diffraction. There are four events that occur when light waves come in contact with an obstacle. These are: reflection, refraction, absorption and diffraction [49].

Hence, because diffraction occurs at the edge as depicted in Figure 11, two properties of the diffracted light can be observed at the aftermath of a diffraction event. They are the angle of the diffracted wave, and the intensity of it. These properties correspond to the diameter of as spherical obstacle or the equivalent (spherical) diameter of an obstacle. This is with an assumption the assumption that particles are spherical and volumetric [74].
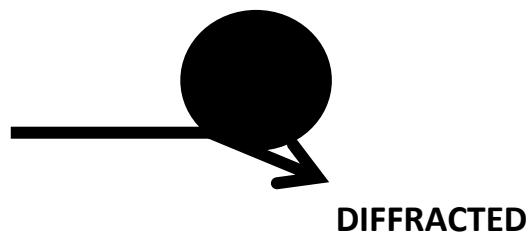
DIFFRACTED

Figure 11: Diffraction occurring at the edge of an opaque spherical particle. This picture is a schematic diagram describing the deflection of light when it is incident on the edge of a particle.

Smaller particles are known to effect wider diffraction angles and lower intensities relative to those effects from larger particles [49]. In order to measure PSD, light from laser sources are emitted unto a particulate medium. Upon interaction with the particles, the light photons tend to scatter at different angles based on the wavelength and the size of the particle. With the aid of photo-detectors, the diffraction angle as well as the intensity of scattered light can be recorded. Mie scattering theory and the Fraunhofer

Approximation Model [49] provide methods of mathematically interpreting these scattering data as particle size distribution data.

Modern LDM based instruments such as the Malvern Mastersizer 3000^{TM} shown in Figure 12 are flexible, fast and have the capacity to measure size diameters between 2 μm and 2000 μm [49, 75, 76]. They are therefore commercially employed across industries.

Figure 12: Malvern Mastersizer 3000 [49] used for analysing the particle size distribution of a given sludge sample. It is a laboratory based instrument which works on the principle of laser diffraction.

2.5.2 Alternative PSD measurement techniques

a. Ultrasonic spectroscopy

Ultrasonic spectroscopy involves the transmission and reflection of ultrasound within a medium for the detection of particulate obstacles of various sizes contained within. In transmitting ultrasonic waves, a number of its properties may be altered by certain characteristics of the particulate medium. The velocity and attenuation of sound waves are usually affected by the number of particulate obstacles within the medium. The frequency of the sound wave however determines what size of an obstacle will have a

significant effect on the wave propagation. By decreasing the frequency, larger sized particles can be detected.

Therefore, by varying the frequency from very high to very low, the presence of sample sizes may be observed. The amount of velocity or attenuation occurring at various frequencies will be mathematically interpreted into particle quantity associated with the respective size class. In implementing particle size analysis using ultrasonic spectroscopy, a wide frequency (f) range allows for the detection of a wide particle size range. The ability to gradually vary this frequency will also improve data resolution.

$$c = f \lambda \qquad\qquad\qquad (2)$$

In summary, ultrasonic spectroscopy requires the development of an Ultrasonic Velocity Spectrum (UVS) or an Ultrasonic Attenuation Spectrum (UAS) which is more widely used [47]. Ultrasonic spectroscopy does not require sample conditioning; it is not destructive and may be designed to be non-intrusive [45].

Another feature of ultrasonic spectroscopy is its suitability for optically opaque systems [77] [78] as well as its non-dependence on the electrical properties of samples [79] [80].

Therefore this technique is able to overcome the problem of opacity of a particulate medium [81] which may influence the performance of other macroscopic but optical techniques. Chapter 7 contains a detailed discussion on the procedure for implementing ultrasonic spectroscopy for PSD measurement.

Alba *et al*. [77] even found ultrasonic spectroscopy to be suitable for volume concentrations ranging from 0.5 to 50%. It can however be argued that concentrations below 2.6% could lead to invalid results as observed by Inam *et al*. [82]. Notwithstanding, it has been reported that some systems become unstable upon dilution [77], while in some other cases, it is desired

to maintain a sample in its original state while being analysed. Ultrasonic spectroscopy therefore becomes a technique of choice.

Furthermore, ultrasonic spectroscopy can be used to measure particle sizes in the range of 10 nanometres to 1 millimetre [78] [77]. In addition to particle sizes, information about the compressibility and dispersion state of the samples can be obtained from ultrasonic spectroscopy data [78].

For example, Hu *et al*. [83] considered the role of an accurate PSD determination on the optimisation of combustion efficiency. To test this, a continuous in-line PSD measurement was conducted on glass beads using a peak detection technique algorithm to analyse the impact of the sample solution on acoustic emissions. Similarly, Pierre *et al.* [84] conducted an experiment involving the transmission of ultrasonic signals of frequency range 60 to 600 kHz through foam bubbles. In this experiment, the ultrasonic attenuation and velocity data was found to be sensitive to the sizes of foam bubbles.

Notwithstanding the numerous merits of ultrasonic spectroscopy, the impact of fluctuating temperature on the measurement of acoustic attenuation has been noted. It has been argued that temperature affects material properties of particulate media thus influencing acoustic behaviour within them [85].

This is however not found to be the case with the measurement of sample concentration [86]. This is because of the adoption of a multi-distance measurement and low frequency technique. Unlike in the measurement of sample concentration, PSD measurement involves high level frequencies. For this reason, it is recommended to measure and seek to limit temperature variation to not more than 2 degrees Celsius for any meaningful result [87].

b.   Sieve analysis

Sieve analysis is one of the traditional methods of particle size analysis. It involves the use of sieves stacked in order of decreasing mesh sizes. The representative sample is first placed on the top mesh and allowed to filter

through to the bottom. If a particle has a diameter size smaller than the mesh size, it filters through to the next smaller size. To ensure that the sieving process is complete, the samples are vibrated mechanically or using sonic methods [48]. The samples collected by the various meshes are then weighed and recorded against their diameter size class. If there is a significant difference between the sum of the overall weights recorded and that of the initial sample, the experiment is repeated. According to [88] a difference below 1% is acceptable. The challenge with this method of analysis is that the chance of a particle of a given size filtering down does not depend solely on its physical diameter but also on its physical shape and orientation as well as its chances of encountering the mesh openings.

c.   **Dynamic light scattering**

Taking advantage of the concept of Brownian motion, where small particles in a medium are understood to engage in constantly random motion, measuring the random changes in intensity of light scattered through such a medium gives an insight into the inherent particle sizes. The dynamic light scattering principle, sometimes called the quasi-elastic light scattering [89] or photon correlation spectroscopy [90] therefore requires a laser source and one or two very fast photon detectors positioned at a known scattering angle, usually 90 degrees (right angle) or 173 degrees (back angle) [49]. As the detector records the fluctuating intensity of scattered light and transmits this data to a digital processing device known as the correlator [49] for analysis of the delay time and diffusion constant obtained, the Stokes-Einstein relationship is employed to produce a particle size distribution. This technique is appropriate for detection of particle sizes which are below 1 nm [89]. For a wider range, more photo detectors positioned at different angles are required.

d.   **Microscopy and image analysis**

Microscopy and image analysis is seen to be a primary technique for particle size characterisation [49].This is because it allows for a direct observation and measurement of the particle shapes and size. The need to expand the capacity of this technique, from the regime of manually

inspecting each sample, to an automated system of analysing much more samples has led to the development of a dynamic image analyser or static image analyser where the samples are directed to flow past the cameras or are made to slide onto an automated stage past the camera, respectively. The underlying principle however remains the same. Particles are placed in the measurement chamber, very high resolution images are captured with the aid of digital cameras. This image taken is processed through an image analysis software such as ImageJ and Image-Pro plus [91] to distinguish between particles and background and to measure shapes and sizes of particles observed.

2.5.3   Recent Development in Particle Size Analysis

There have been efforts towards improving the data processing methodologies involved in the measurement of particle size as well as the introduction of new analytical techniques for particle size measurements. Amongst such methodologies include; the proposal for the use of an analogue computer in processing real time sample images for analysis of particles [92]. There are also proposals for the use of electronic principles similar to the coulter counters, for volumetric particle size analysis [93], and for the use of magnetic properties to predict corresponding particle sizes [94].

There is a proposal for the use of an image analysis method for water treatment applications [95] and a hardware modification to the image analysis technique. This modification involves introducing the concept of multi-flash imaging to enhance image segmentation and consequently, to enhance the computer vision [96]. Other emerging technologies include real-time reflection terahertz time-domain spectroscopy [97], computer synthesized holography [98], use of resonant vibration data [99] and electrostatic charge distribution analysis [100].

Of particular interest is the focused beam reflectance method (FBRM) which is fast becoming a popular technique for *in-situ* particle analysis [101]. This is especially so as the FBRM, just like the ultrasonic spectroscopy technique, does not require a very low sample concentration [102]. In an application to radioactive slurry analysis, Daymo *et al.* [103] noted the capacity technique

to monitor PSD changes at sample concentrations up to 35 vol %. In the FBRM technique, the chord length distribution (CLD) of a sample is measured and mathematically converted to a corresponding particle size distribution (PSD) using established mathematical models [104].

A chord length, being the distance from one edge of a particle to another, is obtained by focusing a laser beam, through a sapphire window on sample. By rotating at a fixed velocity, the focused beam scans across each particle as they flow across. The time between the commencement of laser backscattering at one edge of a particle and its completion at an opposite edge of the same particle is used to determine the chord length [104].

Although particles are likely to be in motion during this event, De Clarcq [105] opines that the motion of the particles is not significant owing to the 8.4 mm scan diameter of an FBRM probe. The FBRM method has been investigated in a number of studies [106] [107] [108]. In one of these studies [108], it was reported that the position of the focal point of the probe also does have an effect on the result.

It is noteworthy that while the CLD data is a sufficient end result in some applications [109], in others, the need to convert CLD to PSD brings up the issues of uncertainty relating to the presumption of particle shapes. To support the analysis of non-spherical particles, Wilkinson and Li [102] proposed a modification in the mathematical model used for CLD-PSD translation. A non-negative least squares method was recommended as against the Least squares or Constrained Least Squares method. This was experimentally validated [110] and observed to have been successful.

In a separate investigation, with regards to waste water treatment applications [105], it was observed that FBRM agrees with image analysis and laser diffraction on number-weighted mean diameters above 150 microns, but records inflated data for below 150 microns. A major problem with FBRM, and perhaps any other technique that may be considered for *in-situ* application is that of fine particles loitering around the probe window thus resulting in a PSD with a false high particle count at small sizes.

2.5.4 Comparative Analysis of some PSD Measurement Techniques

Table 2 provides a comparative analysis in summary of some of the techniques available for PSD measurement.

Table 2: Comparative analysis of some PSD measurement techniques

Techniques	Applications	Advantages	Limitations
Image Analysis & Microscopy	Applied in pharmaceuticals for quality control for particles below 150 microns [111].	It provides absolute information about the particles	1. Time consuming [111] 2. Counting and Sizing is subject to human judgment [111].
Laser Diffraction Method	Applied in Pharmaceuticals [112] and soil science [113]. Modern instruments can analysis sizes between 2 microns and 2000 microns [76]	Useful for bulk analysis and improved accuracy.	1. Requires sample preparation 2. Requires Optical parameters.
Sieving Analysis	Applied in pharmaceuticals [112]	It is the simplest method [112].	It is an offline approach
Ultrasonic Spectroscopy	Applicable to extremely high particle concentrations [114].	1. This technique is applicable to as high as 20% sample concentration [114].2. It does not require extensive sample preparation	It requires thermodynamic and mechanical parameters.

Remarks

In summary, the laser diffraction method (LDM), an indirect and laboratory based method of particle size measurement has been undergoing development over the years into a commercially reliable solution. This is because of the need for an online or *in-situ* measurement solution. Considering that LDM technique requires the samples to be conditioned before analysis, Ultrasonic spectroscopy is considered a viable option. Although relatively new, this technique has been observed to have certain limitations which have affected its wide applicability.

This study seeks to understand the sensitivity of the commercially deployed LDM method, especially as it involves a theoretical assumption that particles are spherical in shape [115]. This assumption in itself introduces some degree of uncertainty to the results derived. It has become important to understand how different choices made in the course of implementing the LDM method contribute to the level of variation or confidence in results.

A number of qualitative analyses conducted with a view to optimise measurement conditions have suggested that there is an influence by experimental factors and conditions on the reliability or otherwise of the various methods for measuring PSD [42, 116].

Nonetheless, there is the need to conduct a quantitative analysis of the influence on the data quality of measurements [43]. This will enable an experimental determination of appropriate conditions and settings required to yield a desired level of precision (as recommended by the British standard [6]). Therefore, the aim of this study is to identify and evaluate the contribution of relevant experimental factors to result variation and confidence.

Furthermore, in line with efforts to advance *in-situ* analysis, the identified limitations of ultrasonic spectroscopy will be discussed and investigated using bench-top experiments and computer simulations as described in Chapter 7.

2.5.5 Experimental Factors involved in LDM

The susceptibility of most analytical techniques to procedural and technical errors is dependent on their principle of operation, thus making it important to investigate the analytical uncertainty related to techniques on an individual basis. Most techniques for particle size analysis operate by taking direct measurement of certain parameters of the investigated sample, and mathematical interpret such observed data into indirectly deduced particle size distribution information. The direct data being measured are most often not a complete reflection of the particle geometry. This is especially the case with automated techniques [117].

These issues raise concern especially if results are to be harmonised or compared. It has become important to understand how different choices made in the course of analysis contribute to the uncertainty in results (analytical uncertainty). This knowledge is useful in deciding which change in measured properties are statistically significant and should be accepted as a true occurrence or be ignored. Although a number of researchers have sought to identify and qualify the effect of some analytical factors on the uncertainty of measurement results, not many have made attempt at quantifying these contributions, particularly factors that are procedural in nature such as sample preparation or handling.

One of such studies was conducted by Gu *et al*. [42] where factors that influenced the result of laser scattering method were investigated with a view to optimising measurement conditions. Another study was conducted by Zhang *et al.* [118] and although it was also research to investigate the influence of experimental factors on the PSD measurements conducted by LDM, the difference was that the focus was on experimental factors relating to the properties of the sample.

The British standard [6] places emphasis on the need for an experimental determination of appropriate conditions and settings required to yield a desired level of precision. It particularly goes on to request that the influence of optical model such as refractive index be investigated. More so, Virden

[43] holds that the success of analytical techniques depends on a thorough and systematic examination of influential factors. The importance of studies on influence quantification is further supported by [116] and [7].

The following experimental factors have been selected for investigation:

a) Measuring Time

The duration for any LDM analysis on a sample may vary from one operator to another. An increase in measuring time is expected to cause the generation of more data about the sample. This will result in an increased data precision and reduced variability. Similarly, insufficient measuring times result in unrepresentativeness and must be avoided [43].

However, excessively long measuring times must also be avoided as it will reduce the efficiency of the analytical process. Storti and Balsamo [119] in a test of laser diffraction technique observed that low strength materials are susceptible to errors due to the measuring time. It is important to identify the significance of the "measuring time" factor on result variability.

The two contrasting settings that will be considered under this factor are 10 seconds and 30 seconds.

b) Stirrer/Pump Speed

Before introducing a sample into the measurement chamber, there is the need to agitate the samples and keep them unsettled for adequate sample dispersion. Sample agitation involves either the use of a stirrer, a pump or ultrasonic waves [43]. Agitation of particles especially dense particles helps to prevent agglomeration while the pump enables flow alignment [43]. Nonetheless, excessive agitation may cause the breaking up of primary particles, and should be avoided.

The speed of the stirrer and the pump has been identified as factors that may contribute to variability in results [120, 121]. It is however important to investigate the extent to which the "Stirrer/Pump Speed" factor affects result variability and confidence.

The two settings that will be considered under this factor are 1500 rpm and 3000 rpm.

c) Dispersion Medium

Samples must be dispersed in a medium which reduces the possibility of agglomeration. Two major dispersants, deionised water and sodium hexametaphosphate (SHMP) are usually considered. In a study, Dias [122] investigated the effect of using each of these two dispersants. Dias concluded that the effect was insignificant.

However, the argument that SHMP helps to prevent agglomeration of particles still arises. Similarly, on the relevance of deionized water, it has been suggested [43] that tap water may introduce flocculation of the particles in the samples and should be avoided. This underscores the need to quantify the contribution of the "dispersion medium" factor on result variability.

The two contrasting settings that will be considered under this factor are tap water and SHMP dispersants.

d) Sample Concentration

The volume concentration of particles in the dispersion medium as well as the sizes of particles in the medium affect the amount of light that is able to travel across to the optical detectors (laser obscuration) [43]. A laser obscuration of 5 to 25 % is desirable [6] in order to avoid multiple scattering.

Variations in sample concentration will cause variations in the PSD results [123]. Such variations may be as a result of deliberate operators' decisions across experiments or as a result of on-going agglomerate decomposition within the same experiment.

The two contrasting settings that will be considered under this factor are 0.5 and 4.0 %V concentration of samples in the dispersant.

e) Optical Parameters – Refractive Index and Absorption Constant

A number of studies [124, 121, 125] have shown that in the use of the LDM technique for PSD analysis, the optical parameters namely: refractive index and absorption coefficient, of the particulate sample and that of the dispersion medium are vital to the computational algorithm. They influence the final PSD result obtained. In order to reduce variations across experiments, the use of generic optimal parameters for unknown sample mixtures has been recommended [124]. In this research, the influence of optical parameters is investigated. This requires the choice of two contrasting optical parameter settings for analysis.

The two contrasting settings that will be considered under this factor are the values 0.1 and 1.0 for absorption constant, and 1.52 and 1.9 for refractive index.

f) Instrument

Lastly, the resolution of the measured PSD is dependent on the number of detectors in place. With more advancement in the LDM technology, in areas such as the sensitivity of the optical detectors and mathematical interpretation algorithms, the accuracy of PSD measurements is expected to improve. There is therefore the need to investigate the effect of using different models of an LDM instrument on the variability of results.

The two contrasting settings that will be considered under this factor are the Malvern^{TM} Mastersizer 3000 and Malvern^{TM} Mastersizer 2000. This is due to significant modifications that have taken place in the design of the Malvern^{TM} Mastersizer Instrument [74] which has made the 3000 model more robust and user friendly.

It should be noted that while individual analytical factors contribute individually to measurement uncertainty, in the event of interactions between factors such combined effect acting together may likely produce an effect greater than their individual sum, as will be observed in Chapter 5. [126].

2.6   Remarks

It has been mentioned in this chapter that an objective of sludge characterisation is the generation of a sludge characterisation map. This is a map showing the spatial distribution of sludge properties across the bed. This map may either be produced as a two-dimensional or a three-dimensional map. In order to carry out sludge characterisation however, a sufficient quantity of representative sludge samples must be retrieved from across the length, width and depth of the sludge bed. An understanding of how to determine what quantity may be sufficient is contained in Chapter 4.

Similarly important is the determination of an appropriate sampling strategy. The theoretical advantage and disadvantages of the various sampling strategy options have already been discussed. Nonetheless, there is a need to understand the influence of such choice on result variation. If the influence is observed to be significant, then emphasis will be placed on the need for adopting stratified random sampling because of its merits.

With regards to the choice of sampling device, this research does not seek to validate any particular type of device. Such reports already exist and have been discussed in this chapter. These reports validate sampling devices based on a number of factors. Two of such factors are the penetration depth and the bias of the sampling device to particle sizes. Other factors include the bias of the device towards samples of a particular density, chemical reactivity and rheology.

However, within the scope of this research, the penetration depth and particle size bias will be considered. It has been mentioned that it is a challenge to design a sampling device that meets all of the desired requirements. However, by evaluating the influence of each of these factors on data quality, a decision can be made on which of the existing sludge sampling devices is the most appropriate.

Aside carrying-out sampling, a comprehensive laboratory analysis of sampled sludge must thereafter be conducted to obtain sampled data. This research identifies seven experimental factors involved in the use of an LDM instrument to measure particle size distribution of sludge samples. The LDM

is being considered because it is the method widely adopted for ex-situ measurement of sludge PSD.

From the foregoing discussion, Table 3 shows the experimental factors which will be assessed for their influence on result variation.

Table 3: The experimental factors to be considered in this research

Label	Description	Remark
Factor A	The Number of Sampled Locations	Experimental Factors Related to Sludge Sampling
Factor B	The Sampling Strategy	
Factor C	The Penetration Depth of the Sampling Device	
Factor D	The Bias of the Sampling Device	
Factor H	The Measuring Time	Experimental Factors Related to PSD Analysis using LDM
Factor I	The Stirrer/Pump Speed	
Factor J	The Sample Concentration	
Factor K	The Refractive Index of Sample	
Factor L	The Absorption Constant of Sample	
Factor M	The Dispersion Medium Used	
Factor N	The Instrument Model Used	

At the end of the PSD analysis of sludge samples, the measured data are fed into a spatial extrapolation algorithm in order to infer PSD data at non-sampled positions of the sludge bed. An understanding of relevant statistical tools required to achieve this is contained in Chapter 3. Also contained in Chapter 3 and Chapter 5 is the deployment of statistical tools to evaluate the influence of experimental factors listed in Table 3.

2.7 Conclusion

A typical sludge characterisation cycle can be allowed to span a sufficiently long period of time. This helps to minimise radiation exposure to operators while allowing for a significant number of sampled locations. In this long period, it may be inevitable to involve various teams of operators at different times, with each team introducing unique methods and procedures. Such variations in procedure could be expected to introduce variation in map results.

It therefore becomes a challenge to combine historical data with recent data to produce one map when adequate records of certain influential factors are not maintained. It also makes it difficult to ascertain genuine changes in the characteristics of the radioactive sludge when comparing characterisation maps produced from historical data with those produced from recent data.

Attempts have been made at limiting the variations in methods and procedures such as the introduction of an international standard on sludge sampling [50] and other standards of procedure documentations. Nonetheless, with continuous technological advancements, variations in methods and procedures over lengthy periods are unavoidable.

3 Chapter 3 - Evaluating the Influence of Sampling Factors on the Accuracy of Sludge Characterisation Mapping

3.1 Introduction

This chapter seeks to understand and quantify the effect of variations in sludge sampling procedures on the variance in the results and their contribution to data quality. The factors of interests which have already been identified in Chapter 2 are as follows:

1. The Number of Sampled Locations
2. The Sampling Strategy
3. Penetration Depth of the Sampling Device
4. The Bias of the Sampling Device

3.2 Spatial Extrapolation and 3D Map Generation

If a population field is completely homogenous in terms of the physical or chemical characteristic being measured, then just one sample collected from only one location will be sufficient to precisely characterise the entire population. Unfortunately, such a population field, like any other field, must be presumed to be heterogeneous as a result of spatial variability until it is perfectly characterised by analysing every sample from every location in the field. In reality however, it is only practical to collect samples from a few selected locations and conduct analysis on these samples. Data for the non-sampled locations can only be predicted by processing the sampled data using an appropriate spatial interpolation/extrapolations algorithm. The success of the data prediction algorithm translates to a reduced spatial uncertainty and improved characterisation accuracy for the population.

The concept of spatial extrapolation is common to 1D and 2D analysis. In environmental applications, particularly in sub-surface monitoring, 2.5D (pseudo-3D) or 3D analyses are necessary to include a representation of the

vertical spatial variability as recognised by French [127]. Contreras *et al.* [66] in estimating the spatial continuity and lateral extent of lithology and flow units penetrated by wells used 3D stack data. The 3D spatial distribution had a vertical resolution that was relative to well logs and 3D data available. Similarly, Heaney [65] in an assessment of the levels of ambient noise in regional waters, considered a 3D modelling approach to estimate the overall impact of man-made sounds underwater. Although a 3D extrapolation introduces further complications in the extrapolation algorithm, there have been some efforts to reduce such complexities. One such effort was reported by Mousa *et al.* [128]where an improvement on an existing algorithm reduced iterations by 98 %.

3.2.1 Methods of Spatial Extrapolation

There are two major approaches to spatial extrapolation; geostatistical and deterministic approach. The deterministic approach is similar to a basic linear regression model as it involves a predetermined assumption of the statistical spread of sampled data, structure of population variance and the autocorrelation amongst population data [129]. Miller *et al.* [129] remarks that these assumptions are not easily applicable to ecological analysis and thus, an approach that seeks to ignore the independence among observed data may not be an entirely appropriate. There have been a few modifications to the approach thereby accommodating a non-linear spread of data. Triangular Delaunay Algorithm (TDA) method is an example of a deterministic approach. In the TDA method, prediction of data at a non-sampled location is made by taking the proportionate contribution of sampled data from the nearest sampled location or from a set of nearest surrounding points weighted by their distance [130].

Geostatistical approach on the other hand is considered most suitable for populations where spatial dependence is suspected [131]. It employs spatial statistics tools, For instance, Ordinary Kriging Algorithm (OKA) method, an example of geostatistical approach, employs an autocorrelation tool to guide predictions [132]. A variogram model is first developed from a statistical analysis (variance and co-variance tests) of all the sampled data and locations. This provides the prediction algorithm with qualitative information about the

spatial correlation between sampled data [133] in the form of sill, range and nugget values.

The predictions at non-sampled locations are then made using a weighted average of all statistically relevant sampled data locations. Two studies [134, 135] provide an extensive description of the Kriging method. It must be stressed however, that the validity of information from a variogram is dependent on the adequacy of number and spread of sampled locations in relation to the degree of heterogeneity in that population. Also, sensitivity analyses conducted in [66] indicated that the predicted results were slightly conditioned by the choice of variogram model used.

Therefore, geostatistical approach is not necessarily the best approach for all ecological monitoring campaign. Bolstad *et al*. [136] in a comparative study on the accuracy of four extrapolation methods in predicting forest vegetation patterns observed that linear regression models were more accurate than the geostatistical approach and thus concluded that the nature of spatial dependence in the population, being not wide spread, would only be captured by dense sampling. Bohling [137] however remarks that an improvement in sampling density, while maintain uniformity of spread, will be beneficial to all types of algorithms.

Furthermore, he opines that except in the event of an uneven spread of sampling points, all algorithms are fairly similar in accuracy, thus defeating the need to undertake a complicated matrix inversion operation where an easier alternative is available. Discussing the relevance of Kriging in the event of sample clustering, [138] agrees that although Kriging is certainly more time-consuming, its dependence on statistical distance as against geometric distance allows for improved data prediction. It is therefore advisable to quantify the spatial uncertainties associated with any chosen extrapolation algorithm [129].

3.3 Materials

The initial study of the experimental factors related to sludge sampling was based on a representative simulated sludge bed. The model which was designed with the aid of MATLAB is a sludge bed having dimensions 100 m × 50 m × 5 m. This nominal size is representative of a pond on the Sellafield site.

This sludge bed was uniformly sub-divided into 200,000 voxels, which are cubic pixels, each having sides of length 0.5 m, with each voxel assigned a specific PSD class value ranging from 1 to 6, with each class representing a range of particle sizes. The reason for this was to section the sludge bed into a population of 200,000 locations with a predefined PSD characteristic for each location.

By doing this, the simulation defines a sampling location as a voxel of dimension 0.5 m × 0.5 m × 0.5 m. This volume is significantly greater than what a typical sludge sampling device can retrieve from one location. Therefore, this simulation adopts the assumption that the PSD within a 0.5 m × 0.5 m × 0.5 m voxel is homogenous.

The diameter of particles typically found in sludge samples can be as high as 15,000 μm. However, the range 10 to 1,500 μm used in the sludge bed model reflects the particle sizes that a common industrial technique for particle size analysis, e.g. Laser Diffraction Method (LDM), can be used to detect [76]. For this reason, samples are first sieved to filter out sizes that are outside of this range. Therefore, the modelling and simulation of PSD characteristics of the sludge bed is based on an assumption that the sludge samples contain only particles within the size range 10 μm to 1,500 μm.

For the purpose of this analysis, the range of particle sizes is segmented into six PSD class values using the following classification for the mean particle size of any sample: Class 1 (0 − 150 μm), Class 2 (150 − 250 μm), Class 3

(250 – 450 µm), Class 4 (450 – 700 µm), Class 5 (700 – 1000 µm) and Class 6 (1000 – 1500 µm). This size classification is as shown in Figure 13.
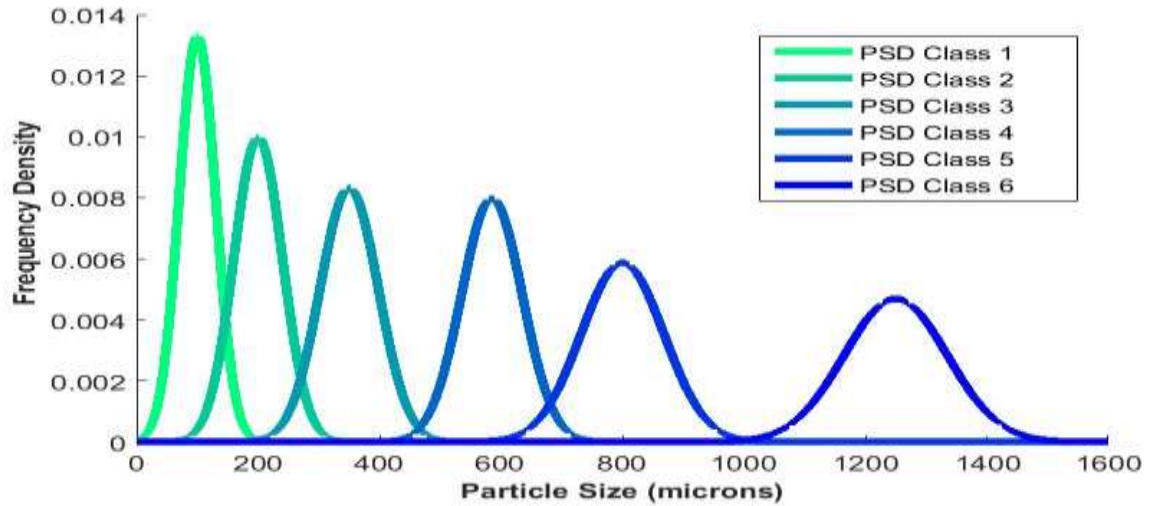
Figure 13: PSD classification used for the sludge bed models. This figure shows that in the sludge bed model used in this study, the mean particle size at any given location ranges up to 1500 micrometres.

The choice of size range, size classes and the number of classes can be modified to model any sludge bed model and should not be restricted to the choice of this research. In essence, such classifications should be designed to suit the purpose for which the sludge characterisation is needed. If the entire range of particle sizes can be approximated as belonging to a single class, then it may be said that the pond is simply homogeneous. Alternatively, if the purpose for which the results are to be applied is sensitive to PSD sizes, then the population may have to be put into several small classes. The more the classes, the more heterogeneous the population appears to be.

The spatial distribution of the various PSD classes in a sludge bed can be influenced by either natural or man-made activities. Examples of natural activities of influence include underwater current, rainfall and wind as these affect the movement of waste into and around the storage pond. Similarly,

human-made activities of influence include the deliberate deposit of certain waste materials in large quantities at specific locations of the pond.

The dominance of natural or human-made activities of influence will result in either of two scenarios. In the first scenario, the PSD map will exhibit continuity at inter-class borders (spatial autocorrelation). By implication, the transition of sludge characteristics from one PSD class to another across borders will be gradual. This is evidenced in a number of reported studies [139] [140]. In one of the studies [140] for example, the regional pattern of the mean particle size of sea-floor samples was used to infer the speed of bottom-current.

In the second scenario, the PSD map will be characterized by immediate transitions across inter-class borders [141]. This scenario may be considered as the worst-case scenario as there could be no predictable pattern in the spatial distribution of PSD across the map.

In modelling a heterogeneous PSD topography of the 3D sludge bed, there are four possible spatial configurations. These configurations depend on the presence or absence of Spatial Auto-Correlation (SAC) of PSD along the horizontal or vertical direction. $\boldsymbol{HSAC}$ and $\overline{\boldsymbol{HSAC}}$ represent the presence and absence of Horizontal Spatial Auto-Correlation respectively while $\boldsymbol{VSAC}$ and $\overline{\boldsymbol{VSAC}}$ represent the presence and absence of Vertical Spatial Auto-Correlation in the PSD topography.

The sludge bed is produced by developing a three dimensional matrix of size $200 \times 100 \times 10$ to represent the $100 \text{ m} \times 50 \text{ m} \times 5 \text{ m}$ size of a nominal sludge bed. By implication, each element in the matrix represents the mean particle size data of a $2 \text{ m} \times 2 \text{ m} \times 2 \text{ m}$ voxel. Each element in the three-dimensional matrix is any of 1, 2, 3, 4, 5 or 6. This number corresponds to the mean PSD class which is found in that coordinate of the sludge bed.

The mean PSD class 1 to 6 is shown in Figure 13. It is based on the understanding that several numbers of sludge samples can be retrieved from a given voxel with each having different mean PSD values. However, the distribution of the mean PSD obtainable from within a voxel will follow a

normal distribution. This distribution is either classed as PSD class 1, 2, 3, 4, 5 or 6.

In modelling a sludge bed therefore, an algorithm was developed (see MATLAB code in Appendix B) to randomly generate the overall PSD mean for each pixel. This algorithm ensured that any PSD mean falls within the range of class values 1 to 6. In allocating PSD mean values (and the corresponding PSD class values) to pixels, the algorithm ensured that there was either a gradual spatial progression of PSD mean along the horizontal or vertical plane, or that the distribution was random. This is what results in the presence or absence of spatial autocorrelation in a sludge bed model.

The four models, Beds 1 to 4 are as shown in Figure 14 (a) to (d) respectively. The colours and PSD of each voxel on the maps correspond to the colours and their corresponding PSD class (1 to 6) as provided in Figure 13.

(a) **Bed 1** $\overline{HSAC}\,VSAC$ (b) **Bed 2** $HSAC\;VSAC$
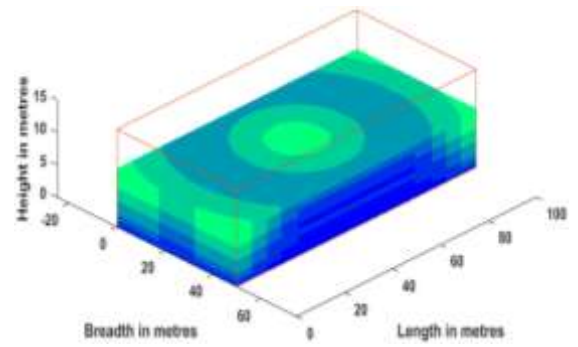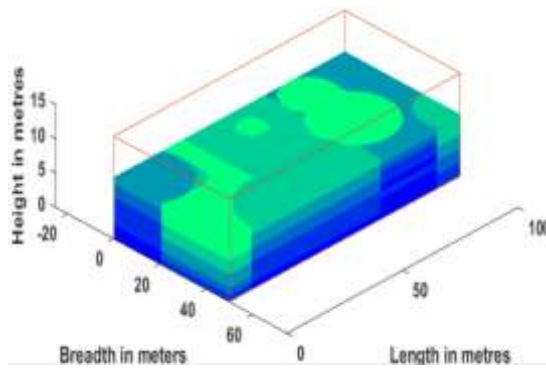
(c) **Bed 3** $\overline{HSAC}\,\overline{VSAC}$ (d) **Bed 4** $HSAC\,\overline{VSAC}$
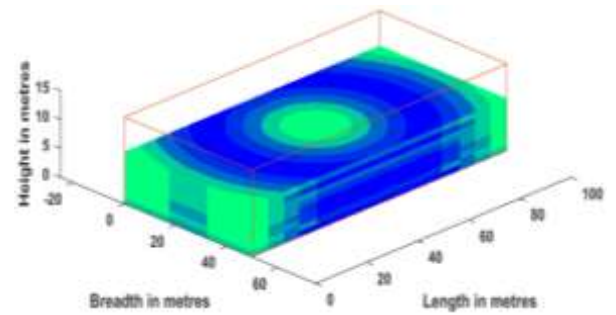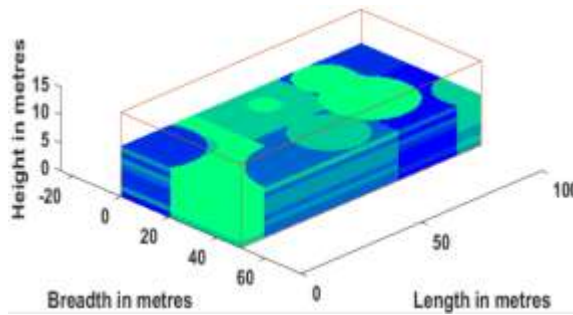
Figure 14: Map showing the spatial distribution of the Particle Size Distribution (PSD) classes in Sludge Bed Models. These picture shows a three dimensional schematic representation of a sludge bed with the different colours indicating the various classes to which the mean particle size found in a given are belongs to.

Figure 14 (c) depicts a scenario for Sludge Bed 3 wherein there exists no spatial autocorrelation along both the vertical and horizontal cross-section of the sludge population. This may be considered the worst-case scenario for a heterogeneous PSD topography. Hence, this research places emphasis on results concerning Bed 3. The patterns of spatial distribution of PSD classes used in the four sludge bed models have not been generated from real-world data.

It is important to note that even in the absence of spatial autocorrelation, it would be noticed that a given number of voxels would fall within the same PSD class value. This is because of the broad range of PSD mean values that define each PSD class.

3.4 Experimental Factors Related to Sludge Sampling

An algorithm was implemented in MATLAB which simulated the process of retrieving and analysing the sludge samples. The input to the sampling algorithm includes the number of sampled locations (Factor A), the sampling strategy (Factor B), the penetration depth (Factor C) and the bias (Factor D) of the sampling device. This allows for variations in sampling procedure and for observation of the outcome. For each of the factors under investigation, two settings are chosen − A high, and a LOW setting as shown in Table 4.

Table 4: A summary of sampling factors and settings tested in the 2k ANOVA

Factor	Description	Low Setting	High Setting
A	Number of Sampled Locations	8 (0.04 % sampling intensity)	200 (1 % sampling intensity)
B	Sampling Strategy	Simple Random	Stratified Random
C	Penetration Depth of Sampler	10% of sludge depth	100% of sludge depth
D	Particle Size Bias of Sampler	Collects only particles that are less than 400 microns	Collects all sizes of particle
OTHER FACTORS CONSIDERED			
Sludge bed topography	Bed 1 $\overline{HSAC}\ VSAC$	Bed 2 $HSAC\ VSAC$	Bed 3 $\overline{HSAC}\ \overline{VSAC}$	Bed 4 $HSAC\ \overline{VSAC}$

A sample number of eight was chosen as the low setting for Factor A because this is a practical setting that is achievable in the real world. While retrieving only 8 samples may not yield an accurate characterisation result unlike the

high setting 200, it is a more practicable choice in a real hazardous environment. This is based on historical sampling campaigns undertaken at Sellafield. This pair therefore offers an opportunity to switch from a low to a high setting of Factor A and to study the effect that this has on result variations and confidence.

For Factor B, the low and high settings chosen are the 'simple random' and the 'stratified random' sampling strategy. This is based on the merits and demerits of both strategies discussed in Chapter 2.

In regards to the penetration depth of a sampling device, the collection of sludge sampling can either be implemented by shallow sampling or by core sampling. Hence, the low and high settings for Factor C are chosen to be 10 % penetration depth and 100 % penetration depth, respectively. By using such a low setting, only the sludge population within the top-most voxel (a three-dimensional pixel) of the bed is available for sampling. The high setting however enables the sampling of sludge at various depths of considerable intervals of a given sampling location.

With regards to the bias of the sampling device, the chosen low setting represents the use of a device which only has the ability to collect only particles that have a diameter less than or equal to 400 μm. This is a low setting in the sludge bed model which is designed to contain particles sizes up to 1500 μm. The use of a syringe sampler having a nozzle of diameter 4 mm in a pond where the maximum particle size is actually 15 mm is a practical example of a low setting for Factor D. A high setting which may not be practicable is the use of an unbiased fit-for-all-purpose sampling device which can collect and retain all the particles in the sampled area.

3.5   Analysis of Simulation Results

3.5.1   2k Factorial Analysis of Variance (ANOVA)

To evaluate the effect of the experimental Factors A, B, C and D on variations in results, a statistical tool known as the 2^k Factorial Analysis of Variance (ANOVA) [36] can be used. This method involves the

implementation of a number of unique sampling configurations (also referred to as treatments). Each configuration is also further repeated a number of times to observe the effect of random errors on result variation.

A sampling configuration refers to the unique combination of 'low' or 'high' setting of each factor. A list of all unique configurations can be made by representing 'high' and 'low' by digits '1' and '0' respectively. For a set of four factors under investigation therefore, there are 16 unique configurations listed as 0000 to 1111. Generally, the total number of unique sampling configurations for a set of k factors is 2^k.

The result of implementing any sampling configuration is observed by comparing the characterisation map generated to the model of the sludge bed. This result can be further quantified by calculating the accuracy of the generated map. This accuracy is obtained using the method of confusion matrix [51, 129].

Sub-chapters 3.5.2 to 3.5.6 describe the methods by which the following can be achieved:
- The generation a characterisation map from available sampled data.
- The estimation of the accuracy of a characterisation map.
- Statistical evaluation of how experimental factors A, B, C and D influence map accuracies.

3.5.2 Spatial Extrapolation Algorithm for Map Generation

The development of a three-dimensional sludge PSD characterization map involves the inference of sludge PSD characteristics at non-sampled positions of the sludge bed. To achieve this, spatial extrapolation is performed by analysing the PSD measurements collected at each of the sampled positions. A general equation [142] for spatial extrapolation is provided by Equation (3)

.

$$\tag{3}$$

$$Z_k = \sum_{j=1}^{n} \lambda_{jk} Z_j$$

Where Z_k is the inferred PSD data at any non-sampled position k, Z_j is the observed PSD data at sampled position j, n is the total number of sampled positions available and λ_{jk} is the weighting factor of the contribution of the any measurement from a sampled position j to the inferred measurement at a non-sampled position k.

Two standard methods of calculating the weighting factor, λ_{jk}, are the deterministic and the geostatistical methods [131]. An example of a deterministic method is the Triangular Delaunay Algorithm (TDA), where λ_{jk} is dependent on the proximity of the position j to the position k [9]. In this method, given a set J of all sampled positions j, let $\{\alpha, \beta, \gamma\} \subset J$ be the vertices of the nearest triangular enclosure around a non-sampled position k as shown in Figure 15.
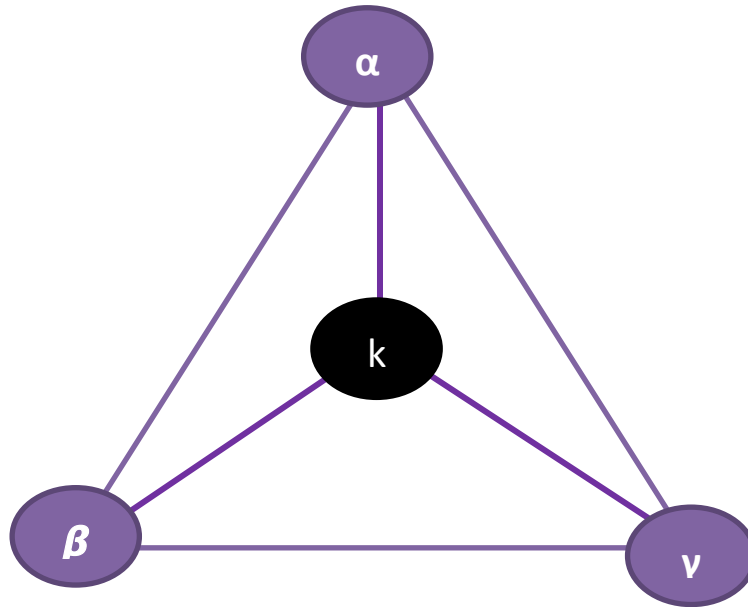
Figure 15: Nearest triangular enclosure around a non-sampled position k. This figure provides a diagrammatic representation of the method of the Triangular Delaunay Algorithm used to infer data at a non-sampled location based on the data from the three nearest sampled locations.

Equation (4) [138] provides a method for calculating λ_{jk}.

$$\begin{pmatrix} \lambda_{\alpha k} \\ \lambda_{\beta k} \\ \lambda_{\gamma k} \end{pmatrix} = \begin{pmatrix} A_{\beta\gamma k} \\ A_{\alpha\gamma k} \\ A_{\alpha\beta k} \end{pmatrix} / A_{\alpha\beta\gamma} \qquad (4)$$

$\lambda_{jk} = 0$, for all $j \notin \{\alpha, \beta, \gamma\}$

Where A represents the area of a triangle. For example A_{123} refers to the area of a triangle with vertices at positions 1, 2 and 3. This can be calculated using available mathematical techniques where the position vectors of the three vertices are known.

The Ordinary Kriging Algorithm (OKA) [134] is an example of a geostatistical method. In this method, a spatial autocorrelation tool known as a variogram is used in the calculation of λ_{jk} [132]. The variogram is a plot of covariance between all possible pairs of sampled data against their proximity. An example of a variogram is as shown in Figure 16 [143]. This method is considered most suitable for populations where spatial autocorrelation is suspected [130].
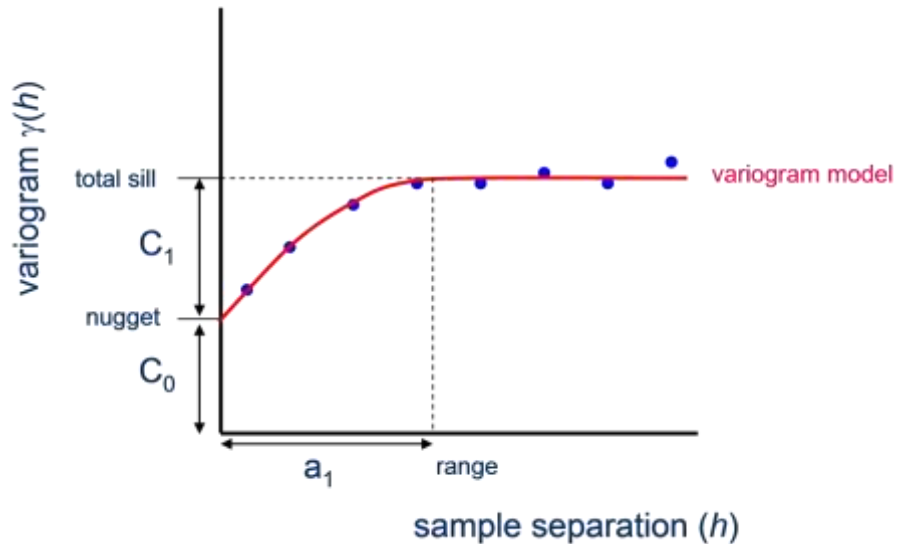
Figure 16: An example of a variogram, typically obtained as a line of best fit on a scatter diagram of sampled data variance against spatial distance across samples.

From the variogram, the peak co-variance between sampled data points, known as the sill ($\sigma_o{}^2$) and the distance at which this occurs, known as the range (a) are obtained. These are parameters that are known to characterize the spatial dependence of the data. Based on the variogram plot observed, a suitable variogram model is adopted for estimating the co-variance matrix element v_{jk} between any two positions j and k. Equations (5) and (6) respectively, may then be applied to calculate λ_{jk} [138].

$$v_{jk} = \sigma_o{}^2\, e^{-\frac{3}{a}|h_{jk}|} \tag{5}$$

$$
\begin{pmatrix} \lambda_{1k} \\ \vdots \\ \lambda_{jk} \\ \vdots \\ \lambda_{nk} \\ \mu_k \end{pmatrix}
=
\begin{pmatrix}
v_{11} & \cdots & v_{1n} & 1 \\
\vdots & \ddots & \vdots & 1 \\
v_{j1} & v_{jj} & v_{jn} & 1 \\
\vdots & \ddots & \vdots & 1 \\
v_{n1} & \cdots & v_{nn} & 1 \\
1 & \cdots & 1 & 0
\end{pmatrix}^{-1}
\begin{pmatrix} v_{1k} \\ \vdots \\ v_{jk} \\ \vdots \\ v_{nk} \\ 1 \end{pmatrix}
\tag{6}
$$

Where h_{jk} is the distance between two positions j and k.

The Triangular Delaunay Algorithm (TDA) and the Ordinary Kriging Algorithm (OKA) techniques have been selected to represent the deterministic and geostatistical methods respectively. Both techniques are compared in order to determine which method is appropriate for the given case study. Although it is generally suggested [129, 131] that geostatistical methods such as OKA are particularly relevant in the presence of spatial autocorrelation.

However, OKA is dependent on the choice of variogram model used [66]. In addition, the suitability of an OKA method to a population which has a significant presence of spatial autocorrelation depends on the accuracy of the variogram plot. The accuracy of any variogram is also dependent on how adequate and representative the collected samples are. The implication of this is that while it is generally expected that OKA should produce a more accurate spatial extrapolation in the presence of spatial autocorrelation, such

performance may be limited by sampling intensity and sampling strategy factors.

Linear regression based methods may even be more accurate [136] in the presence of spatial autocorrelation. It is therefore important to compare the performance of OKA and TDA in the presence and absence of spatial autocorrelation under certain experimental conditions.

For example, a study [144] compared the performance of four different spatial extrapolation methods in a complex terrain different from the expected spatially continuous surfaces. It was found that OKA performed poorly due to the absence of spatial autocorrelation, while the method involving linear regression proved to be more appropriate under this condition.

However, the use of the OKA technique is common in geological and ecological related studies. This is because of the general expectation of the existence of spatial autocorrelation. Recent examples of the usage of OKA can be found in [145], [146] and [147]. The similarity in these three studies is the existence of spatial autocorrelation within the population under study.

The general expectation is therefore that a method such as the OKA is most appropriate in the presence of special autocorrelation. It is similarly expected that TDA is most appropriate in the absence of spatial autocorrelation. This research is however concerned about the usage of either of this two methods for conducing spatial extrapolation on an unknown population where such knowledge of the existence of spatial autocorrelation is lacking. By determining the significant performance of the TDA in the presence of spatial autocorrelation, and comparing that to the performance of OKA in the absence of spatial autocorrelation, a suitable choice would be made.

3.5.3   Estimating Map Accuracy using Confusion Matrix

In modelling and simulation studies, the ground-truth map (T) of the sludge bed model is known. Therefore, when an inference map (P) is generated, both the inferred and the ground-truth data can be compared to assess the performance of both the sampling method and the inference algorithm used.

One method of achieving this is by observing the ratio of the number of correct inferences made to that of incorrect inferences. This involves the use of a confusion matrix [51].

A confusion matrix CM is a matrix that classifies as either TRUE or FALSE the agreement of each voxel on map P with its corresponding voxel on map T. The accuracy of the map is considered to be equal to the proportion of the total number of correct inferences to the total number of inferences made. The confusion matrix therefore provides information about the total number of inferences that are true or false for each of the classes of PSD.

Figure 17 gives a basic illustration of how a confusion matrix is obtained. The map accuracy as obtained by method of confusion matrix is considered to be equal to the proportion of the total number of correct inferences to the total number of inferences made. It is calculated using Equation (7). Where tr is the sum of the diagonals of a given matrix and $cm_{b,c}$ refers to an element of the confusion matrix CM located on row b and column c.

$$Map\ Accuracy = \frac{\text{tr}(CM)}{\sum_{c=1}\sum_{b=1} cm_{b,c}} \qquad (7)$$
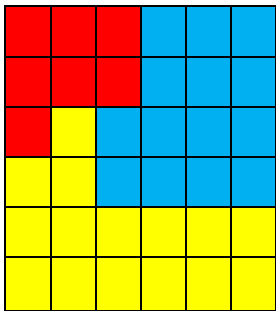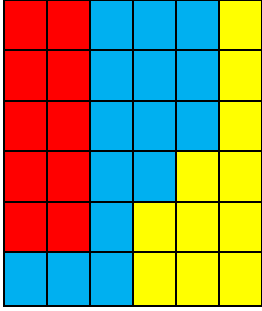
GROUND TRUTH MAP	INFERRED MAP	CONFUSION MATRIX			
			Inferred Red	Inferred Blue	Inferred Yellow	**TOTAL**
		Truly Red	5	2	0	7
		Truly Blue	0	9	5	14
		Truly Yellow	5	4	6	15
		TOTAL	10	15	11	**36**

Figure 17: An illustration of a confusion matrix. This figure is an example of the application of confusion matrix. The confusion matrix is a statistical method of determining the percentage agreement between any two maps.

From the illustration shown in Figure 17, the map accuracy is given by:

$$Map\ Accuracy\ =\ \frac{5+9+6}{36}\ x\ 100\ \%\ =\ 55.56\ \%$$

An inference map accuracy of 55.56 % implies that on average, in every 100 inferences made, approximately 56 of them were correct.

Understandably, this method of evaluating map accuracy is not feasible in real applications where the ground-truth map remains unknown. In such situations, alternative methods for assessing the performance are discussed in Chapter 4.

Furthermore, the results of all sampling runs and their corresponding sampling configurations can be analysed using statistical tools such as the F-ratio statistics, P-value, Half-normal plot of effects and the eta squared effects. These tools are used in evaluating the influence of each experimental factor. They also detect the presence of interactions (interdependence) among factors. Factor interactions indicate the interdependencies amongst interacting factors. This implies that the influence of one of the interacting factors on result variability depends on the set value of the other interacting factors. For example, supposing the interaction between Factors B and A (represented as BA) is observed to have significant influence on result variability, this would imply that the effect of varying either factor A or B may or may not be significant enough to cause result variability. The significance would depend on the current setting of its interdependent factor.

3.5.4   The F-ratio Statistic and Probability (P) Values

For each experimental factor, the entire set of results obtained from a 2^k ANOVA experiment can be divided into two equal sets: the 'group 0' and 'group 1' sets. 'Group 0' is a set of results obtained from all ANOVA experiments in which the given experimental factor was set to its LOW setting. While the 'group 1' is a set of results obtained from all ANOVA

experiments in which the given experimental factor was set to its HIGH setting.

Similarly for analysing interactions that exist among μ number of factors, the entire set of results obtained from the 2^k ANOVA experiment can be divided into 2^μ equal sets. For example, to analyse the F-ratio of the interaction between two experimental factors, ANOVA results will be divided into the following groups: 'group 00', 'group 01', 'group 10' and 'group 11'.

The F-ratio of any factor or interaction is the ratio of the mean squared error between the groups ($MS_{between}$) to the mean squared error within the groups (MS_{within}) [148]. An F-ratio greater than 1 implies that the variation due to a change in the settings of that factor is greater than the variation which could have occurred by chance. While an F-Ratio value close to or less than 1 implies that a change in the settings of that factor has no significant influence on the variability of the result [149].

Nonetheless, the significance of any F-ratio needs to be examined. This can be achieved by obtaining a Probability (P) value. This represents the probability that the F-ratio may be false and misleading, thus an indication of the risk of a type I error [150] in which an F-ratio may have occurred by chance. It is therefore desirable to have a Probability (P) value to be less than 0.05, an acceptable risk benchmark corresponding to a 95 % confidence in rejecting a null hypothesis. By rejecting a null hypothesis, it can then be held that a factor has a significant influence on result variability.

3.5.5 The Half Normal Plot of Effects and Interactions

Following the completion of an ANOVA, a half normal plot of effect provides a graphical indication of the significance of the influence of all the factors and interactions on result variation [151, 152]. The construction of a half normal plot involves the calculation of the effect of each factor or interaction using Equation (8) [153]. The absolute values of the calculated effects are then ordered from smallest to largest and are assigned values i, (where $i = 1, 2, ..., 2^k - 1$). This list is used in obtaining a corresponding list

of theoretical half-normal probability Q_{th} values using Equation (9), also known as Blom's proportions [154, 155].

$$Factor\ Effect\ =\ Y_+ - Y_-$$ (8)

Where Y_+ and Y_- denotes the average of the result of "group 1" and "group 0" for which the factor takes on a "high" or a "low" setting respectively. In the case of factor interactions, there will be more groups as explained in the subchapter 3.5.4.

$$Q_{th}(i)\ =\ 0.5\ +\ \frac{i - 0.055}{2(2^k - 1) + 1.2}$$ (9)

The half normal plot of effect is then produced as a scatter plot of the magnitudes of these effects against the theoretical probability values. A line of best fit can be drawn for low ranking factors and interactions. A number of factors and interactions may be observed to deviate from this line. For any factor or interaction, the degree of deviation from the drawn line provides a qualitative assessment of the influence of such factor or interaction on result variation, uncertainty and confidence [156, 157].

3.5.6 The Eta-Squared Effects

The eta-squared effect η^2 is a useful tool for quantifying the actual influence of any factor or factor interactions [158]. Similar to the eta squared effect value are the partial eta squared effect, the omega squared effect and the epsilon squared effect values [158] which have their advantages and disadvantages. The eta-squared effect value η^2 is defined by Equation (10). Where $SS_{between}$ is the sum square between groups in factor i and SS_{total} is the total of all sum squares in the ANOVA.

$$\eta_i^2 = \frac{SS_{between}}{SS_{total}}$$ (10)

The eta-squared effect for all influence factors, factor interactions and the residual (unexplained) error indicates their proportional contributions to the overall uncertainty.

3.6 Results and Discussions

3.6.1 Ordinary Kriging versus Triangular Delaunay Spatial Extrapolation Algorithm

Firstly, in order to select a suitable extrapolation algorithm, the accuracies of the inferred maps from both Ordinary Kriging (Kriging) and Triangular Delaunay (Nearest) algorithms were compared. An attempt to run the 3D Kriging algorithm simulation using up to 100 % depth of penetration or a number of samples collected greater than 200 could not yield a timely response. Hence, this comparison was made over different bed models (Beds 1 to 4), and using stratified sampling strategy, 30% depth of sampler's penetration and no particle size bias of sampler as factorial settings while varying the number of samples collected from 2 to 200.

Figure 18: Kriging versus Delaunay (nearest) - for Bed 1 ($\overline{HSAC}\ VSAC$). In this figure, the sludge bed model has spatial auto-correlation only along the vertical. This data was obtained by simulation.
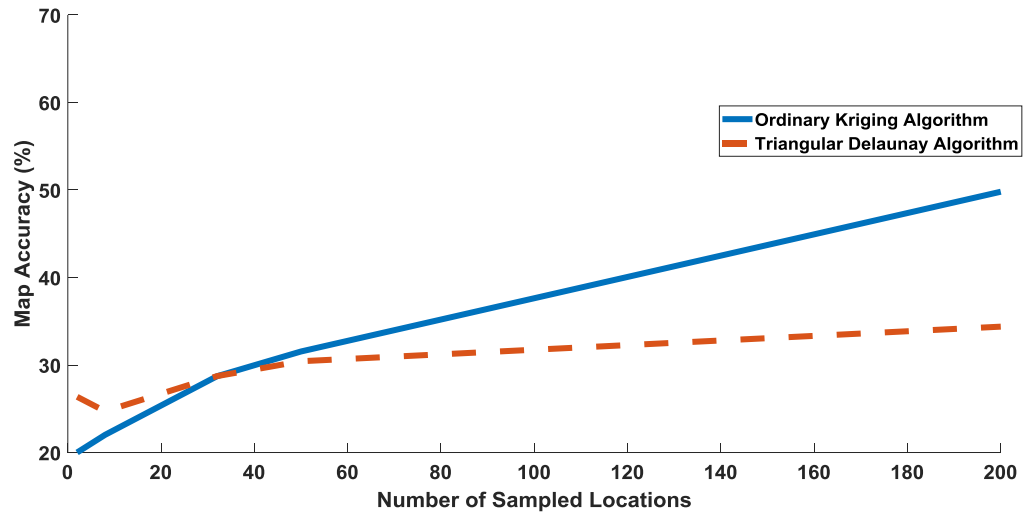
Figure 19: Kriging versus Delaunay (nearest) - for Bed 2 ($HSAC\,VSAC$). In this figure, the sludge bed model has spatial auto-correlation along the horizontal and vertical. This data was obtained by simulation.
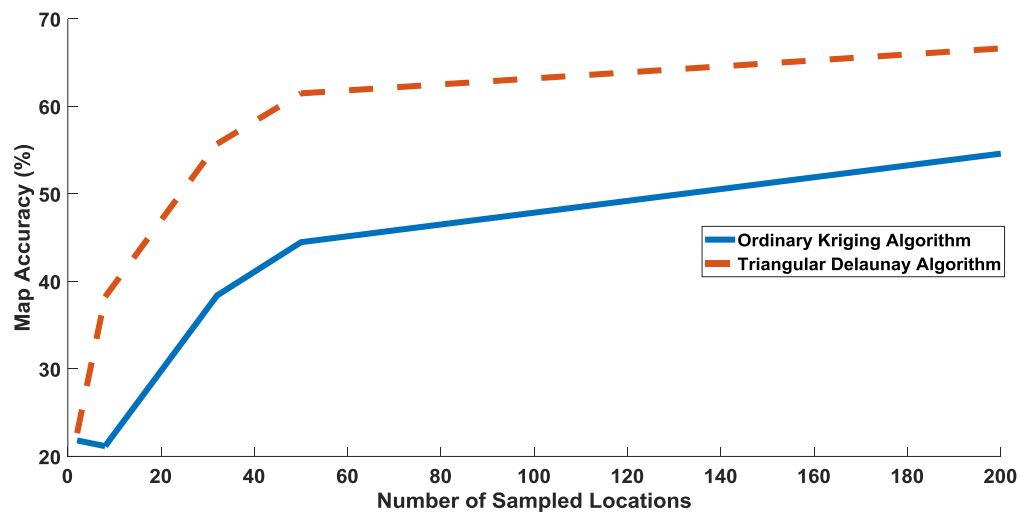
Figure 20: Kriging versus Delaunay (nearest) - for Bed 3 ($\overline{HSAC}\,\overline{VSAC}$). In this figure, the sludge bed model no spatial auto-correlation along the horizontal or vertical. This data was obtained by simulation..
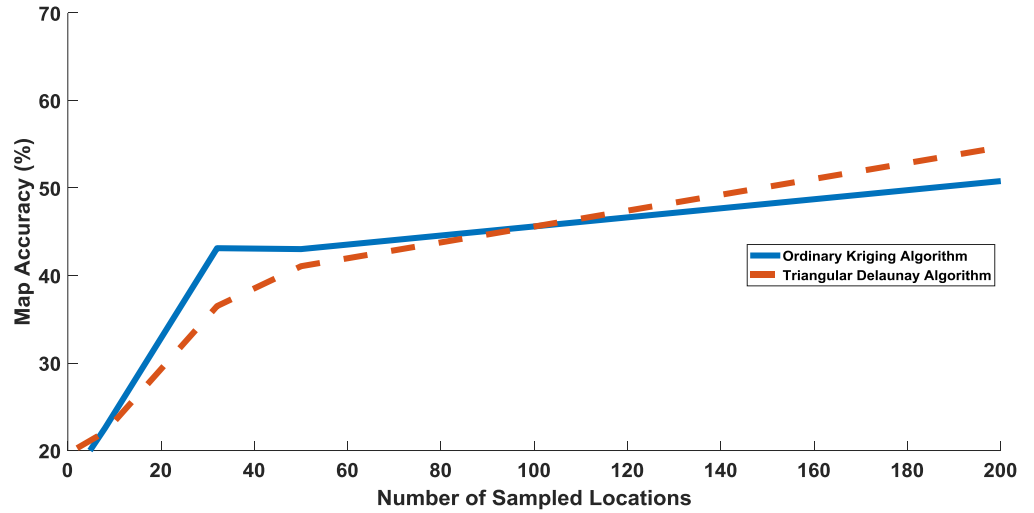
Figure 21: Kriging versus Delaunay (nearest) - for Bed 4 ($HSAC\ \overline{VSAC}$). In this figure, the sludge bed model has spatial auto-correlation only along the horizontal. This data was obtained by simulation.

Figure 22 shows the result from Bed 3 of TDA prediction accuracy as number of sampled locations and depth of penetration increased.
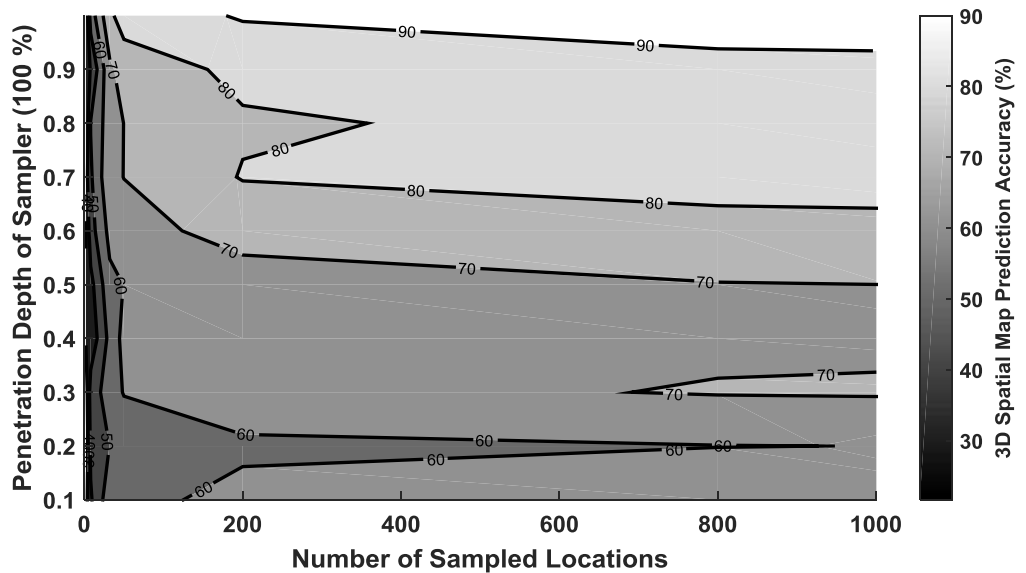
Figure 22: Map Accuracy against Number of Sampled Locations and Penetration Depth of the Sampling Device for Bed 3. The darker contours correspond with regions on the graph where accuracy is low

Discussion

The graphs in Figure 18 to Figure 21 shows the behaviour of OKA and TDA (nearest) as spatial auto-correlation (SAC) becomes present or absent either along the horizontal or vertical. Figure 18 shows that in Bed 1 ($\overline{HSAC}\ VSAC$) where only vertical SAC exists, TDA is more accurate than OKA when the number of sampled locations is below 85 (about 0.4 % sampling intensity). With an increase in number of sampled location, OKA can be seen to become more accurate than TDA. Figure 21 shows that in the case in Bed 4 ($HSAC\ \overline{VSAC}$) where only horizontal SAC exists, OKA only performs better than TDA when the number of sampled locations is set between 5 and 100.

Figure 19 and Figure 20 represent the best and worst case scenario of PSD topography as represented by Bed 2 ($HSAC\ VSAC$) and Bed 3 ($\overline{HSAC}\ \overline{VSAC}$) respectively. While Figure 20 shows that OKA works increasingly better than TDA for Bed 2 (when SAC exists in along all directions), TDA gives about 15 % higher map accuracy compared to OKA in Bed 3 ($\overline{HSAC}\ \overline{VSAC}$). It can therefore be concluded based on the performance of TDA in Bed 3 ($\overline{HSAC}\ \overline{VSAC}$) that in the case of an unknown PSD topography, TDA is the more suitable method.

Furthermore, TDA (nearest) proved to be a faster algorithm as it required an average data processing time of 10 seconds while OKA took from 50 seconds to 5 minutes data processing time. As sampled data increased even further particularly by increasing penetration depth to 30 % of sludge depth, OKA became almost non-responsive as it kept running one analysis for over 48 hours and had to be terminated. This is because the OKA involves matrix inversion. The size of the matrix is dependent on the number of sampled data available. An attempt to invert very large sized matrixes may result in singularity problem, hence the need to adopt the pseudo inverse approach which makes the process more time consuming. TDA (nearest) algorithm on the other hand involves computational logic and thus, faster.

From Figure 22, it can be seen that 3D map inference accuracy increases with penetration depth and number of sampled locations. This provides an understanding of how both factors interact in order to improve map accuracy.

3.6.2 ANOVA RESULTS: F-Ratio Statistics and P Values

Figure 23 and Figure 24 show the result of an ANOVA test carried out on experimental factors A, B, C and D. The interaction amongst a number of factors is represented by a combination of their names. For example, BA represents the interaction between Factors B and A. Other examples include CBA and DCBA. F and P represent the values obtained for the F-Ratio statistics and the Probability values, respectively. These results are also depicted in Table A1 (see Appendix A), respectively.
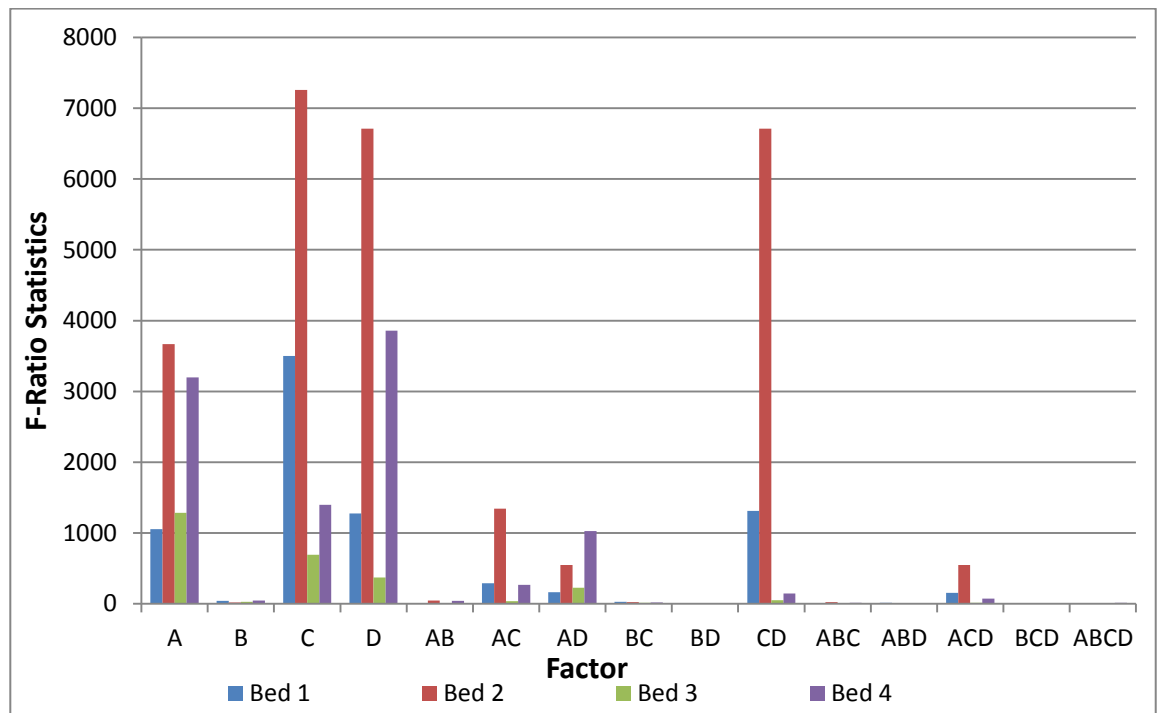
Figure 23: Chart Showing F-Ratio Statistics for all factors on all bed models. This chart provides the result for the four configurations of sludge bed models as represented by the different colours.
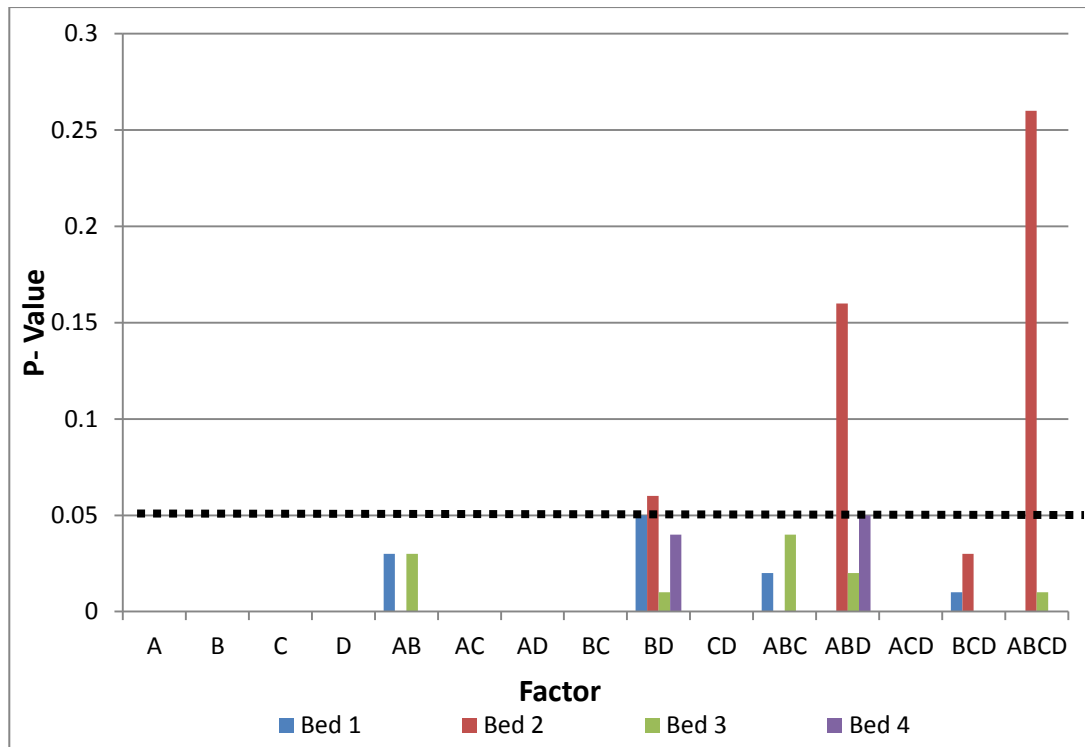
Figure 24: Chart Showing P-Values for all factors on all bed models. **This chart provides the result for the four configurations of sludge bed models as represented by the different colours.**

Discussion

The F-Statistic value obtained from an ANOVA test indicates how influential a factor is to result variation. Any factor with an F-Statistic value greater than 1 is understood to have a significant degree of influence. This implies that where a factor is known to be of significance, any attempt to change its settings from the high to the low or vice versa will cause the entire result to vary. On the other hand, the Probability value represents the probability that the F-statistic may be false and misleading, thus an indication that the null hypothesis is true. Note that the null hypothesis simply says that a factor has no significant influence on result variability.

It is therefore desired for the Probability value to be less than the adopted risk factor, usually 0.05 for a 95 % result confidence for one to conveniently set aside the null hypothesis. This is achieved by increasing the number of runs for each treatment. The result used in this ANOVA test is the TDA (Nearest)

map prediction accuracy obtained from all sampling procedure treatments as required by ANOVA.

It can be seen from Figure 23 that the F-ratio statistics of the four main factors A, B, C and D are greater than 1 in all of the four sludge bed models. This confirms the expectation that the four identified experimental factors involved in sludge sampling do contribute to result variability. However, Factor A and B having the highest and lowest value, respectively, is an indication of the strength of their influence. All the F-ratio statistics recorded were satisfactorily valid because their Probability values were below 0.05.

The presence of factor interactions was also observed. This may be ignored where the F-ratio statistics are relatively insignificant compared to the main factors. Nonetheless, for strong interactions such as 'AD', a further ANOVA test involving only Factors A and D may be required before any interpretation may be given. In other cases, theoretical explanations are available. For example, Factors A and C are both factors which contribute to the overall number of sludge samples collected, hence the presence of a strong interaction AC is as expected. This is also similarly in the case of Factors C and D which are both factors related to the choice of any sampling device.

3.6.3   Half Normal Plot of Effects

For a graphical interpretation of the ANOVA results, the Half-Normal Plot of effects could be relied on.

The red dots belong to the four experimental factors (A, B, C and D) and their interactions (such as BA, CB, DA, DBA, CBA, DCBA) and represent the actual positions of their effects. The straight blue dotted line represents the expected half-normal plot of effects when all effects are insignificant. The distance of a red dot from the blue straight line therefore indicates the significance of such effect [157]. The blue straight line is a line of best fit of the ten lowest effect sizes (not seen in the abridged figures) obtained using Matlab functions *polyfit* and *polyval*.
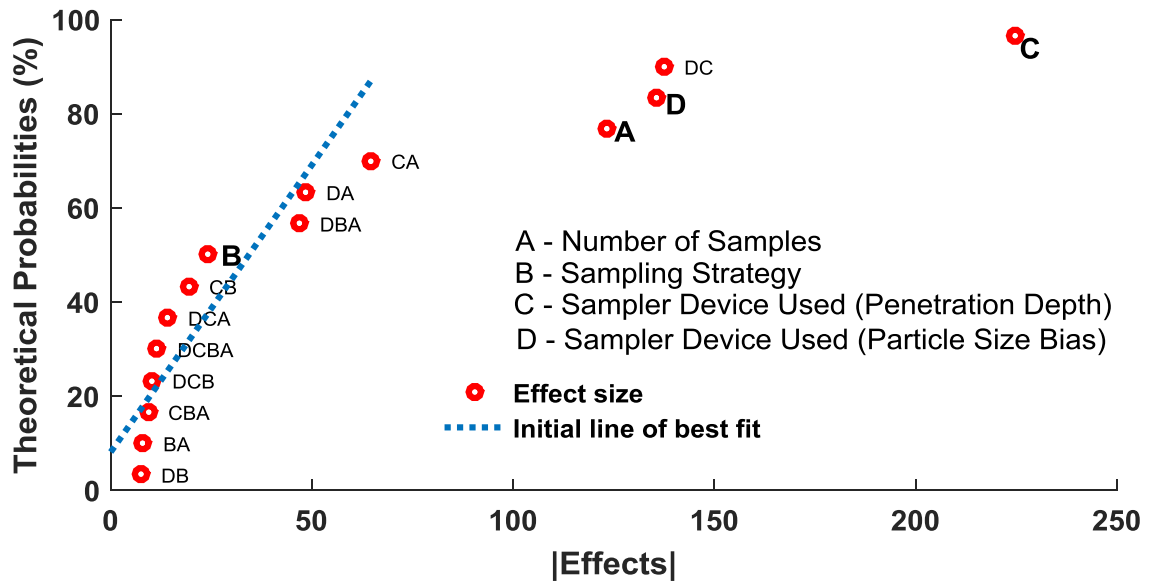
Figure 25: Half normal plot of effects - Bed 1. This is a pictorial representation of the ANOVA Results. It indicates how significant a main factor or factor interaction is to the variation of the result of an inferred map. The result depicted in this figure pertains to sludge bed model 1
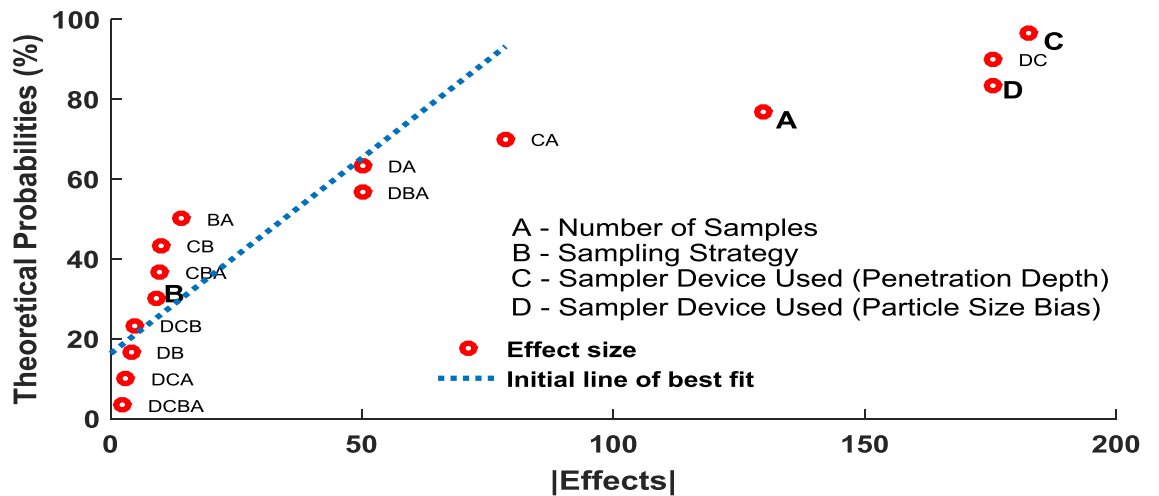
Figure 26: Half normal plot of effects - Bed 2. This is a pictorial representation of the ANOVA Results. It indicates how significant a main factor or factor interaction is to the variation of the result of an inferred map. The result depicted in this figure pertains to sludge bed model 2.
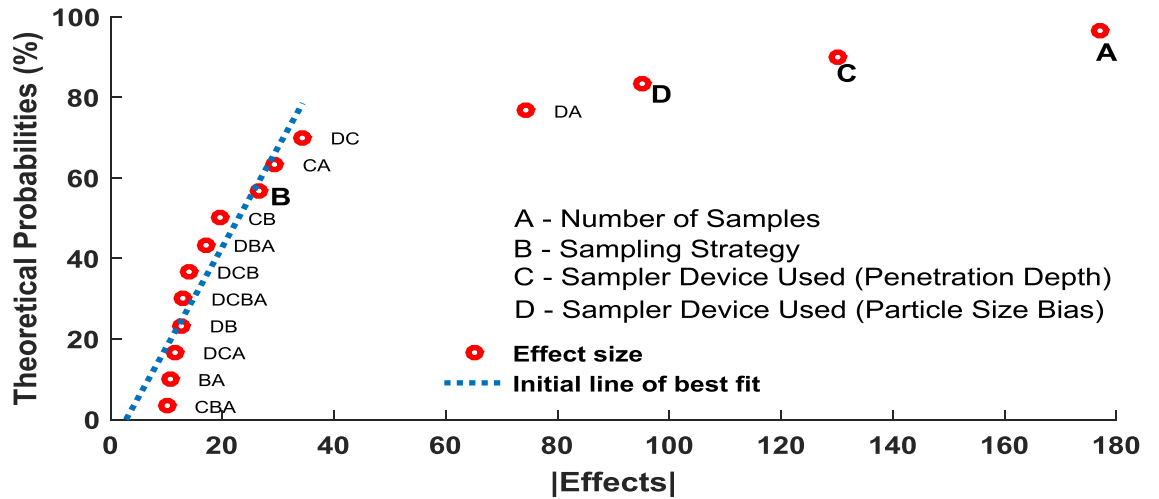
Figure 27: Half normal plot of effects - Bed 3. This is a pictorial representation of the ANOVA Results. It indicates how significant a main factor or factor interaction is to the variation of the result of an inferred map. The result depicted in this figure pertains to sludge bed model 3.
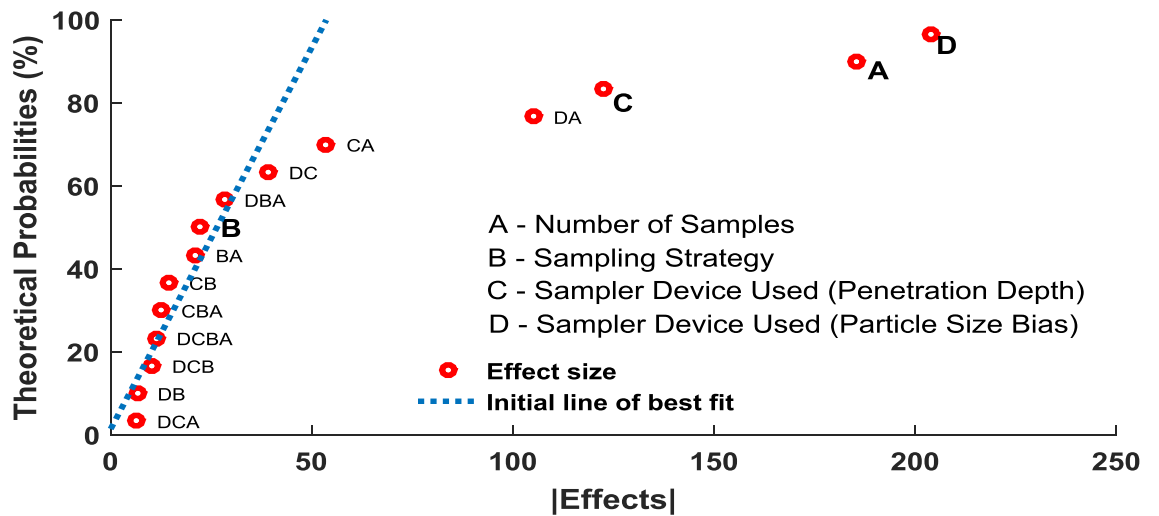
Figure 28: Half normal plot of effects - Bed 4 This is a pictorial representation of the ANOVA Results. It indicates how significant a main factor or factor interaction is to the variation of the result of an inferred map. The result depicted in this figure pertains to sludge bed model 4.

Discussion

The half-normal plots of effect shown in Figure 25 to Figure 28 further confirm the relative significance of factors and their interactions on result variability. The blue dotted line shows the path which effect sizes ought to follow if they were normally distributed. The red dots however represent the actual effect sizes observed. Any red dot that deviates from the blue dotted line is considered to have significant influence on variability. These plots are therefore a pictorial description of the results in the ANOVA.

It can be seen from the figures that Factors A, C and D showed significant deviations from the normal path (represented by the blue dotted line) with Factor A being most significant factor for sludge Bed 3. It is clear from the figure that Factor B (sampling strategy) appears to be the least significant factor for all four sludge bed models. It must be noted that Factor B still remains a significant factor of influence, except that its influence is overshadowed by that of the other three factors and their interactions.

3.6.4 Eta-Squared Effect of Factors and Interactions

Having observed the qualitative significance of all factors and interactions, it is useful to quantify their contributions to overall result variation. The eta-squared effect has been earlier described as the tool required for such evaluation. Figure 29 shows the percentage contribution of each factor and interaction to result variation.
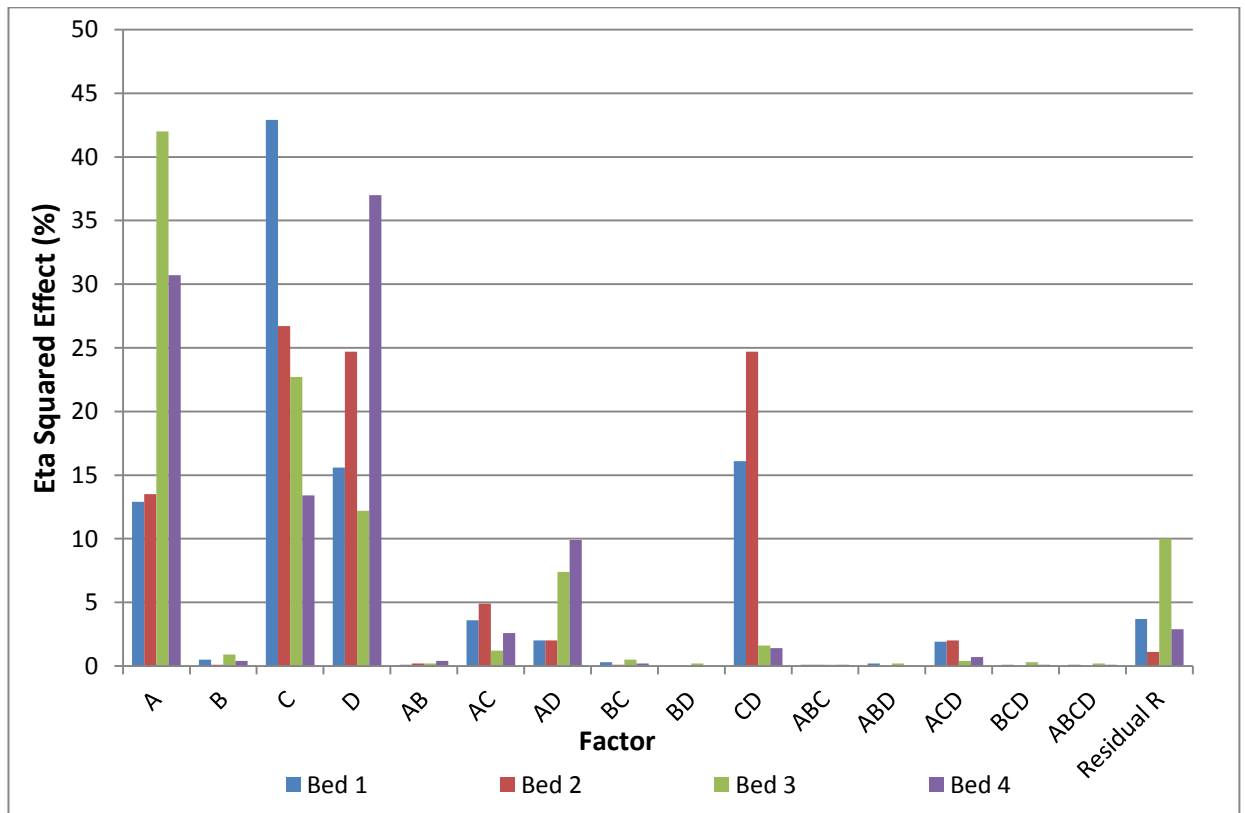
Figure 29: Bar Chart showing Eta-Squared Effects for all bed models. This chart shows the percentage contribution **of each of the four experimental factors related to sludge sampling and their interactions to the variation of the inferred map produced from any given sludge characterisation exercise.**

<u>Discussion</u>

This discussion is based on the results pertaining to bed 3 (the worst-case scenario). As can be observed from Figure 29, the 'number of sampled locations' (Factor A) accounts for 42 % of the variation in the results of sludge characterisation mapping. This reflects the sensitivity of results to the number of locations sampled. Similarly, the 'depth of penetration of the sampling device' (Factor C) has a high influence of 22.7 %. This describes the sensitivity of the resulting 3D characterisation map to the penetration capabilities of a sampling device in a heterogeneous sludge bed.

It was also observed that the 'Residual R' (unexplained) variance accounted for 10 % of the result variation. The residual variance of any ANOVA test

refers to the variance that is not strictly associated with only one factor or interaction group. It is the variance that may best be considered to have occurred due to the inherent randomness of any experiment. Hence, by maintaining the same sampling configuration of Factors A, B, C and D across a number of sludge characterisation exercises, only 10 % of the result variations observed in this experiment will occur. The source of this residual contribution can be further investigated by introducing other experimental factors present in sludge characterisation.

In this simulation study, the residual contribution was a result of the randomness introduced into the sludge sampling algorithm. In order words, a sludge sample belonging to PSD class A was modelled to have particle sizes that are randomly chosen within the domain of the expected mean and spread for that class. In real applications however, additional factors present in the laboratory analysis of sludge may be involved.

3.7 Further evaluation of the four experimental factors related to sludge sampling

The foregoing discussion has sought to evaluate the four experimental factors related to sludge sampling. In this attempt, four examples of a sludge bed models were used. These models included one example each of the four possible spatial autocorrelation configurations. The results from statistical analyses have so far indicated that the sludge bed model (Sludge bed 3) which has no spatial autocorrelation (either along the horizontal or vertical plane) may sometimes behave differently compared to the other three sludge bed models. This sludge bed model, by nature of it not having spatial autocorrelation, could be regarded as being the worst case scenario for any sludge bed and hence, should be the focus of evaluating experimental factors.

For example, in the determination of an appropriate method of spatial extrapolation, the other sludge bed models (sludge bed models 1, 2 and 4) indicated no significant preference (based on map accuracy performance) for either TDA or OKA. However, results from sludge bed 3 indicated that the TDA was a more accurate method of spatial extrapolation in the absence of

ground truth and in the event of no spatial autocorrelation. This led to the conclusion that the TDA would be most appropriate as it is of greater performance in a worst case scenario.

A similar observation occurred in the determination of the level of significance of the various experimental factors and factor interactions related to sludge sampling in relation to their influence on result variability. From the ANOVA table of results, it was observed that for sludge bed 3, the number of sampling locations recorded the highest significance amongst all other experimental factors.

However, results from sludge bed models 1, 2 and 4 indicated that this factor was not the most significant of all experimental factors. One way to interpret this observation is that the influence of the various experimental factors on result variability may be dependent on the presence or absence of spatial autocorrelation. However, from another perspective, it could be argued that the particular sludge bed model 3 designed for this simulation is only one example and does not provide an overall assessment of the behaviour of sludge bed in the worst case scenario of no spatial autocorrelation.

It is therefore important to consider further evaluation of the four experimental factors using five more examples of sludge bed models which have no spatial autocorrelation. The sludge bed models 5, 6, 7, 8 and 9 are as shown in Figure 30.

Although all the five additional bed models have no spatial autocorrelation along the horizontal and vertical planes, sludge bed model 9 is modelled to represent an extreme case with a higher degree of heterogeneity in the spatial distribution of PSD class. Hence, sludge bed model 9 may be observed to behave differently from the other models.

Using these bed models, the results earlier observed on sludge bed model 3 are re-evaluated and are discussed in the following sub-chapter.

(a) Bed 5 $\overline{HSAC}\,\overline{VSAC}$ **(b) Bed 6** $\overline{HSAC}\,\overline{VSAC}$
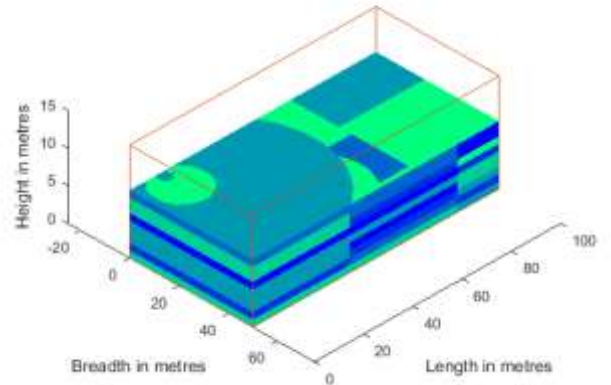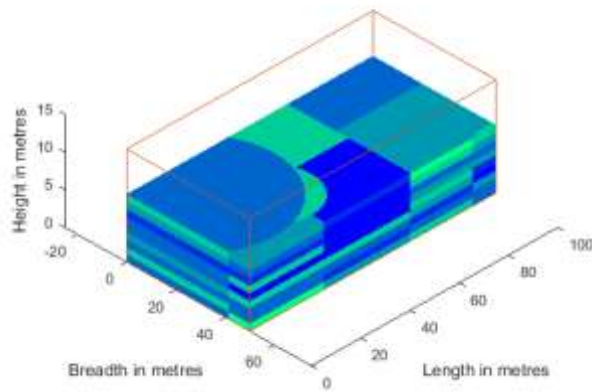
(c) Bed 7 $\overline{HSAC}\,\overline{VSAC}$ **(d) Bed 8** $\overline{HSAC}\,\overline{VSAC}$
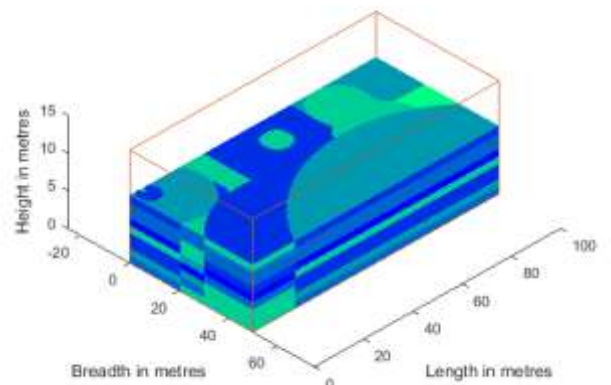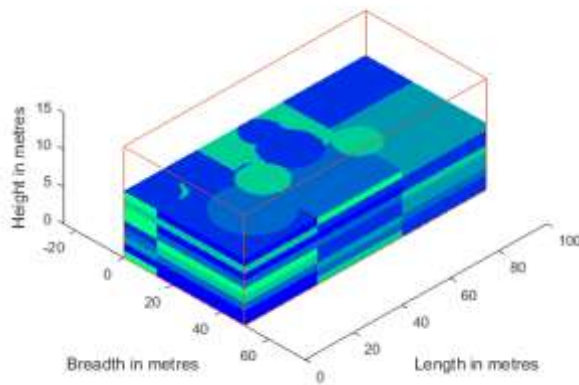
(e) Bed 9 $\overline{HSAC}\,\overline{VSAC}$
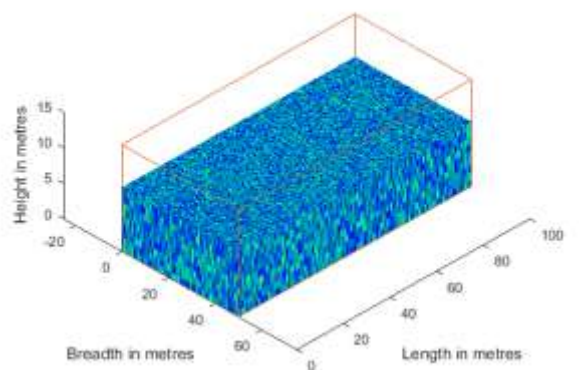
Figure 30: The five additional sludge bed models developed for re-evaluation purposes. These are sludge bed models which have no spatial autocorrelation. The coloured pixels indicate the class size values of the particle size distribution of sludge found

3.7.1 Re-evaluation of the Comparison between the Ordinary Kriging and the Triangular Delaunay Spatial Extrapolation Algorithm
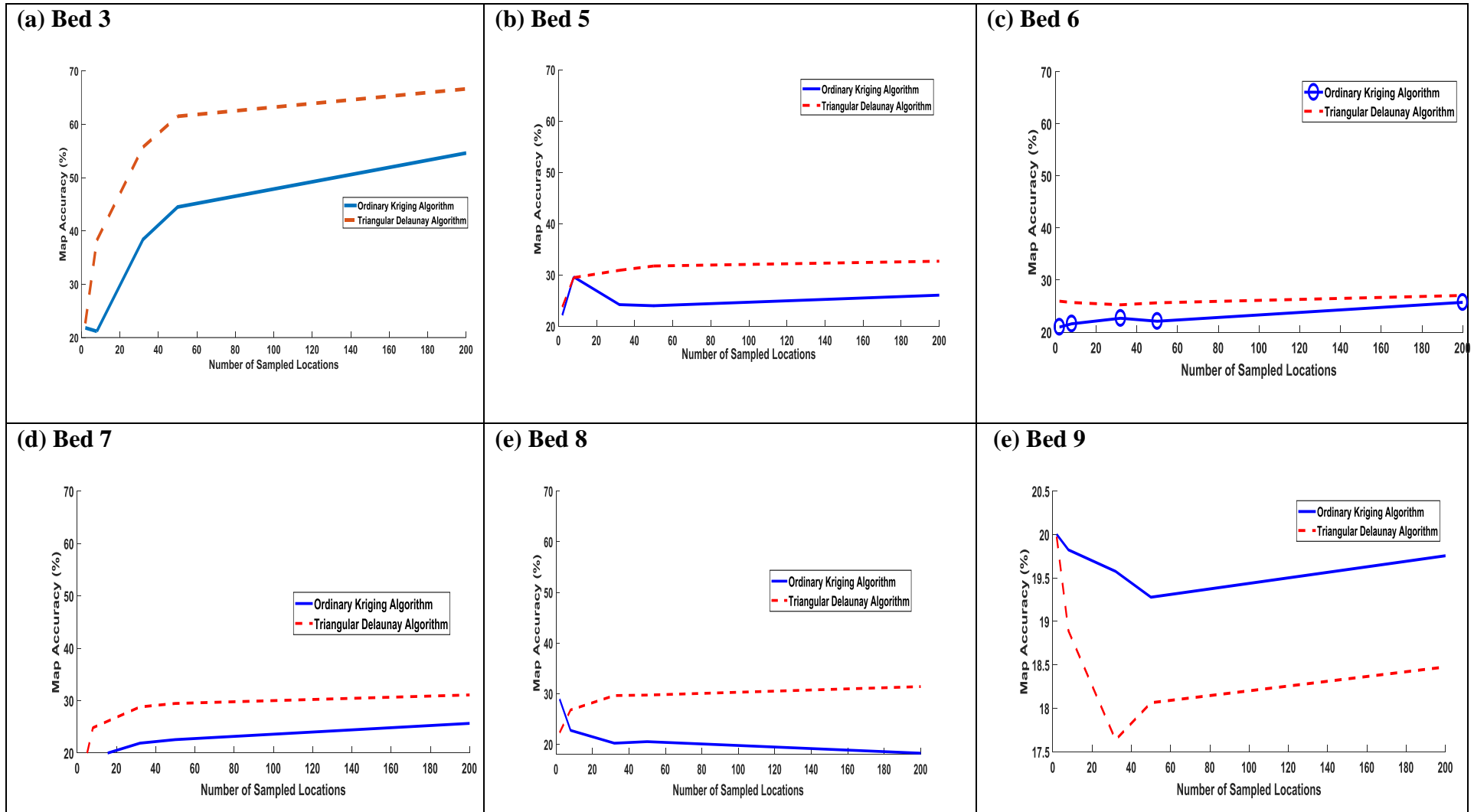
Figure 31: Kriging versus Delaunay (nearest) for $\overline{HSAC}\ \overline{VSAC}$ Beds

Figure 31 shows the performance of both the OKA and TDA methods of spatial extrapolation in each of the five additional sludge bed models and bed 3. When compared to sludge bed model 3, it is evident that the sludge bed models 5, 6, 7 and 8 all agree with the earlier observations that in the absence of spatial autocorrelation, TDA delivers higher map accuracy than OKA.

However, as may be expected, sludge bed model 9 gives a different result. In this result it shows that although OKA performs better than TDA, the accuracy is relatively low under such extreme heterogeneity conditions. The observation in sludge bed model 9 was carried out on a similarly heterogeneous sludge bed model with the same outcome. It can therefore be concluded that the observations in sludge bed model 3 remain valid for the worst case scenario of a no spatial autocorrelation.

3.7.2   Re-evaluation of the ANOVA Results: F-Statistics and P Values

In the ANOVA results of sludge bed models 1 to 4 of varying spatial autocorrelation configurations, sludge bed model 3 was the only model which indicated that Factor A (number of sampling locations) had the most significant influence (as represented by the magnitude of the F-Statistic value). In the other sludge bed models, Factor A was in a third position behind Factors C and D (Sampler device). However, results from Table 5 shows that the five additional sludge bed models 5 – 9 do not agree with sludge bed model 3.

Table 5: A summary of the ANOVA test showing F-Statistic and Probability (P) results

	Factor	Bed 3 $\overline{HSAC}\ \overline{VSAC}$		Bed 5 $\overline{HSAC}\ \overline{VSAC}$		Bed 6 $\overline{HSAC}\ VSAC$		Bed 7 $\overline{HSAC}\ VSAC$		Bed 8 $\overline{HSAC}\ VSAC$		Bed 9 $\overline{HSAC}\ VSAC$	
		F	**P**	**F**	**P**	**F**	**P**	**F**	**P**	**F**	**P**	**F**	**P**
Main Factors	A	1284.5	0	147.33	0.00	133.84	0.00	778.78	0.00	459.84	0.00	2.79	0.10
	B	28.9	0	24.97	0.00	39.68	0.00	49.39	0.00	33.18	0.00	0.28	0.60
	C	693.2	0	3680.85	0.00	5287.96	0.00	7489.69	0.00	8131.77	0.00	0.83	0.36
	D	371.3	0	4096.60	0.00	905.10	0.00	4442.71	0.00	5609.13	0.00	1355.60	0.00
Factor Interactions	AB	4.7	0.03	7.06	0.01	1.95	0.16	1.33	0.25	1.59	0.21	1.53	0.22
	AC	35.3	0	48.84	0.00	19.10	0.00	472.08	0.00	220.53	0.00	13.33	0.00
	AD	226.2	0	112.27	0.00	61.29	0.00	247.33	0.00	112.58	0.00	0.48	0.49
	BC	15.7	0	12.93	0.00	22.03	0.00	27.73	0.00	33.80	0.00	0.11	0.74
	BD	6.6	0.01	5.22	0.02	6.85	0.01	2.79	0.10	1.33	0.25	1.03	0.31
	CD	48.35	0	343.55	0.00	979.71	0.00	3394.85	0.00	3419.22	0.00	0.05	0.83
	ABC	4.1	0.04	13.93	0.00	6.37	0.01	5.87	0.02	0.92	0.34	0.77	0.38
	ABD	5.4	0.02	11.75	0.00	14.95	0.00	15.29	0.00	16.98	0.00	0.17	0.68
	ACD	11.8	0	37.15	0.00	51.46	0.00	356.10	0.00	129.92	0.00	2.45	0.12
	BCD	8.1	0	12.12	0.00	11.20	0.00	1.05	0.31	4.31	0.04	1.84	0.18
	ABCD	6.9	0.01	6.84	0.01	10.14	0.00	18.33	0.00	8.60	0.00	1.40	0.24

In each of the sludge bed models 5 to 8, Factor C and D displayed higher significance compared to Factor A. While Factor C (penetration depth of the sampling device) had the most significant F-Statistic in bed models 6, 7 and 8, Factor D (particle size bias of the sampling device) had the most significant F-Statistic in bed model 5 and 9. This result is significantly different from what was observed in sludge bed model 3. Plots of half normal effect as shown in Figure A1 – A5 (see Appendix A) further confirm these observations.

3.7.3 Re-evaluation of the eta-squared effect of factors and interactions

Table 6: Eta Squared Effect of Sampling Factors and their Interactions

	Factor	Eta-Squared Effect (%)					
		Bed 3 $\overline{HSAC}$ $\overline{VSAC}$	Bed 5 $\overline{HSAC}$ $\overline{VSAC}$	Bed 6 $\overline{HSAC}$ $\overline{VSAC}$	Bed 7 $\overline{HSAC}$ $\overline{VSAC}$	Bed 8 $\overline{HSAC}$ $\overline{VSAC}$	Bed 9 $\overline{HSAC}$ $\overline{VSAC}$
Main Factors	A	42.0	1.7	1.7	4.4	2.5	0.2
	B	0.9	0.3	0.5	0.3	0.2	0.0
	C	22.7	41.5	67.3	42.5	44.0	0.0
	D	12.2	46.2	11.5	25.2	30.3	80.4
Factor Interactions	AB	0.2	0.1	0.0	0.0	0.0	0.1
	AC	1.2	0.6	0.2	2.7	1.2	0.8
	AD	7.4	1.3	0.8	1.4	0.6	0.0
	BC	0.5	0.1	0.3	0.2	0.2	0.0
	BD	0.2	0.1	0.1	0.0	0.0	0.1
	CD	1.6	3.9	12.5	19.3	18.5	0.0
	ABC	0.1	0.2	0.1	0.0	0.0	0.0
	ABD	0.2	0.1	0.2	0.1	0.1	0.0
	ACD	0.4	0.4	0.7	2.0	0.7	0.1
	BCD	0.3	0.1	0.1	0.0	0.0	0.1
	ABCD	0.2	0.1	0.1	0.1	0.0	0.1
	Residual R	10.0	3.4	3.9	1.7	1.6	18.0
	TOTAL	**100**	**100**	**100**	**100**	**100**	**100**

Table 6 shows the Eta Squared Effect of the experimental factors related to sampling. It can be seen in this table that unlike what was observed with sludge bed model 3, the highest contribution of Factor A to result variability is 4.4 %. The table also shows that in the extreme case of heterogeneity (bed model 9), Factor D accounts for about 80 % of the result variability observed in sludge PSD campaigns. In sludge bed models 5, 6, 7 and 8, Factor C has an average contribution of about 48 % to result variability while Factor D has an average contribution of 23 %. Factor A takes a distant third position with an average contribution of 2.6 %. This observation is significantly different from what was previously observed. It can here be concluded that the penetration depth and particle size bias of the sampling device being used are the most significant and influential experimental factors related to sampling.

Nonetheless, this observation does not eliminate the significance of Factor A (number of sampling locations).

3.8   Conclusion

The performance of both the Ordinary Kriging Algorithm (OKA) and the Triangular Delaunay Algorithm (TDA) methods of spatial extrapolation have been compared against each other. While the results confirm the general expectation that the accuracy of the OKA method is greater than TDA in the presence of spatial autocorrelation, this observation only held where the number of sampled locations was greater than 30. However, in the absence of spatial autocorrelation, it was observed that the accuracy of TDA was about 15 % more than that of OKA. By considering that the worst case scenario of an unknown sludge bed is where there is a total absence of spatial autocorrelation, the results hereby suggest that TDA is the more suitable method to be used.

The 2^k ANOVA test conducted on the four identified experimental factors related to sludge sampling provided a measure of their influence. The result of the test indicated that all main factors had their F-ratio statistics above the

threshold value of 1, and their P-values were satisfactorily below the threshold value of 0.05. This confirmed that all of the four main factors are of significant influence to the variability of sludge characterisation results.

In evaluating the influence of each of the experimental factors using their Eta Squared Effect, the 'sampling strategy' factor recorded the least percentage influence, below 1 %. In the absence of spatial autocorrelation, the 'number of sampled locations' factor recorded the third highest influence of about 4.4 %. Under this condition, the 'penetration depth of the sampling device' factor and the 'bias of the sampling device' factor recorded 48 % and 25 % influence respectively.

Going forward, with an observed influence of 4.4 % due to variations in number of sampled locations alone, it is important to understand how to determine an adequate setting. In seeking such understanding, Chapter 4 establishes an algorithm that can be used to support field operators in real-life sludge characterisation. It is also expected that the development of an *in-situ* sampling mechanism will enhance the capacity of sampling devices to collect and analyse sludge samples from an adequate number of locations, with minimal bias, deep penetration and less variation in procedures.

4 CHAPTER 4: Estimating and Improving Confidence in Radioactive Sludge Characterization Maps

4.1 Introduction

A number of experimental factors that influence the success of any such sludge sampling have now been identified and their influence has been evaluated. It has also been observed that one of the significant sampling-related experimental factors is the number of sludge sampling locations used.

With about 4.4 % influence on the variation of characterisation map accuracy, it has become necessary to determine how to choose an adequate setting for this influential factor. If this setting is determined and maintained across multiple sludge characterisation exercises, result variability would decrease.

From Chapter 3, it has also been shown that as the number of sampled locations increases, the map accuracy increases. This increase is similar to an exponential rise. By implication, with further increase in the number of sampled locations, the rate of change of map accuracy decreased. This was as map accuracy approached the 100 % limit.

Unlike with computer simulated sludge bed models, the observations in Chapter 3 cannot be made on real-life sludge beds. This is because map accuracies can only be obtained when the ground-truth map is available for comparison with generated maps. This means field operators need an appropriate method of evaluating the quality of map results in the absence of such ground-truth map.

This chapter considers two questions in regard to sludge characterization mapping:

- What are the percentage confidence estimates in the results inferred at non-sampled areas relative to that of the actual samples?
- What is the number of samples that are required, such that any further samples are unlikely to significantly improve the accuracy or confidence of the resulting characterization map? [57]

A measure of the percentage confidence in the data presented on the three-dimensional characterization map will be useful in evaluating the adequacy of any sampling choices made and the reliability of the results [38]. This chapter provides results from computer simulated sludge bed models and a real-life sludge bed.

4.2   Percentage Confidence in Generated Map

The confidence in a resulting three-dimensional map depends on three factors:

- the method used in the collection of the sample [51], covered in Chapter 3,

- the method of spatial extrapolation [138], and

- the method of sample analysis undertaken in the laboratory [159].

In many real-life applications, it is not possible to quantify the accuracy because the actual sludge characteristics across the entire bed will be unknown. In fact, regardless of the method of spatial extrapolation used, the generated map of sludge characteristics will not always be accurate. What can be quantified however, is the probability that the ground-truth value at a specific location lies within an interval $\pm\varepsilon$ of the value that has been inferred. This is referred to as the percentage confidence ($\%C_k$) in the inferred measurement. The error margin $\pm\varepsilon$ is referred to as the confidence interval.

In calculating the value of $\%C_k$ for any inferred measurement, the desired value of ε should be fixed. For example, if the data of interest is the PSD class value at a position, which is expected to be any integer from 1 to 6, an ε value of 0.5 is appropriate as it provides the class boundary for each PSD class. The method of calculating $\%C_k$ depends on the chosen method of spatial extrapolation. If OKA is utilized then this relies on the relationship that has been established between variance and error [149], which uses Kriging variance σ_k^2, defined in Equation (11) to represent the degree of uncertainty in an inferred measurement at any position k.

$$\sigma_k^2 = \sigma_o{}^2 - \left(\sum_{j=1}^{n} \lambda_{jk} v_{jk} + \mu_k \right) \tag{11}$$

In contrast, the TDA is based on regression, which is achieved using the modified t-distribution equation given in Equation (12) [160]

$$\varepsilon = t_{\left(\frac{\Phi}{2}, n_p - 2\right)} \sqrt{s^2 \left(1 + \frac{1}{n_p} + \frac{(x_k - \bar{x}_o)^2}{S_{xx}} \right)} \tag{12}$$

Where t is the t-score, $\Phi = (1 - \%C_k \times 0.01)$ is the risk of error, n_p is the number of particles in the reference samples, s is the standard deviation at the reference sampled position, x_k is the position of a non-sampled point, $\bar{x}_o$ is the mean position of the reference sample, and S_{xx} is the variance of x.

By re-arranging Equation (12) and replacing ε with 0.5, Equation (13) is derived and can be used to estimate $\%C_k$ at a specific inference point k.

$$\%C_k = 100\,\% * t_{n_p - 2}^{-1} \left(\frac{0.5}{\sqrt{s^2 \left(1 + \frac{1}{n_p} + \frac{(x_k - \bar{x}_o)^2}{S_{xx}} \right)}} \right) \tag{13}$$

Where t^{-1} is the t-score inverse function.

From Equation (13), it can be seen that by increasing n or by decreasing s^2, $\%C_k$ at location k will increase. Similarly, as the proximity $(x_k - \bar{x}_o)$ between the non-sampled position and the reference sampled position increases, $\%C_k$ decreases.

It is important to note from Equation (13) that the percentage confidence $\%C_k$ at a non-sampled location is not directly dependent on the total number of sampled locations used. It is also not directly dependent on the bias of the sampling device or the penetration depth of the sampling device. Similarly, $\%C_k$ is not dependent on the sampling strategy adopted.

What can be deduced from Equation (13) however, is that $\%C_k$ directly depends on the size of the sludge sample collected from sampling location $\bar{x}_o$. This is because the size of the sample may determine the value of n_p. This underscores the need to maximize sludge samples and the need to adopt an analytical technique which supports the analysis of bulk samples as discussed in Chapter 2.

From Equation (13) it can be further observed that $\%C_k$ at any non-sampled location is directly dependent on the distance between such non-sampled location and its nearest sampled location. This implies that the further away a non-sampled location is from any sampled location, the less the percentage confidence in the inferred PSD at that non-sampled location. By implication, $\%C_k$ is indirectly related to the sampling strategy. By ensuring that sampling locations are uniformly distributed across the population space, $\%C_k$ may be improved. Similarly, $\%C_k$ is indirectly related to the number of sampled locations and penetration depth of the sampling device because with more sampled locations spread uniformly across and through the depth of the population space, the distance between a non-sampled location and a sampled location would decrease.

The direct dependence of $\%C_k$ on the standard deviation s within a sampled location implies an indirect dependence on the sample bias of a sampling device. This is because a sampling device which is biased has the potential to distort the measured PSD standard deviation obtained from the sampled location.

4.2.1   Development of a Confidence Map

The $\%C_k$ value, when obtained for locations within the sludge bed and plotted on a map, provides a pictorial representation of the spread of percentage confidence across the population. This confidence map is used to qualitatively assess the adequacy of the sampling factors.

To illustrate confidence mapping, consider the computer simulated sludge bed model Bed 3 ($\overline{HSAC}\ \overline{VSAC}$). Given that this sludge bed is sampled at

eight sampling locations, with a non-biased sampling device which penetrates only through 10 % of the sludge depth. The resulting PSD inference map is shown in Figure 32.
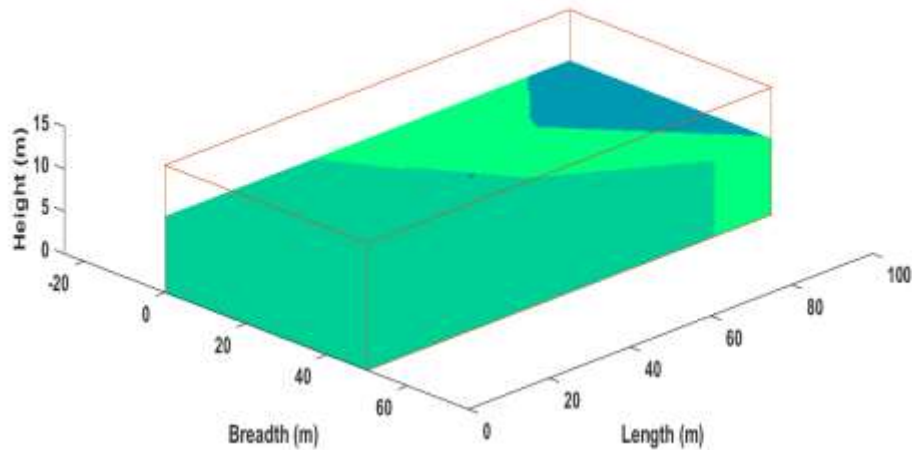
Figure 32: PSD inference map with 8 sampled locations. The different colours indicate the various classes to which the mean particle size found in a given are belongs to.

In order to show the percentage confidence that there is in accepting that the PSD class values inferred on the map are within ± 0.5 of their true values (relative to the accuracy of the measured PSDs), Equation (13) was applied. The resulting confidence map is shown in Figure 33

Line drawn across the length of the pond and 16 m into the width
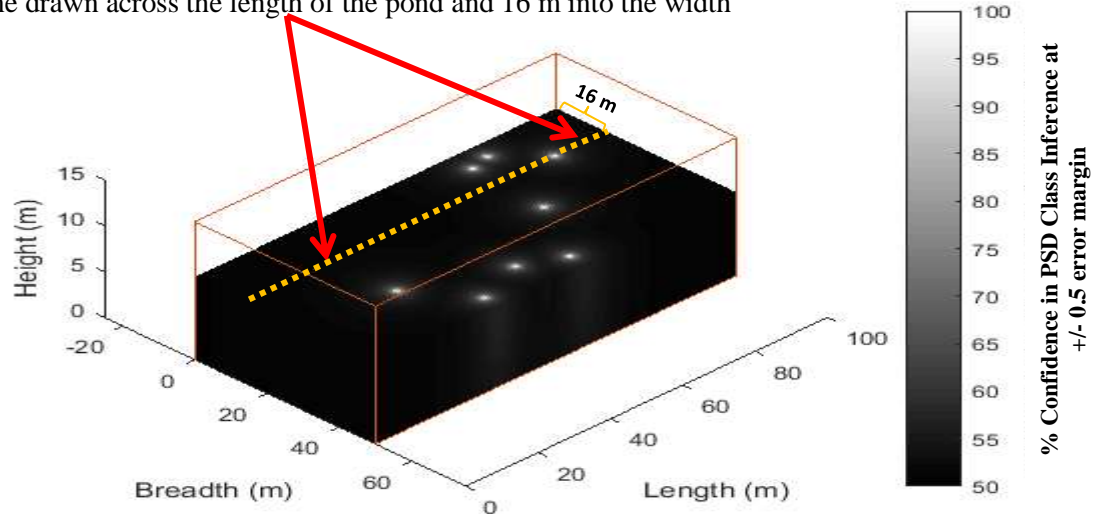
Figure 33: Map of sludge bed showing percentage confidence for 8 sampled locations. The sampled positions are the eight white spots visible on the map

At each of the 8 sampled locations, a 100 % confidence value can be observed. This 100 % confidence at a sampled location does not imply that the measured PSD at that location is 100 % accurate relative to the ground truth. This is because the accuracy of any measured PSD is dependent on the adequacy of the sampling device used and the accuracy of the PSD measurement. In effect, the 100 % confidence is relative to the accuracy of the measured PSD value. The percentage confidence values are observed to decrease as the samples go further away from sampled positions. This is illustrated in Figure 34 which shows the variation of the % Confidence values along the length of the pond at the surface of the sludge bed and 16m into the width of the pond.
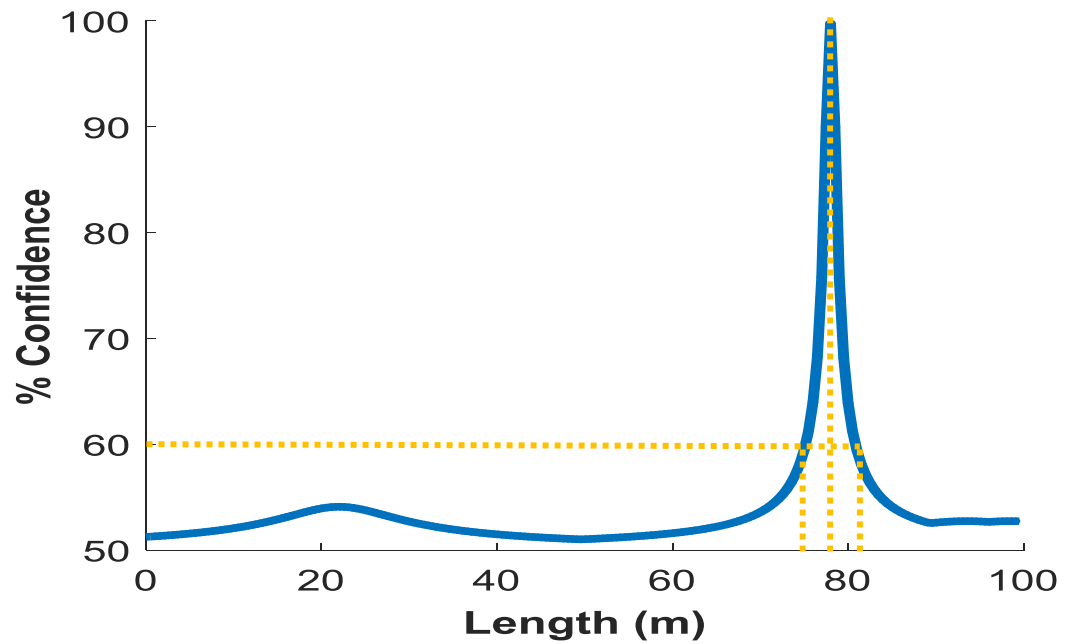
Figure 34: Plot of Percentage Confidence against distance along the length of the pond and 16 m into the width (reference to Figure 33.) The plot was taken from data points on a line drawn on the surface of the sludge bed confidence map produced using eight sampling locations.

The plot on Figure 34 indicates that there is a 100 % Confidence value at length 78 m, 16 m into the width of the pond. This can be verified on Figure 33. However, it shows how the Percentage Confidence decreases as distance from the sampled point increases. From Figure 34, it was observed that the Percentage Confidence 2.8 m away from the sampled location was 60 %. The gradient decreases as Percentage Confidence further drops to 50 %. The observed average Percentage Confidence along the length was 53.83 %

To further illustrate the significance of percentage confidence, corresponding locations in the PSD inference map and confidence map to the same location in the ground truth map were compared. It can be seen in Figure 35 that the inferences at locations having 100 % confidence were true (see red arrows). It can also be observed that the worst results were of positions of 50 % confidence where PSD inferences were observed to have been either true (see yellow arrow) or false (see blue arrow).
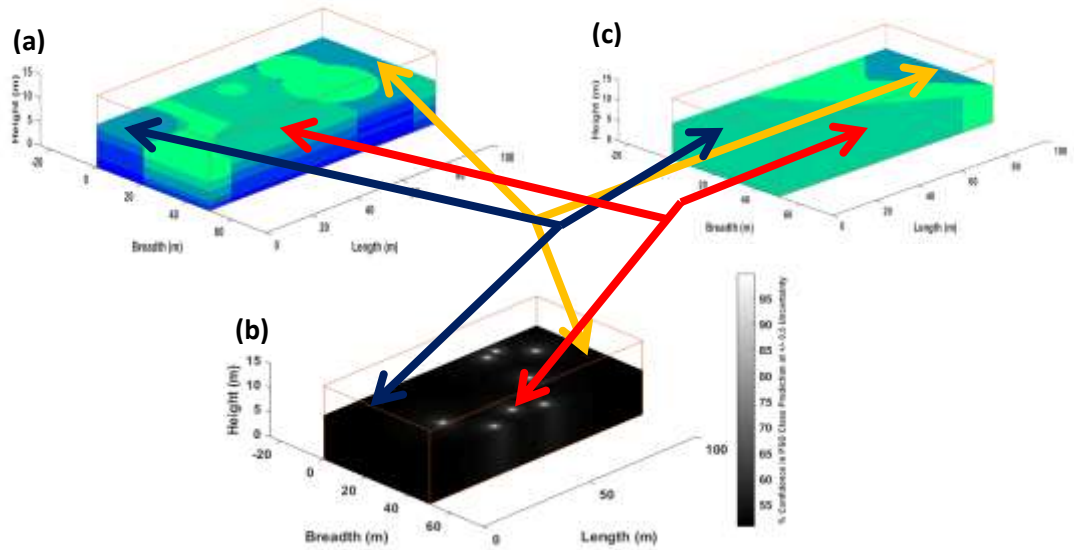
Figure 35: Comparing (a) Ground truth, (b) Inference map and (c) Confidence map. This figure illustrates how the percentage confidence values validate the inferred data.

Therefore, in order to increase the general percentage confidence across the sludge bed, the number of samples may be increased. Given that the number of sampled location is increased to 200, with sampling devices penetrating through 100 % of the sludge depth, the result of the confidence map is shown in Figure 36. This result indicates that deeper penetration enhances percentage confidence in sampled/non-sampled data from all positions of the bed.
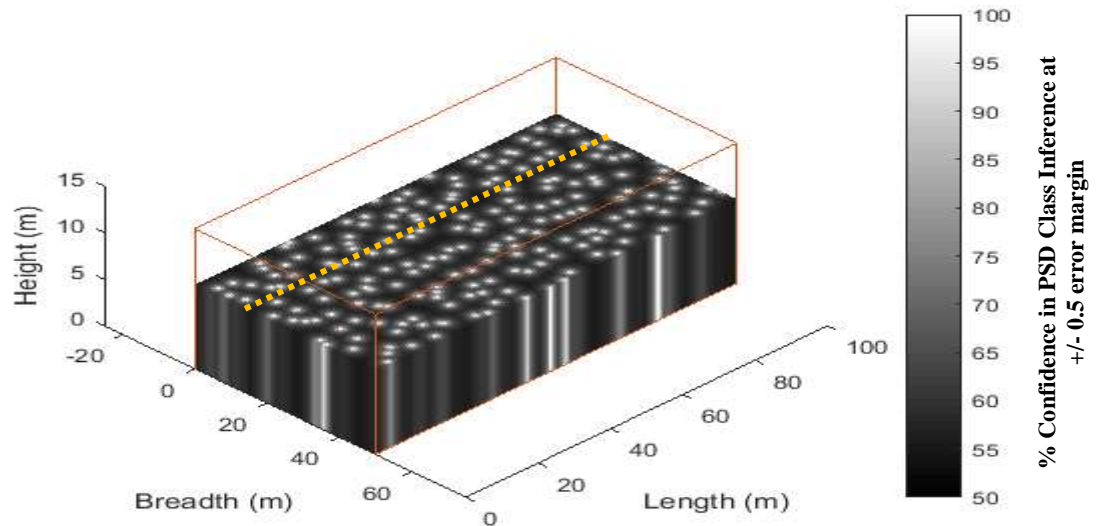
Figure 36: Map of sludge bed showing percentage confidence for 200 sampled locations. The map was generated using two hundred sampled locations.

The improvement in the general Percentage Confidence across the bed can be observed in Figure 37 which is the plot of Percentage Confidence along the length and 16 m into the width of the pond. This graph shows significant improvement compared to Figure 34 as the OBSERVED average percentage confidence along the length has increased to 63.78 %.
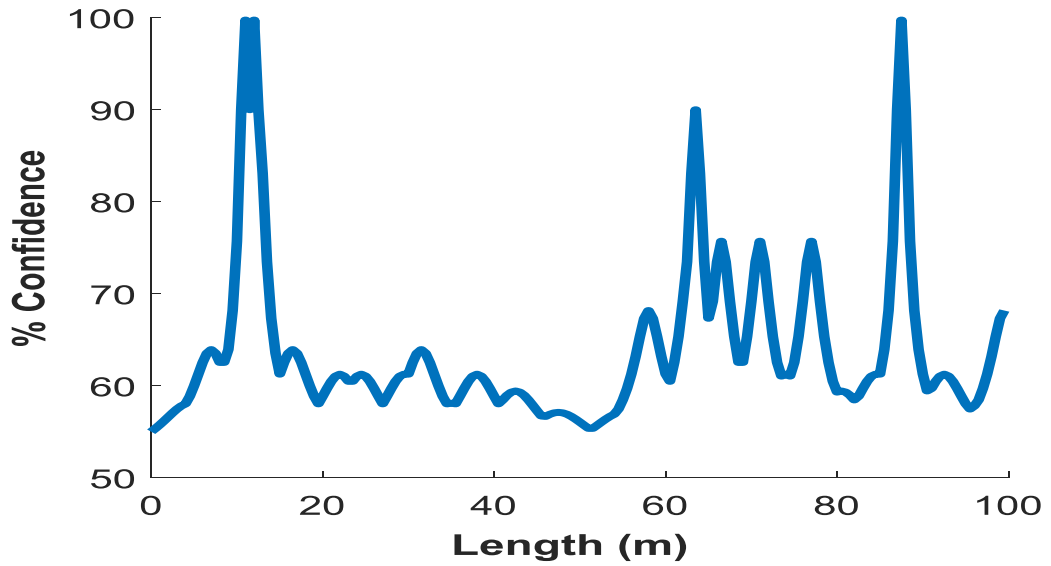
Figure 37: Plot of Percentage Confidence against distance along the length of the pond and 16 m into the width (reference to Figure 38). This plot was taken from data points on a line drawn on the surface of the sludge bed confidence map produced using eight sampling locations.

4.2.2 Remarks

Figure 33 also shows that for a 10 % penetration depth of the sampling device, the confidence reduces vertically. This is different in Figure 36 where a 100 % penetration depth has been used, resulting in a uniform percentage confidence in the vertical direction. This confirms the expected benefit of using deep penetrating sampling devices on data confidence and map accuracy.

Considering that the percentage confidence in Equation (13) is significantly dependent on the specific sampling procedure, the confidence map obtainable does not provide a tool for comparing the results from one sludge characterisation campaign to another. It may therefore be known as a measure of "single-campaign" confidence. In Chapter 6 however, the results from Chapter 3 and 5 which indicate the influence of various experimental factors on result variation will be adopted and introduced to Equation (13) in order to

develop a measure of "cross-campaign" confidence. It will then become possible to compare and harmonise the results from a number of sludge campaigns.

However, the scope of this chapter is focussed to a specific sludge characterisation campaign, and seeks to identify and improve the single-campaign confidence in the sampled/non-sampled data from each position within the sludge bed.

From a general perspective, the concept of confidence maps suggests that data quality and resulting confidence may continually increase with the number of sampled locations. However this may be bounded such that beyond a certain number of measurements, any further samples have little impact on the inference map produced of the bed. A plot of map accuracy against the number of sampled locations can be used to determine such adequate number of sampled locations.

4.3   Improving Map Accuracy

In real applications where the ground-truth map is unknown, alternative methods for assessing the accuracy of maps include the single-deletion jack-knife cross-validation with replacement method and the model-based uncertainty estimates method [160]. Evaluating the accuracy of inferred data over time as new sampled data become available has also been suggested [161, 162].

These existing techniques can be used for comparing different spatial extrapolation methods or for validating them. This is achieved by estimating the mean absolute error and other error statistics of extrapolations made at positions that have already been sampled. Methods such as leave-one-or-more-out cross-validation can be incorporated within these techniques to avoid over-fitting. However, reliance on such error statistics does have some limitations. One of these is that the method of cross-validation does not provide an assessment of the inference error at non-sampled locations. Another limitation is that the method of confidence estimation as mentioned

earlier relies, in part, on the same assumptions as the extrapolation algorithm used [160].

A key objective in this study is to determine when an adequate number of locations have been sampled such that a satisfactory inference map of the sludge bed can be obtained. This requires measuring the map accuracy, however without reference to a ground-truth map (T), and observing how the map accuracy improves as the number of sampled data points increases.

To enable this, a new algorithm referred to as the Recursive Relative Accuracy (RRA) is introduced. This algorithm takes advantage of both the leave-one-or-more-out cross-validation method and the confusion matrix method of calculating absolute map accuracy. One advantage of this method is that unlike existing techniques, it maintains the use of map accuracy as a parameter for assessing map validity rather than relying on the error statistics measured only at sampled positions. Another benefit with the proposed method is that it does not require knowledge of the ground-truth map.

4.3.1   The RRA Method

The first step in implementing the RRA algorithm is to generate inference maps using a selection of subsets of the data points that are available. The relative accuracy of the resulting inference maps is then compared to the inference map produced using all the data points.

Let n be the total number of sampled data points collected at a given time. The proposed technique works by initially generating an inference map P using all n data points. This inference map will be denoted by $P_{1,n}$.

Inference maps are then generated from a data subset obtained by choosing one or more of the n data points at a time but not exceeding $(n-1)$ data points. Let the number of data in a given subset be denoted by i. For any $i \in \{1, 2, 3, \ldots n-1\}$, the data subset to be created from the n available measurements can be chosen in $\binom{n}{i}$ unique ways.

If i is very large, then time restrictions may prevent the processing of all possible $\binom{n}{i}$ data selections. In the investigations described in this paper, a limit of 20 possible data selections for any i was applied.

Let r, an integer in the range $1 \leq r \leq \binom{n}{i}$, denote the serial number of each unique data subsets containing i number of data points. The inference maps so generated are then denoted by $P_{r,i}$. The total number of $P_{r,i}$ maps that are generated is given by $\sum_{i=1}^{n-1}\binom{n}{i}$.

For example, if there are 4 sampled measurements available at a given time, then all 4 measurements will be used to generate the initial map denoted by $P_{1,4}$. Subsequently, several other inference maps can be generated using all the unique combinations of the measurements. This will result in 14 more maps denoted by:

$P_{1,1}, P_{2,1}, P_{3,1}, P_{4,1}, P_{1,2}, P_{2,2}, P_{3,2}, P_{4,2}, P_{5,2}, P_{6,2}, P_{1,3}, P_{2,3}, P_{3,3}$ and $P_{4,3}$.

The next step involves the calculation of the relative accuracy, denoted by $RRA_{r,i}$, of each of the $P_{r,i}$ maps. In the proposed approach this determines the confusion matrix, when the unknown ground-truth map T is replaced by $P_{1,n}$, using Equation (14).

$$RRA_{r,i} = \frac{tr(CM_{r,i})}{\sum_{c=1}\sum_{b=1} cm_{r,i\ (b,c)}} \qquad \textbf{(14)}$$

Where $CM_{r,i}$ is the confusion matrix (previously described in Chapter 3) between $P_{r,i}$ and $P_{1,n}$ and $cm_{r,i\ (b,c)}$ refers to any element of the matrix $Cm_{r,i}$ located on row b and column c.

All the values of $RRA_{r,i}$ are then plotted against i, either as a scatter-plot or an error-plot. By observing the response of RRA to an increase in i, it is possible to determine whether the response is in a transient state or at a steady state. If the value of i is relatively low and unable to adequately represent the entire population, then the response will be transient. Each new data point will continue to add information to the inference map to improve its relative

accuracy. However, as i increases, the response will begin to approach steady state, as it approaches 100 %. In interpreting this steady-state observation, it can be said that beyond a certain number of sampled measurements i_o, any further measurements introduced into the spatial extrapolation algorithm will make no significant change to the inference map.

The proposed method is recursive because until a steady-state response is observed, further measurements would have to be collected, thereby increasing the value of n and recalculating the $RRA_{r,i}$ values. A weakness of this algorithm is the possible occurrence of false-maxima. This is a situation where the RRA value successfully reaches 100 % when there are very few measurements. These false-maxima can only be avoided by using *a-priori* understanding of the properties of the sludge bed.

It is important to note that although RRA may converge to 100 % at steady state, this is not an indication of absolute map accuracy. 100 % absolute inference accuracy of the map can only be determined if the ground-truth map is known.

4.3.2 An Illustration of the RRA Method on Simulated Sludge Bed 3 Model

To illustrate the outcome of the RRA algorithm and how it can be interpreted, consider the simulated sludge bed model Bed 3 ($\overline{HSAC}\ \overline{VSAC}$) as the population to be sampled. For the purpose of the RRA algorithm, it is assumed that the simulated bed is unknown. By conducting sludge sampling in a given number of locations, e.g. 200, a PSD inference map of the population is then produced and named $P_{1,200}$. The RRA algorithm can be implemented by following the flow chart of Figure 39.
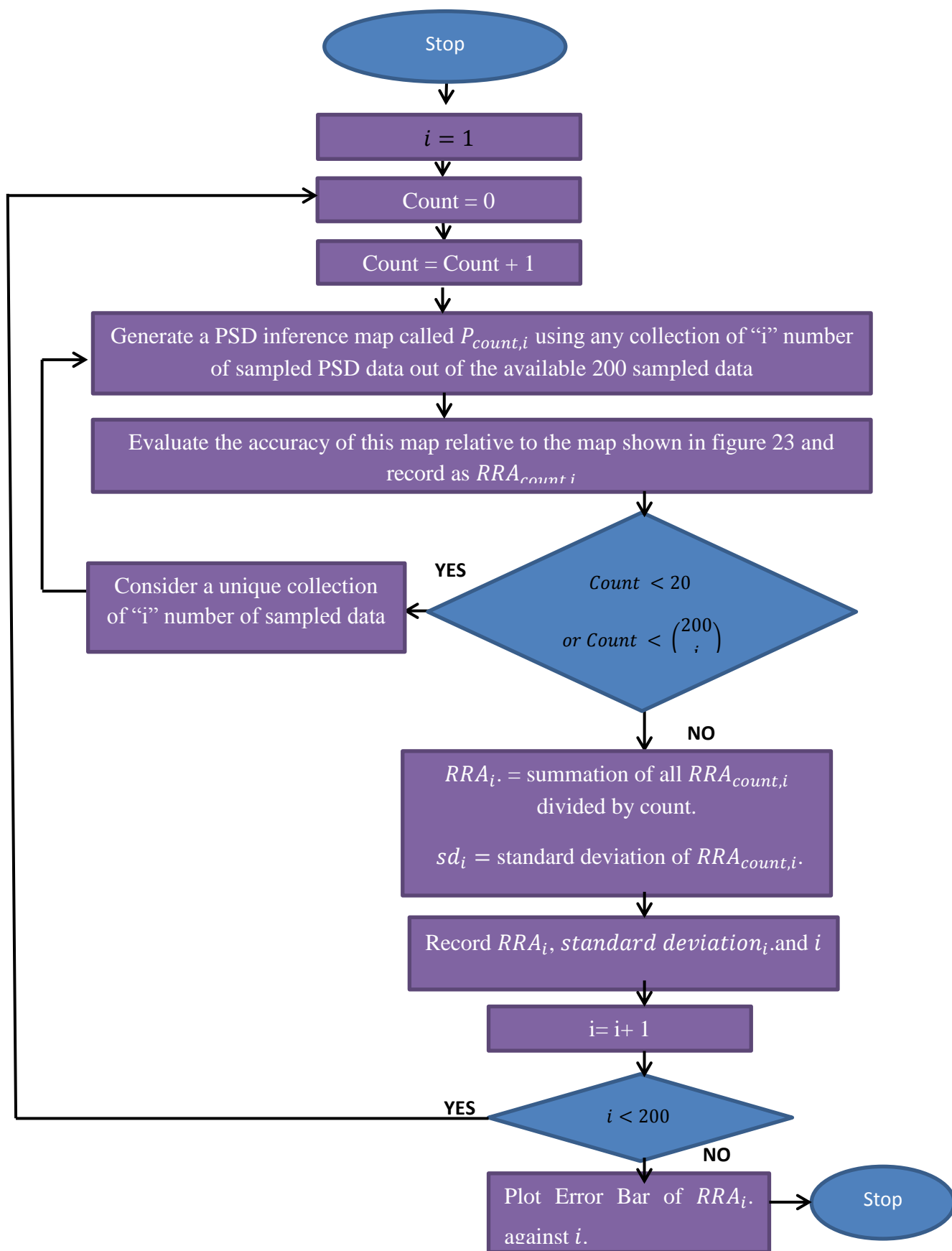
Figure 39: A flowchart for the RRA algorithm

The flowchart considers a case where the total number of available sampled data is 200. However, this may not always be the case. For example, field operators may decide to implement an RRA algorithm when only 8 sampled data are available. The outcome of which would be used to determine whether to carry out further sampling.

Figure 40 shows the result of implementing RRA on Sludge Bed 3. In this exercise, four scenarios were examined. The four scenarios had n and penetration depth values as being: 8 at 10 %, 200 at 10 %, 200 at 30 % and 200 at 100 % depth respectively.
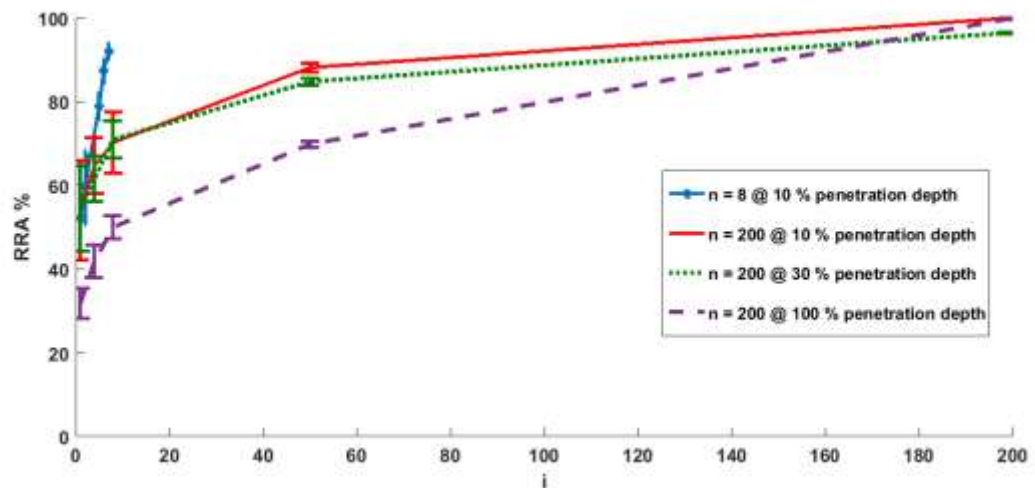
Figure 40: Plot of recursive relative accuracy (RRA) with error bars against number of sampled locations (i) – from simulation. This figure helps to understand how the accuracy of an inferred map improves with an increase in the number of sampled locations.

From Figure 40, it can be observed that the RRA error-plot for $n = 8$ did not approach steady state. However, by recalculating the RRA values using $n = 200$, and increasing the penetration depth from 10 % to 100 %, it can be observed that the plot begins to approach steady state. In fact for penetration depths of 10 % and 30 % there would appear to be limited value in taking more than approximately 50 samples.

Figure 40 has a significant resemblance to the "map accuracy versus number of sampled locations" plots of Chapter 3. The similarity in the shape of the plots can be observed. This is in spite of Figure 40 being non-reliant on the use of a ground-truth map for result validation. This result suggests that for this simulation, the RRA plot provides a convenient tool in identifying how the inferred map accuracy improves as the number of samples increases. In particular, the estimation that 50 is a sufficient number of sampled locations in the case where the sampling depth is 10 % or 30 % agrees with the accuracy plots of Chapter 3. This confirms the reliability of the RRA algorithm in the absence of ground truth. Similar results were also obtained when this technique was applied to different simulated sludge bed.

4.4   Experimental Validation using a Real-Life Sludge Bed

For result validation purpose, a real-life sludge simulant tank shown in Figure 41 was used. This six year old simulant sludge bed is located at the National Nuclear Laboratory's (NNL's) facility in Workington, UK. The aim of the validation experiment was to demonstrate the real-life application of the RRA algorithm. This was done using a test bed which is considered to be representative of a nuclear storage pond. The test bed used contained non-radioactive Corroded Magnesium Sludge (CMgS) with dimension of 120 cm $\times$ 30 cm $\times$ 14 cm.
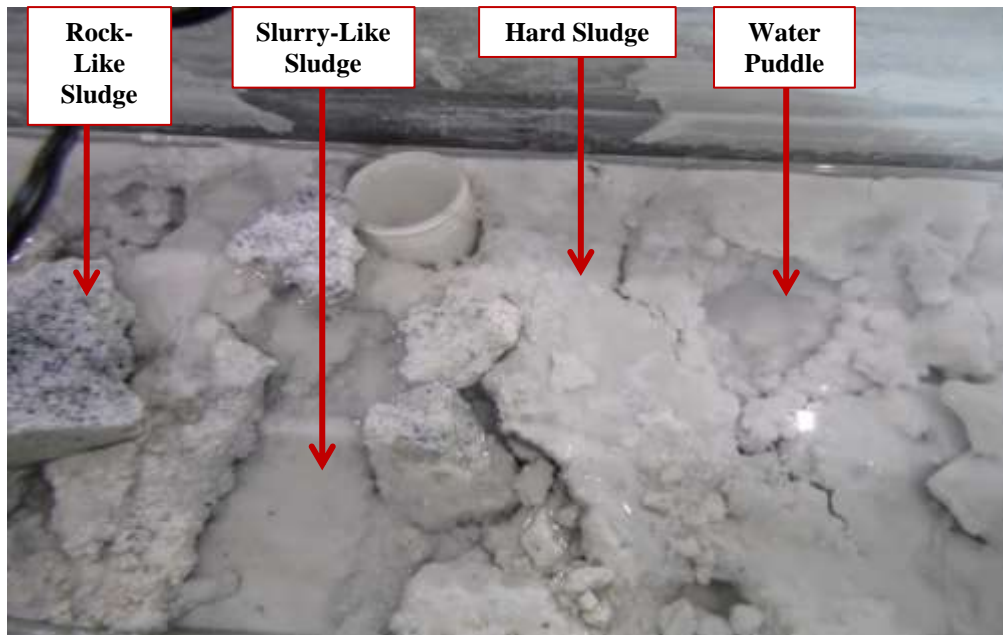
Figure 41: Top View of a Corroded Magnesium Sludge Simulant Tank at the National Nuclear Laboratory, UK (2017). This picture shows that there are a number of different sludge formations in the bed.

4.4.1 Sludge Sampling

Figure 42 shows 20 locations earmarked for sample collection. This choice of these locations was based on stratified random sampling. The strata demarcation was made to be spherical, rather than square shaped. This was because of historically facts available. In 2011 when this particular simulant tank was commissioned, sludge was introduced into the tank at sampling location "1". Hence, outward dispersion of sludge from location "1" would be spherical. Each sample location/pixel is of surface dimension 2 cm × 2 cm and is further subdivided into 5 depth intervals of 2.8 cm each for three-dimensional spatial characterisation. This is because the diameter of the sampling device was about 1.5 cm and the depth of the sludge was about 14 cm.
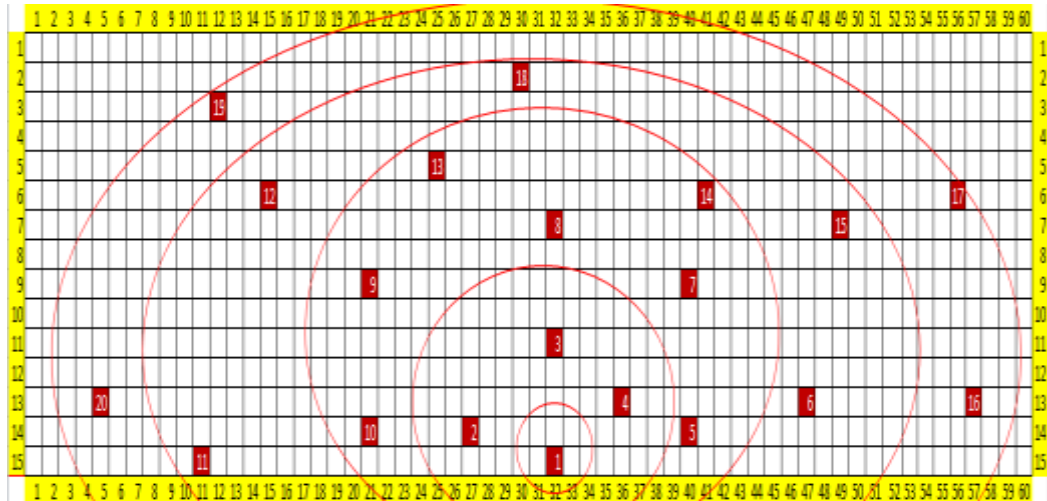
Figure 42: Plan view of sampling locations. This figure shows (from a plan view) how the method of stratified random sampling may be applied to the sludge bed at the National Nuclear laboratory, Workington, UK in order to select twenty sampling locations.

The $\times$ and Y coordinates were identified with the aid of a cross wire system. This is shown in Figure 44. Samples were collected using a combination sampler methods; syringe and core sampler. As samples per location were collected along one consistent depth, they were deposited into labelled sample containers in order of the depths they were collected from. Figure 43 shows an array of labelled samples in containers. Challenges faced and observations are discussed in the subsequent section.

Figure 43: An array of sludge samples collected at the National Nuclear Laboratory (NNL), UK from various sample locations and depth.

4.4.2 Experimental Observations during Sampling

Holding the sludge samples in the collection tube was challenging as the pressure differential produced by the syringe was not enough to oppose the weight of the sample. Secondly, penetrating the top layer of the sludge bed was challenging. This was observed at sampling location "4" (see Figure 44) of the sludge bed where increased downward thrust was required. This was beyond the capabilities of the collection tube. A steel rod had to be attached to the collection tube for support penetration.

Interestingly and in most cases, under such hard surface of sludge was a layer of water before another layer of sludge. This created a scenario whereby excessive water from surrounding non-sampling locations found their way into the collection tube, replacing already collected but loosely held sludge samples.

In some cases as it was observed, very fine sludge particles formed into agglomerates of very high viscosity and compactness to the extent of blocking access to and out of the collection tube. This was particularly the case at sampling location 16. There were also some obvious rock-like sludge formations within the tank which suggests the agglomeration capabilities of the sludge with time.

Furthermore, while the sampling procedure required that samples collected from any single location be subdivided into sample bottles based on sample location depth, it was observed that there was recombination and resettling of particles within the collection tubes. There were areas which were inaccessible as a result of refuse deposit within the tank such as at sampling location "18" which had to be moved 2 cm downwards.

It is also important to note that the cross-wire used was not adequate. The recorded sampled locations could therefore have had errors. Care was taken to minimise errors such as by attaching a metal rod to the collection tube. This was useful in keeping maintaining a vertically downward penetration.
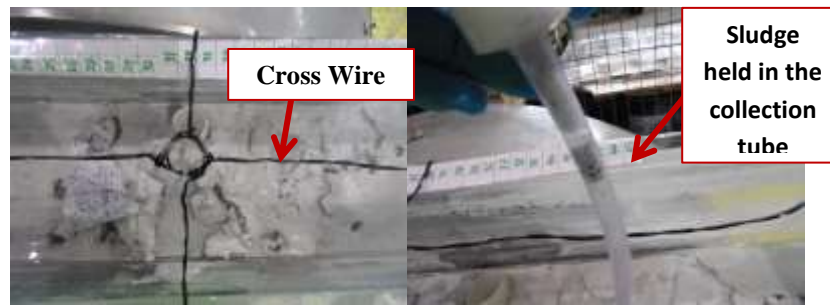
Figure 44: Sludge sample collection set-up. The picture on the left shows the use of cross-wire for sample localisation. The picture on the right shows the use of syringe for sludge retrieval.

4.4.3 Remarks on the Sludge Sampling Regime and Methodology

Unlike in the sludge bed sampling simulations discussed in Chapter 3, this experiment presented a relatively smaller sized sludge bed. The minimal pixel size is the surface area of the sludge sample which can be captured using the sampling device. In a larger sludge bed, this choice of pixel size could be constrained by a limited data processing power, but in this sludge simulant tank of size 1.2 m × 0.3 m, a pixel size of 0.02 m × 0.02 m does not present any significant data processing challenge. Hence, this was adopted as the pixel size.

In using the method of stratified random sampling, grids (or strata) need to be created. While the aim is typically to ensure equal sized square grids, the reliance on historical background could influence the bias in the distribution of grid sizes and shapes. In this particular experiment, the historical background of the sludge bed is that sludge was introduced into the tank by pouring corroded magnesium sludge into the tank, but at a particular location. This location is therefore labelled as 'sample location 1'. In order to ensure that sample is collected at this critical location, the location itself must be made a grid.

In creating other grids, and for the purpose of understanding how the sludge particles filtered into the rest of the sludge tank from 'location 1', the grids were created in a circular shape. This is with background knowledge that filtration into the tank must have occurred in all directions. The number of

sampled locations was made to be 20 only. Physically, it was possible to retrieve more samples and increase the overall sampling intensity. However, doing so would deplete the sludge bed at NNL and affect its use for other research. Secondly, doing so would make the exercise achieve a sampling intensity which is highly unrealistic in a real-life sludge bed on a nuclear site.

The method of retrieving sludge samples from specific pre-determined locations required a method of two dimensional localisation of the sampling device. This informed the decision to use a cross-wire system. However, due to the construction of this cross-wire system, it may not be accurate and may introduce positional errors which would create further uncertainties in the spatially extrapolated results for non-sampled locations. The use of a LIDAR based positional system would have been a more suitable solution.

4.4.4 Laboratory analysis of Particle Size

Prior weighing and measurement of sample volume and density were carried out. The samples were analysed for their PSD using a Malvern Mastersizer 3000TM instrument with method development parameters set as follows:

Sample concentration: 1.0 % v/V [161], average sample density: 1.525 g cm^{-3}, Dispersion medium: Water, Dispersant density: 1.0 g cm^{-3}, Stirrer/pump speed: 2500.0 rpm, Sample refractive Index: 1.559, sample absorption constant: 0.1, dispersant refractive index: 1.33, measuring time: 30.0 seconds, number of runs per aliquot: 5

4.4.5 Experimental observations during analysis

There was the need to combine samples from different depth levels within a sampling location in order to meet the sample concentration requirement of 1 % V/V. This however did not reduce the obscuration levels which ranged from 39 % to about 99 %. This was found to be as a result of the high proportion of tiny particles within the sample volume, thus leading to a high total amount of particles in the sample. A further limitation faced was the limit of 2000 μm recommended for the laser diffraction technique within which measurements can be reliable. This limit may have been exceeded as some particles in the sample were visibly large and results from some

analyses indicated extreme sizes. In fact, high level agglomeration was observed during the analysis of samples from position 13, 16 and 18.

4.4.6 Data Processing

Given the PSD results from only 20 sampling locations out of 900 possible sampling locations, the TDA was used in predicting the mean, lower and upper quartiles and the median size of the PSD at non-sampled locations within the tank. 3-D spatial maps of PSD predictions and percentage confidence were obtained. Attempts were also made to obtain prediction and confidence maps for scenarios where even less than 20 locations were sampled.

The accuracies of these predictions were estimated relative to the result from 20 sampled locations. Accuracy measurements were based on size classification from class 1 to 201. This classification is based on the fact that the Malvern Mastersizer 3000 detects particle sizes within the range 1 to 3500 µm at a resolution of 0.0554 on the logarithmic scale.

4.5 Experimental Results and Discussions

The characterisation map of the sludge simulant bed was obtained and is shown in Figure 45. Similarly, the confidence map was obtained and is shown in Figure 46.
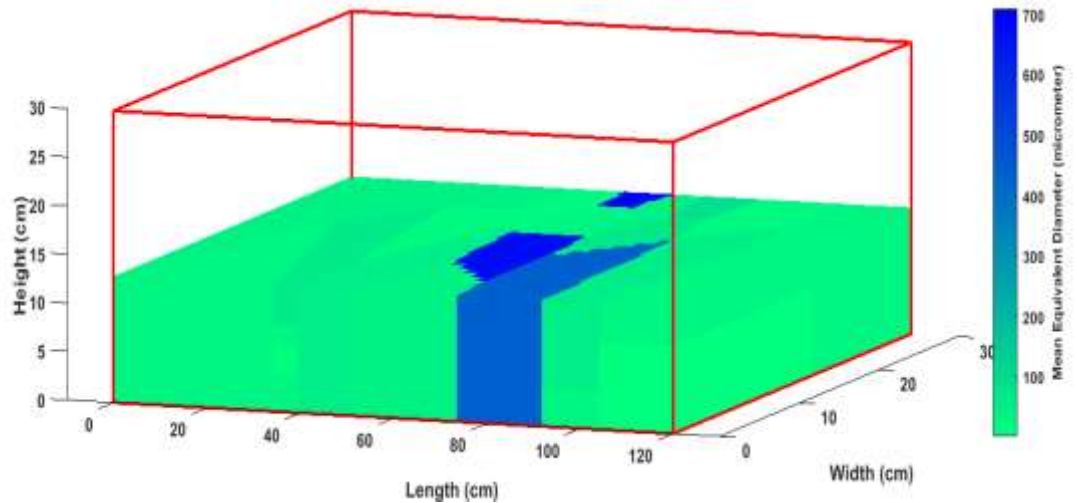
Figure 45: 3-D Characterisation Map of Sludge Simulant Tank at NNL showing Inferred PSD. The different colours show the class of mean particle size which can be found in the different locations. This map was produced by inferring data at non-sampled locations from the data collected at 20 sampled locations. The method of data collection was by the use of a laser diffraction method (Malvern Mastersizer 3000).
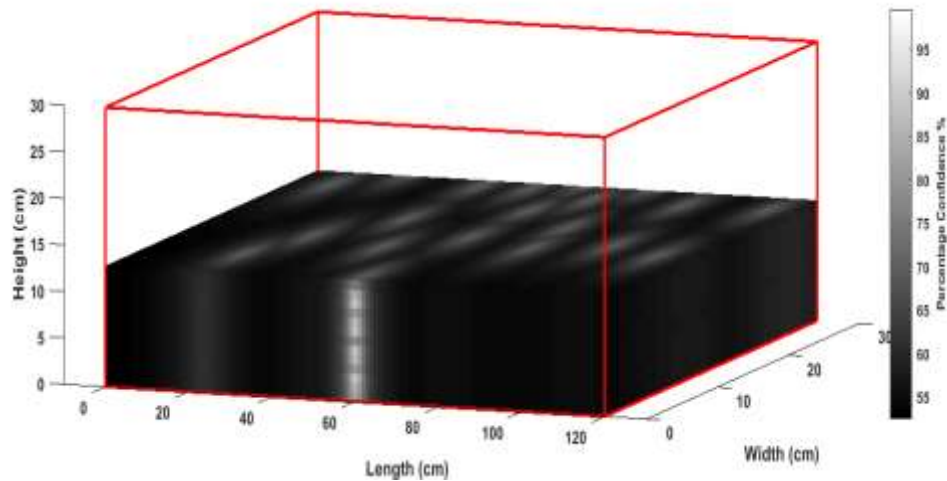
Figure 46: 3-D Confidence Map for the Inferred PSD of Figure 45. This map was generated based on the sampling locations selected for the sludge simulant tank

With 20 being the maximum number of sampled locations across the sludge simulant tank, Figure 45 shows the expected distribution of particle sizes within the sludge bed. Considering that samples from some locations were combined, and the analysis result distributed along the depth, it would appear that the sizes do not vary vertically at some locations. For some other

sampled locations where samples from each depth was individually analysed, there was no fixed pattern of variation along the depth. While some locations had larger particles at lower depths, some had the same mean size at all depths. At position 1 however, it was observed that the particles at the top were larger than particles below.

The reason for this inconsistency may have been the mixing of samples collected from different depths within the collection tube as a result of water in flow from neighbouring locations. This could be understood as suggesting the in adequacy of syringe sampling system for a sludge bed of varying viscosity and hardness.

Figure 46 shows the distribution of percentage confidence when 20 sampled locations are used to make PSD predictions. This % confidence shows the probability of predictions made at non-sampled locations to be true within an error margin of +/- 0.5 of the predicted particle class size (1-201). Considering that the class size increases logarithmically, this tends to favour higher particle size predictions.

In assessing the performance of the accuracy of the PSD predictions and estimated percentage confidence, Figure 46 shows (in black print) the actual mean particle size at each of all 20 sampled locations measured. In red print however are the predicted particle sizes at 12 locations which for the purpose of this test, were deemed to be non-sampled locations and thus were not supplied to the TDA extrapolation algorithm. It can be seen that there is a wide disparity between what was predicted and their actual results. At those positions, the percentage confidence had suggested a close to 50 % probability of the result being within the size class.

4.5.1 Interpreting the Results from the RRA Method on Real-Life Sludge Bed at NNL
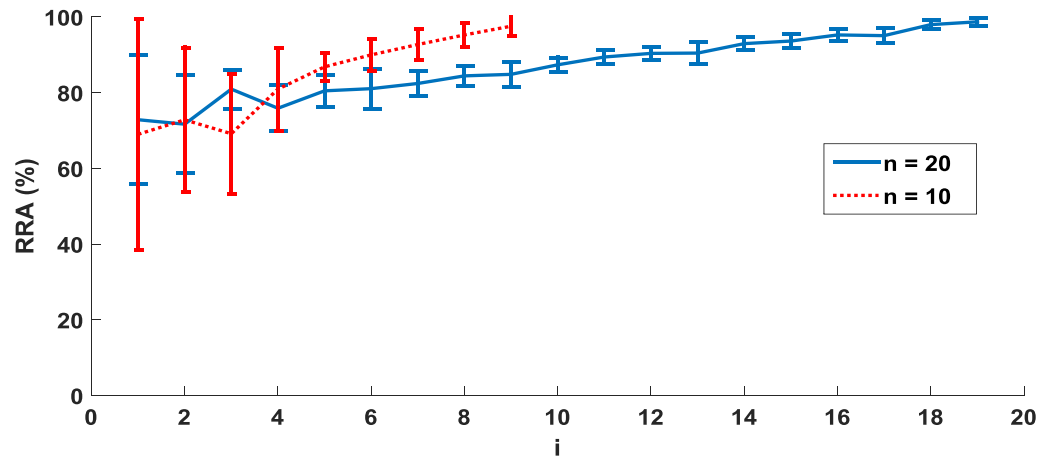
Figure 47: Plot of recursive relative accuracy (RRA) with error bars against number of sampled locations (i) – from experiment. The plot in red was obtained after sampled data from a total of 10 sampling locations were available, while the plot in blue was obtained when the total available sampling locations had been increased to 20.

Figure 47 shows the result of an RRA implementation on the characterization of sludge in the simulant tank at the National Nuclear Laboratory. The RRA algorithm was repeated twice: after practically retrieving samples from 10 locations and subsequently when the number of sampled locations was increased to 20. In both cases, it can be observed that as the number of measurements increases, so too does the relative accuracy of the inference map. This means that every sample contributes extra information about the characterization map of the population.

It is evident that even with 20 samples collected, steady state has not been reached, however it is noticeable that beyond $i = 4$, the slopes of both RRA plots remain consistently low and positive. Hence, the benefits in further sampling may not be entirely significant. This is also an indication of the degree of homogeneity of the sludge characteristics, based on the PSD classification of Chapter 2.

4.6 Summary

A suitable method for estimating the percentage confidence in inferences made has been presented. The resulting percentage confidence maps indicated a visible increase in the spread of confidence in non-sampled locations when there was an increase in the quantity of samples obtained.

The quantity of samples needed for improved map accuracy can be determined by using the recursive relative accuracy (RRA) method. In the simulated exercise, it was observed that with a sampling device of 30 % penetration depth, the maximum map accuracy was about 60 %. The RRA plot suggested that with a penetration depth of 30 % there was limited benefit in sampling from more than 50 locations. While the confidence map provides guidance in choosing areas for further sampling, the *RRA* provides indication of when to stop further sampling.

5 Chapter 5 - Evaluating the Influence of Experimental Factors on Particle Size Distribution Measurement Using Laser Diffraction

5.1 Introduction

Notwithstanding the importance of adequate sludge sampling (as exemplified in Chapters 3 and 4), the success of laboratory analyses of sludge samples is as well critical to the overall objective of a sludge PSD characterisation campaign. This is because such measured data will be relied upon in inferring the PSD at non-sampled positions of the sludge bed. Hence, in this chapter, the focus is on the procedure involved in the laboratory analysis of sludge samples from which measured data is obtained.

Just as PSD is vital for sludge waste management decisions, it is also vital for measuring the quality and efficiency of general industrial products and processes. Evidence can be found in the detergent making [163, 35], drug manufacturing [112, 111], food processing [164, 34], and wastewater management [165, 166] related industries. To this effect, the relevance of PSD has been established by a number of authors [163, 34, 159, 33] with a focus on the quality of measurements obtainable.

To address these quality concerns, seven experimental factors which are suspected to have the potential of influencing result variation have been identified (see Chapter 2). These are factors which relate to the use of Laser Diffraction Method (LDM) as a technique for measuring PSD. They are:

1. Measuring Time
2. Stirrer/Pump Speed
3. Sample Concentration
4. Refractive Index of Sample
5. Absorption Constant of Sample
6. Dispersion Medium
7. Instrument Model

5.2 Background Theory

5.2.1 Sources of Error in LDM

LDM involves the illumination of adequately dispersed samples by a laser beam generated from a monochromatic source [6]. The interactions between this laser beam and individual particles lead to a variety of optical phenomena including laser scattering and absorption [43]. Smaller particles produce a lower intensity scattering while larger particles produce higher intensity scattering. Similarly, the scatterings due to smaller particles are at wider angles compared to that due to larger particles. Forward scattered lights are detected and recorded by multi-element detectors, and characterised by their angle of scattering and the intensity as expressed in Equation (15). This recorded data provides a signature which is mathematically translated to a volumetric particle size distribution by method of de-convolution and using an appropriate mathematical algorithm such as the mie algorithm or Fraunhofer approximation.

$$\begin{array}{c} De-\text{convolution} \\ I(\theta) \qquad \rightarrow \qquad v(x) \end{array} \tag{15}$$

Where, $I(\theta)$ is the angular intensity distribution and $v(x)$ is the particle size distribution obtained by de-convolution using a pre-determined scattering theory and mathematical model.

The data interpretation process either takes into consideration the optical property of the sample components or makes appropriate assumptions about them, as well as about the shapes and condition of the measurement cell. In all of the steps involved, a few sources of likely errors are likely, they are discussed below.

1) Errors due to technicalities

   There are few aspects in the design of laser diffraction method that are bound to introduce some random errors. One of these technical errors is the assumption that scattered patterns originate from spherical particles. Thus, any deviation of the real shape of a particle from the ideal spherical

shape will introduce uncertainty in the measurement outcome. Another assumption made is that the scattering signature recorded during measurement is the sum of all individual scatterings received [6]. This implies that all scatterings, with the inclusion of multiple scatterings are all recorded as single scattering. This will result in technical error.

In addition, the record of scattering angles is only as definite as the physical stability of the optical bench on which detectors are mounted, the focus lenses and the light source. In the event mechanical disturbances caused by electrical noise or wind draft, there could be a disturbance to the pre-set optical alignment. Any such disturbance causes the LDM instrument to lose calibration. In the Malvern Mastersizer 2000 instrument, this disturbance leads to downtime of about three minutes.

Lastly, the resolution of particle sizes measured is dependent on the number of detectors in place. Hence, with inherent limitations in the obtainable size measurement resolution, technical errors may be unavoidable.

Technical errors may however be avoided by adopting precautions such as the following:

a) Ensure that samples are dispersed in a suitable dispersion medium such as diluted water at an adequate concentration and that such dispersion is sufficient to maintain adequate laser obscuration; preferably 5 % to 25 % [6] depending on the size of particles involved. This is to reduce the likelihood of multiple scattering. A modified algorithm that reduces technical errors in the data interpretation process was proposed by a study on LDM [167]. Another study [168] also sought to improve the robustness of data interpretation algorithms by proposing a 'mahalanobis' distance.

b) Place the instrument on a rigid bench and away from electrical, mechanical and thermal noise to avoid realignment of the optical bench [6].

c) Proper calibration tests should be performed on the instrument to identify any existing system bias [6].

d) Run the experiments more than once to detect random errors.

2. <u>Errors due to sample preparation</u>

To determine the particle size distribution of any given sample, as earlier mentioned, it is advisable to run the test more than once. Hence, the first step in reducing result variation is the division of a bulk sample into the corresponding number of test samples, known as an aliquot. It must be ensured that the aliquots are 'representative' of the bulk sample. This is done by coning [7] or by using a rotary riffler [6] to achieve an unbiased distribution of heterogeneous particles in each aliquot.

This does not totally eliminate sampling errors, but any attempt to distribute samples manually may increase the likelihood of an error thereby rendering the results invalid. It has been pointed out [43] that sampling errors are possibly the greatest errors in laser diffraction method, especially if the data being sort is a percentile data such as the D90. The reason is that LDM is volume sensitive, and any drop in volume of either larger or smaller particles will create a significant shift in the volumetric particle size distribution. In fact, the British standard [6] discourages the use of such specification based data.

The second step in sample preparation is the selection of an adequate dispersant. There have been arguments concerning the need to investigate the role of dispersant suitability on result variation. In a study, Dias [122] considered the effect of using deionized water and using sodium hexametaphosphate $Na(PO3)6$ (SHMP). The argument had always been that SHMP helps to prevent agglomeration of particles, but after a series of experiments, Dias concluded that the suspension medium has an insignificant effect on the results, with the exception of a 74% glycol solution that resulted in a consistently lower median gran size. This only supports calls for further investigation into the role of a dispersion medium in affecting analytical uncertainty. On the use of water as a dispersant, and choice of pH, [43] makes a case for deionized water on the basis that tap water may introduce flocculation.

Finally, sample concentration is equally critical. As mentioned previously, adequate sample concentration is necessary in attaining an appropriate laser obscuration. It has also been observed that the wider a particle size distribution is suspected to be, or the bigger the particle sizes are in general, then the higher the volume of samples required in an aliquot while maintain concentration [43].

3. <u>Errors due to method development</u>

One of the first steps to take in a laser diffraction experiment before running the samples into the measurement zone is to mechanically excite the samples and keep them unsettled for optimal sample dispersion. To do this, there are three complementary methods that may be employed; the use of a stirrer, a pump, and sonification [43].

The stirrer speed and sonification agitate the particles, thus preventing agglomeration while the pump speed allows for flow alignment [43] especially where the particles have high aspect ratios. However, the speed at which agitation and pump are set to must not be too high as to cause primary particles to break up. It is also noteworthy that more dense particles would require higher agitation [43].

The measurement time is another critical factor to consider. It is expected that the longer the measurement duration, the higher the precision. Although excessively long measurement duration will be inefficient, obtaining an unrepresentative result due to insufficient measurement time must be avoided [43].

Storti and Balsamo [119] in a test of laser diffraction technique under a number of conditions, observed that while low strength materials are susceptible to errors due to the choice of agitation, pump speed and measuring time, high strength materials are not affected. Nonetheless, it may be interesting to determine the limit at which agitation could begin to affect material strength.

5.3 Laboratory Experiment to Investigate Influence Factors related to Laser Diffraction Method

The challenge is to investigate the influence factors involved in LDM technique using an ANOVA test. This test will be conducted on results obtained from laboratory data. There are two forms of experimental data which may be used to represent a PSD; mean size of particles, or the percentile values of the distribution such as D90 or D10.

To evaluate the contribution to PSD result variance of the experimental factors, a laboratory experiment is required. For this purpose, soda-lime glass microspheres of well-defined characteristics were purchased from Whitehouse Scientific Ltd. 100 bottles each containing 10 grams were purchased. The density of the glass beads was given as $2.49 \, g \, cm^{-3}$. The particle size range of each bottle was 170 μm – 710 μm. This was the widest PSD range available within the 10 nm – 1500 μm suitable for LDM application.

When re-distributing samples into aliquots, it is important to avoid bias. One instrument that is recommended for unbiased distribution of samples is a rotary-riffler. In this experiment, a rotary-riffler (shown in Figure 48) was constructed at low cost and used to obtain sub-samples of 2.5 grams and 4 grams aliquots (depending on the intended sample concentration).

Inclined Funnel

Collection Bottles

9V Battery
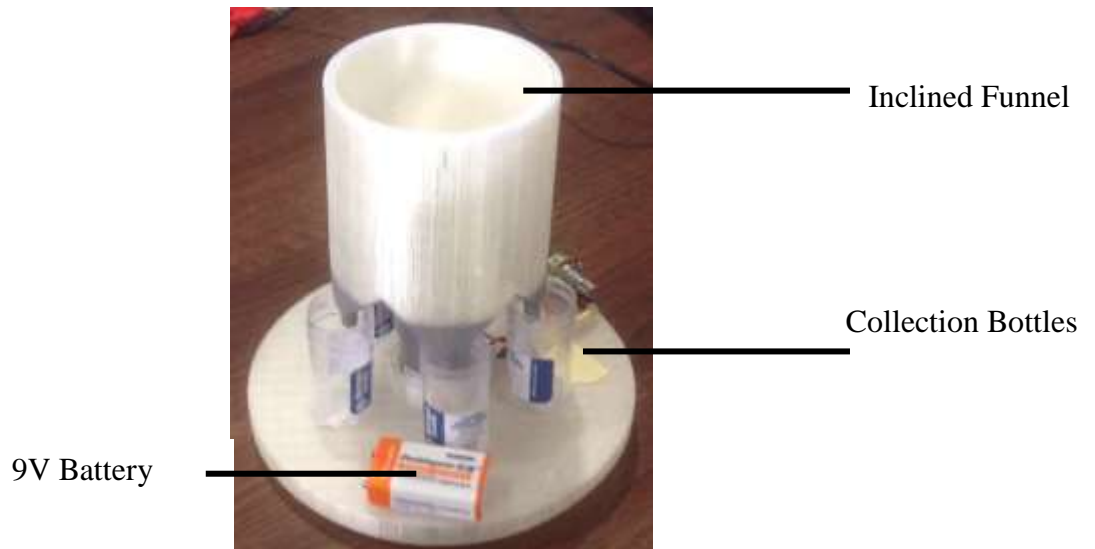
Figure 48: In-House built rotary riffler for unbiased distribution of samples. It allows for a continuous spin of the funnel or of the cups while the other part remains static.

Other materials used include: SHMP, tap water, weighing scale, Malvern Mastersizer 3000^{TM} at the National Nuclear Laboratory (NNL) Workington, United Kingdom, the Malvern Mastersizer 2000^{TM} at The Mill, The University of Manchester, United Kingdom, and the use of MATLAB.

5.3.1 Method

A statistical tool used in analysing the influence of k number of experimental factors on PSD result variance is the 2^k analysis of variance (ANOVA) test [36]. This test involves the repetition of an experiment $m \times 2^k$ number of times. After every run, the experimental conditions are changed and this is repeated from one run to another.

To vary the experimental conditions, a pair of contrasting "high" and "low" settings should be determined for each of the k experimental factors under investigation. 2^k represents the total number of unique experimental conditions (treatments) available and m is the number of experimental runs subjected to the same treatment.

In compliance with the procedure for conducting a 2^k ANOVA test, a total of 256 aliquots of soda-lime glass microspheres were required. PSD measurements were conducted on each of them using the principle of LDM as

represented by the Malvern Mastersizer Instrument. The measurements were conducted in the laboratory under varying experimental conditions.

There were 128 unique experimental conditions (treatment) to choose from. Each treatment was characterised by a unique selection of experimental conditions based on "high/low" settings of the experimental factors (Factors H to N) under investigation, as given in Table 7.

Table 7: A summary of experimental factors and their contrast settings

Factors	Description	Low Setting	High Setting
H	Measuring Time	10 Seconds	30 Seconds
I	Stirrer/Pump Speed	1500 rpm	3000 rpm
J	Sample Concentration	0.5 %V	4.0 %V
K	Refractive Index of Sample	1.52	1.9
L	Absorption Constant of Sample	0.1	1.0
M	Dispersion Medium	Tap Water	SHMP
N	Instrument Model	Malvern^{TM} 2000	Malvern^{TM} 3000

Each treatment was applied to the PSD measurement of 2 separate aliquots of soda-lime glass in order to allow for random errors resulting from irregular aliquot distributions. There were only 2 aliquots per treatment due to limited material resources. Further repetitions were made by repeating the PSD measurement of each aliquot 10 times within the Malvern Mastersizer instrument.

Of the 256 aliquot technically required for this test, only 64 aliquots were physically required. This is because Factors K and L (the absorption constant and refractive index) represent optical parameters. Variations in these two factors were simply implemented offline on the mathematical interpretation

algorithm of raw LDM data. This reduced the number of required aliquots from 2^7 to 2^5.

At the end of the laboratory experiment, all PSD results are collated and statistically analysed on MATLAB to determine the F-ratio statistics [148], half-normal plot of effects [157], and Eta-squared effect [158]. These provide a measure of the influence of each factor on PSD result variation. They also indicate the degree of interactions that may exist among experimental factors.

PSD results may be represented by the mean value, or by a measure of the spread. A number of field operators are more interested in the measure of spread of PSD rather than the mean PSD. However, the British Standard [6] cautions on the reliance on PSD spread as a parameter. The reason is that LDM is volume sensitive, and any drop in volume of either larger or smaller particles will create a significant shift in the cumulative curve, thus affecting the percentile values [43].

This study will however analyse the results of both the PSD mean and the PSD spread. The measure of PSD spread used is the ratio of the 90th percentile to the 10th percentile (D90/D10) of the particle size distribution.

5.4 Results and Discussions

5.4.1 ANOVA Test for PSD Measurement

F-ratio statistic provides an indication of how significant the contribution of a factor is to result variation. An F value greater than "1" implies that the factor is of significant influence. Table 8 and Figure 49 show the F-ratio statistic (F) and Probability values (P) of the ANOVA test for the seven experimental factors under investigation.

However, a "type I error" [150] which in statistical hypothesis testing refers to the acceptance of a "false positive" finding may occur. The probability of a type I error occurring is represented by the P value. Where P is less than 0.05, it is more than 95 % probable that the F-ratio statistic value is true.

144

Table 8: Abridged ANOVA table showing F-Ratio Statistic (F) and Probability (P) values for experimental factors of influence on PSD mean

	PSD Spread (D90/D10)		PSD Mean	
Factor	**F**	**P**	**F**	**P**
H	9.87	0.00	0.43	0.51
I	0.16	0.69	0.91	0.34
J	0.46	0.50	61.32	0.00
K	58.15	0.00	0.01	0.94
L	36.25	0.00	0.00	0.98
M	24.83	0.00	0.08	0.77
N	7.37	0.01	359.32	0.00
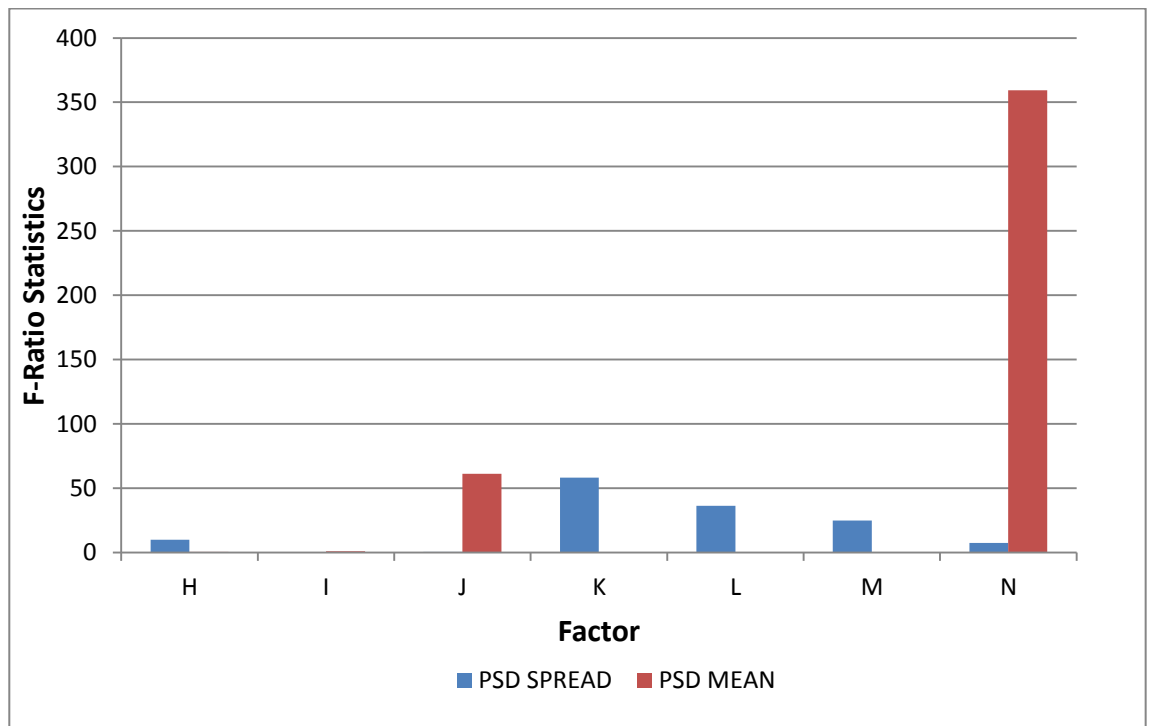
Figure 49: Chart Showing F-Ratio Statistics for all factors related to laser diffraction method. This chart shows the significance of each of the seven experimental factors related to particle size analysis to the variation of the result of particle size measurements using a laser diffraction method based Malvern Mastersizer.

It can be seen from Table 8 that Factors J and N (the sample concentration and the instrument model used) are the only two factors of significant influence to variations in the result of mean PSD observed. However, variations in PSD spread (D90/D10) values are more significantly influenced by Factors K, L and M (the optical parameters and the dispersion medium used).

Factors H and N (measuring time and the instrument model used) also have some significant influence on variations is the PSD spread observed.

Similarly, the presence of factor interactions can be observed on

Table 9. The table shows only the four most significant two-way factor interactions present. Factor interaction refers to the degree of mutual dependence in the contribution of two or more factors to result variations. This indicates that choosing a certain pair of settings for two interacting factors may influence the PSD result [169].

The most significant factor interactions occurred between Factors I and N (stirrer/pump speed and the instrument model used) with an F-ratio statistic value of 169.8.

Table 9: Abridged ANOVA table showing F-Ratio Statistic (F) and Probability (P) values for experimental factors of influence on PSD mean

PSD Spread (D90/D10)			PSD Mean		
Interactions	F	P	Interactions	F	P
IN	40.92	0.00	IJ	29.99	0.00
JK	38.11	0.00	IM	17.67	0.00
KM	51.32	0.00	IN	169.8	0.00
LM	36.62	0.00	JN	43.52	0.00

5.4.2 Half-Normal Plot of Effects for PSD measurement

The half-normal plot of effects provides a graphical representation of the influence of each experimental factor. It involves the calculation of the absolute value of standardised effects and plotting these values against the theoretical half-normal distribution probabilities. The algorithm for implementing this is well established in a number of literatures.

Figure 50 and Figure 51 show an abridged half normal plot of effects in regards to the influence on PSD mean and PSD spread results respectively.
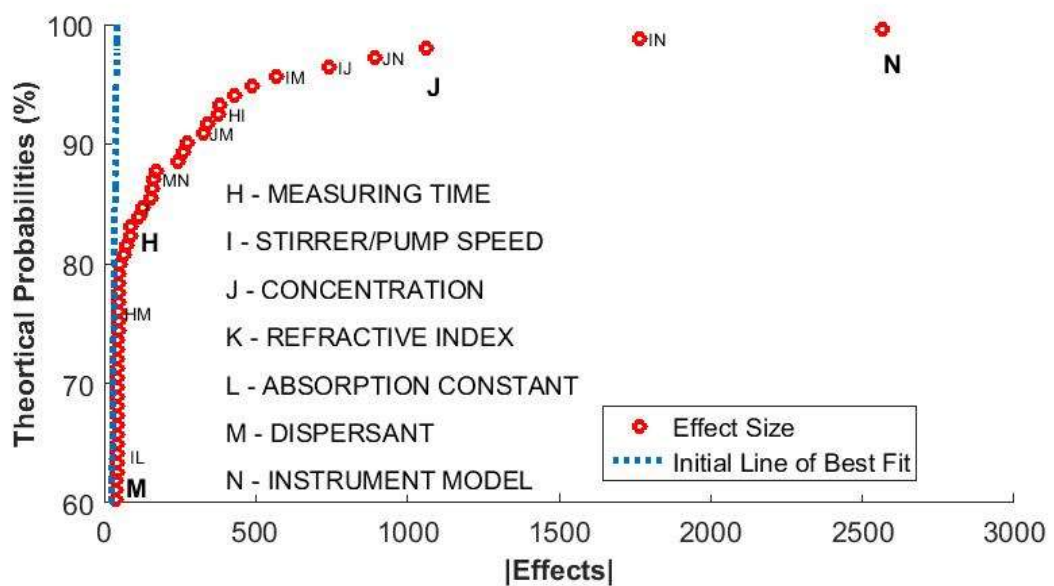
Figure 50: Half-Normal plot of effects - PSD mean. This figure indicates how significant a main factor or factor interaction is to the variation of the result of an inferred map. The significance is assessed by the distance of the red dot (the observed effect of a given factor or factor interactions) from the blue line (a line of best fit from the 10 lowest effect sizes). The 10 lowest effect sizes with which the blue line of best fit was drawn are not seen in the figure for the purpose of high resolution.
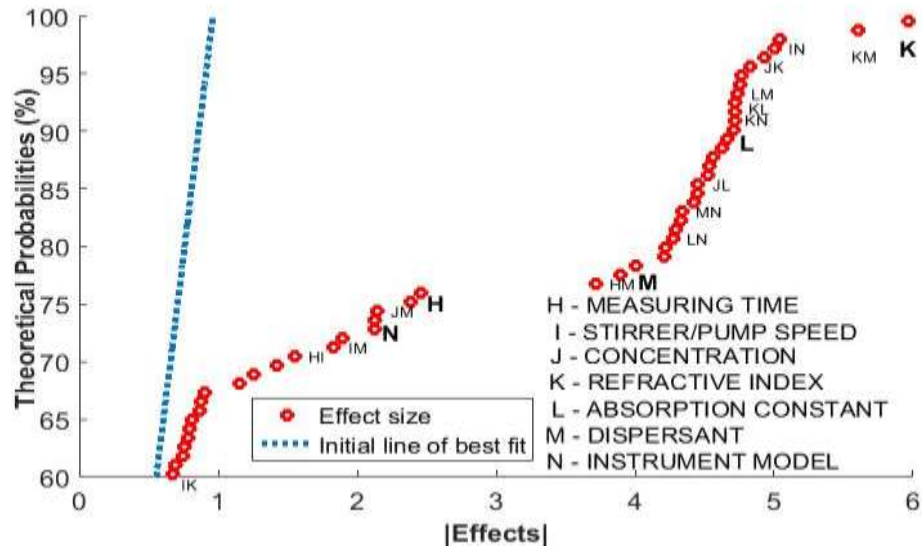
Figure 51: Half-Normal plot of effects - PSD D90/D10 Ratio. This figure indicates how significant a main factor or factor interaction is to the variation of the result of an inferred map.

To reduce congestion on Figure 50 and Figure 51, only a few of the red dots have been labelled. It can be seen on Figure 51 that Factor N (Instrument model used) had the most significant effect on PSD mean result variation. The figure also shows that Factor M (the dispersion medium) had no significant effect.

On Figure 51 however, Factor K and L (optical parameters) can be seen to have the most significant effects on the PSD spread result.

5.4.3   Eta-Squared Effects for PSD measurement

To quantify the actual contribution of individual experimental factors to PSD result variation, a statistical tool known as the eta-squared effect can be used. The eta-squared effect [170] of a factor is obtainable from the ANOVA table as a ratio of the sum squared due to changes in settings within that factor to the total variance observed in the 2^k ANOVA test.

Table 10 shows the eta squared effects of the experimental factors on PSD measurement. Similarly, Figure 52 provides a bar chart representation of this result.

Table 10: Eta-squared effect of the experimental factors on PSD results

	Eta squared effect (%)	
Factor	**PSD Spread**	**PSD Mean**
H	0.78	0.05
I	0.01	0.10
J	0.04	6.94
K	4.61	0.00
L	2.87	0.00
M	1.97	0.01
N	0.58	40.66
Interactions	78.94	37.74
Residual	10.20	14.50
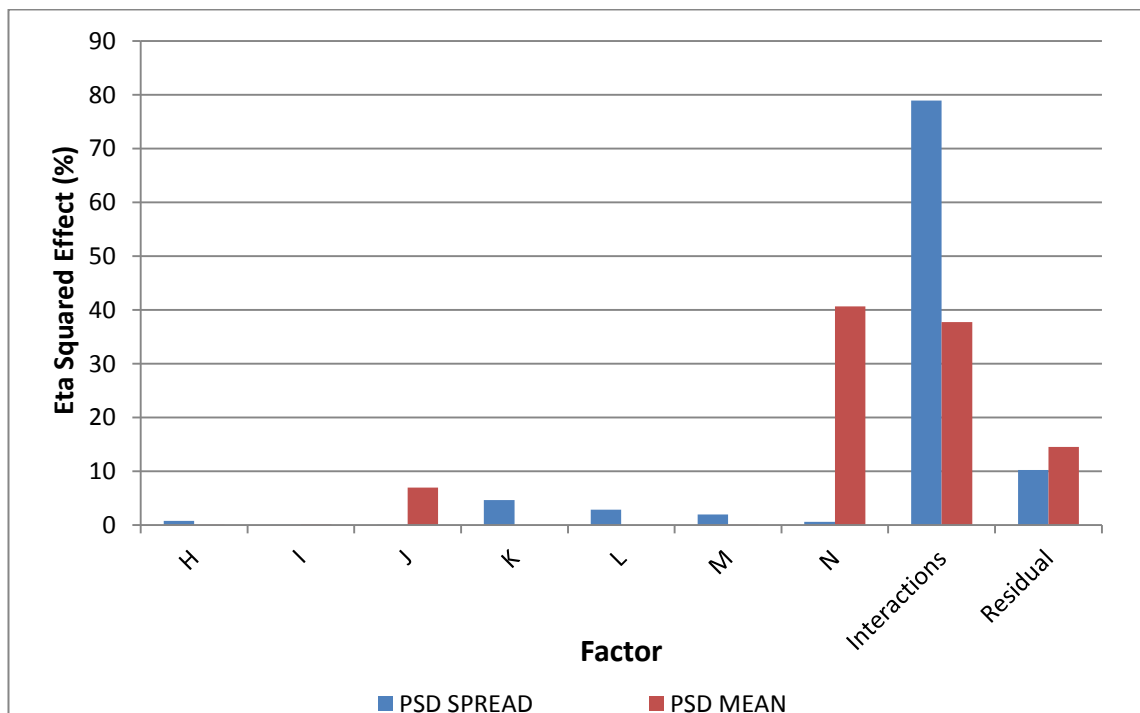
Figure 52: Bar Chart showing Eta-Squared Effects for Factors related to laser diffraction method. The result in this chart pertains to the mean particle size measurements obtained from a series of experiments involving soda-lime glass microspheres from Whitehouse Scientific Laboratory, UK.

From Table 10, it is evident that factor N (the instrument model used) contributed 40.7 % of the total influence on result variation in PSD mean measurements, while factors K, L and M (Optical parameters and the dispersion medium used) had the least effect. About 37.7 % of the total influence was as a result of multi-factor interactions.

Similarly, with regards to their influence on PSD spread variations, the most influential factors observed were Factors K and L (the optical parameters − refractive index and absorption constant) with effect sizes 4.61 % and 2.87 % respectively. However, the highest contributions to result variations were observed to be due to multi-factor interaction. This contributed a total of 78.94 %.

The residual factor which refers to unknown sources of random errors was observed to contribute significantly to result variations. It had a contribution of 14.5 % to PSD mean results and 10.2 % to PSD spread results.

5.4.4   Remarks

It has been observed that Factors N (the instrument model used) and J (sample concentration) had the most significant influence on the variation of the PSD mean size result observed. This observation is in agreement with theoretical expectations [43].

Laser diffraction method is sensitive to laser obscuration levels within the sample. Hence, any variation in sample concentration will cause variations in laser obscuration. This will therefore affect the accuracy of the PSD measurement.

Furthermore, the half-normal plot of effects indicates a significantly high interaction (JN) between the sample concentration (J) and the instrument model used (N). This was also observed for the interaction (IN) involving the stirrer/pump speed (I). This underscores the influence of agitation on laser obscuration level.

While the sample concentration factor (J) was observed to have significant effect on PSD mean results, it did not have a similar effect on PSD spread (D90/D10). This may imply that the PSD spread parameter, being a ratio of

the upper and lower percentile, would not change in a case where both percentiles D90 and D10 are affected in equal proportion by any factor.

5.5 Conclusion

The variance recorded in PSD results obtained by repeating such experiments is a measure of the uncertainty caused by any variations in experimental conditions, as well as residual random experimental errors. This also translates to a measure of percentage confidence in the results obtainable in any single experiment.

The choice of the instrument model (a choice between the Malvern Mastersizer 3000 model and the Malvern Mastersizer 2000 model) used for the PSD measurement and the choice of the sample concentrations (a choice between 0.5 and 4.0 % V) are two experimental factors which are directly responsible for 40.66 % and 6.94 % (respectively) of the variations in PSD mean size results observed across experiments. This is based on an assumption that the samples used across experiments are of the same true PSD value. Similarly, the measuring time, optical parameters, dispersion medium and the type of instrument model used all affect the variations of the PSD spread results observed. Indirect contributions to variations may be attributed to multiple factor interactions and random experimental errors.

It is therefore important to decide on a unique setting for each influential experimental factor. By doing so, contributions to uncertainty will significantly reduce and cross-campaign confidence will improve.

6 CHAPTER 6 – Evaluating the Cross-Campaign Confidence in a Sludge Characterisation Campaign

6.1 Classification of Errors

Errors are classified into two; random errors and systematic errors. Random errors affect precision and introduce variability in results while systematic errors affect accuracy and introduce a bias in the result. Reducing random errors, and consequently, reducing variability, generally requires an increase in sample size, an improvement in analytical methods and an increase in the number of observations [171] [172] [72]. While random errors can be statistically determined, systematic errors cannot, thus the need for adequate calibration of instruments before use [173] [174]. In cases where the magnitude and direction of a systematic error is largely unknown, such an error cannot be eliminated [72].

In analysing uncertainties however, one may only focus on random errors [174] or 'technical errors of measurement' (TEM) as considered by Harris and Smith [149] where TEM was explained to be a part of the residual variance in a statistical test which if analysed, provides a basis for determining statistically significant differences. Technical errors are usually due to a number of sources of variability such as data collection method, instrument used, sample handling and any other procedural variability.

The remaining residual variance may be due to having different operators, or differences in samples analysed as suggested by Cameron [175]. It may therefore be sufficient to centre the discussion on errors on two broad classes; technical (or procedural errors) and general random errors. For example, if an operator who is required to prepare a 1% sample concentration goes ahead to prepare a 1.2% concentration, such a flaw may introduce a procedural error especially where sample concentration has been established to be a major influential factor. If the contribution of this error has been earlier quantified, it may be possible to reverse its effect. The issue of uncertainty becomes vital

where one is not sure of the procedural flaws that may have been involved in the course of several experiments.

It is important to make clear that there may be a minor conflict in the choice of nomenclature amongst researchers in this field. Batista-Fouget *et al.* [148] while maintaining the concept of random and systematic error classification, suggests that systematic errors may be further decomposed into two components; bias and variance, where the variance component is the error introduced by varying the experimental methods or influence factors. It is however easy to see that there is a consensus in that errors may be categorised based on their sources as follows; bias of the system, variability of the procedure and noise.

6.2 Adoption of Eta-squared Effect as a Tool for Variance Harmonisation

In investigating the influence of different experimental factors to variance, there are three steps; the first step is to identify the sources of uncertainties in an experiment, the second step is to estimate the uncertainty in each component that makes up the overall result, the third step is to combine the individual uncertainties to give the overall uncertainty in the final result [176] [173]. Combining individual uncertainties is commonly done by the method of error propagation as discussed in the uncertainty analysis of non-destructive nuclear waste assays [177].

It has however been mentioned that the mathematical method of error propagation as extensively explained in [178] is only applicable when there exist a mathematical relationship between the error variables [173], in the absence of which a statistical method becomes most appropriate.

Thus, the use of t-test and ANOVA test [148] [149] have been suggested as viable statistical methods. Other methods have been suggested such as the test-retest, intra test and the inter-rater reliability tests [149]. In bringing all of these individual uncertainties together to form the overall uncertainty, the eta-

squared effect value (described in Chapter 3) becomes a useful tool [158]. Similar to the eta squared effect value are the partial eta squared effect, the omega squared effect and the epsilon squared effect values [158] which have their advantages and disadvantages when compared to the use of the eta-squared effect value η^2 as recalled in Equation (16).

$$\eta_i^2 = \frac{SS_{between}}{SS_{total}} \tag{16}$$

Where $SS_{between}$ is the sum square between the two treatment group as categorised by settings within the factor i and SS_{total} is the total of all sum squares. Thus, the eta-squared effect of an experimental factor is a ratio of a factor's contribution to variance and the total variance observed in the ANOVA test.

The eta-squared effect when calculated for all influence factors, factor interactions and the residual (unexplained) error, indicates their proportional contributions to the overall uncertainty. By decomposing the overall uncertainty into controllable and uncontrollable uncertainty; where the controllable uncertainty refers to the contributions of influence factors and interaction of factors, while the uncontrollable uncertainty refers to the residual error inherent in the experiment, it thus can be suggested that by conducting an experiment using any procedure, the random error variance observed can be extrapolated to infer an overall variance which takes account the potential impact of procedure variation. This provides a platform for the comparison of experimental results obtained by different operators. Furthermore, it can be suggested that by restricting procedure variation, a certain fraction of the overall uncertainty can be eliminated.

For example, consider an experiment to determine the influence of two factors namely: "duration" and "temperature" on the electrical energy consumed by a kitchen oven. Given that at the end of an ANOVA analysis, Table 11 was obtained as a summary of the ANOVA results:

Table 11: Summary of an ANOVA test (For illustration purpose only)

Factor	Sum Squared (J^2)	Eta-Squared Effect (%)
Temperature	1355.34	40.31
Duration	600.20	17.85
Temperature*Duration	407.98	12.13
Error (residual)	998.54	29.70
Total	**3362.06**	**100**

Therefore, uncontrollable variance is equal to 29.7% of overall variance inclusive of procedure variation. Overall variance is (100/29.7) times the residual variance.

If a number of runs of the experiment is conducted using a particular Duration and Temperature Setting, and a variance of 65.5 J is observed, then the overall experimental variance can be estimated for experiments involving variable Temperature and Duration Settings. Based on the Eta-Squared Effects of Table 11, if a number of operators repeat the same experiment, each using a randomly different procedure, then the overall experimental variance will be;

$$Overall\ variance\ = \left(\frac{100}{29.7}\right) * 65.5\,J\ =\ 220.5\,J \qquad \textbf{(17)}$$

Furthermore, considering that factor 'Temperature' accounts for 40.3% of the overall variance, it implies that if all operators are instructed to stick to the same procedural setting under factor 'Temperature', say all operators are instructed to use a temperature of 40 degrees Celsius, the overall variance is reduced by 40.3%. The contribution of factor interaction 'Temperature*Duration' to uncertainty can be further decomposed by conducting further correlation analysis. Factor interaction means that the effect of one factor is affected or determined by the setting of another factor.

6.3 Method of Variance Harmonisation

The eta-squared effects of experimental factors obtained in Chapters 3 and 5 indicate the percentage influence of the identified experimental factors on result variability. In making use of these eta-squared effects to determine the cross-campaign uncertainty associated with a sludge characterisation map result, the flowchart in Figure 53 provides an algorithm. The algorithm describes how the uncertainty contributions of the various experimental factors can be harmonised to produce the overall cross-campaign uncertainty in sampled data as well as in predicted data. The key to the flowchart is as follows:

LV: Laboratory observed variance due to random errors during experiments. LV is obtainable from laboratory data; hence it is a known value.

AnV: This is the analytical variance and it is caused by variability in analytical procedures as influenced by analytical factors and their interactions: {H, I, J, K, L, M, N, HI, HJ, . . ,HIJKLMN, residual r}. The percentage contributions of each of these factors and interactions have been calculated as shown in Table 10 of Chapter 5. The 'residual r' component here represents the LV value.

SmV: This is the sampling variance and it is caused by variability in sampling procedures as influenced by sampling factors and their interactions: {A, B, C, D, AB, AC, . . . ABCD, RESIDUAL R}. The percentage contributions of each of these factors and interactions have been calculated as shown in Table 6 of Chapter 3. The 'RESIDUAL R' component here represents the AnV value.

SpV: Spatial Prediction variance (applicable to predicted data for non-sampled locations) SpV is obtainable from the spatial extrapolation algorithm method used and hence it is a known value but unique to each spatial position. It has a value of zero for data at sampled locations.

Also, let 'r %' and 'R %' represent the percentages of residual components in the analytical and sampling uncertainties, respectively.
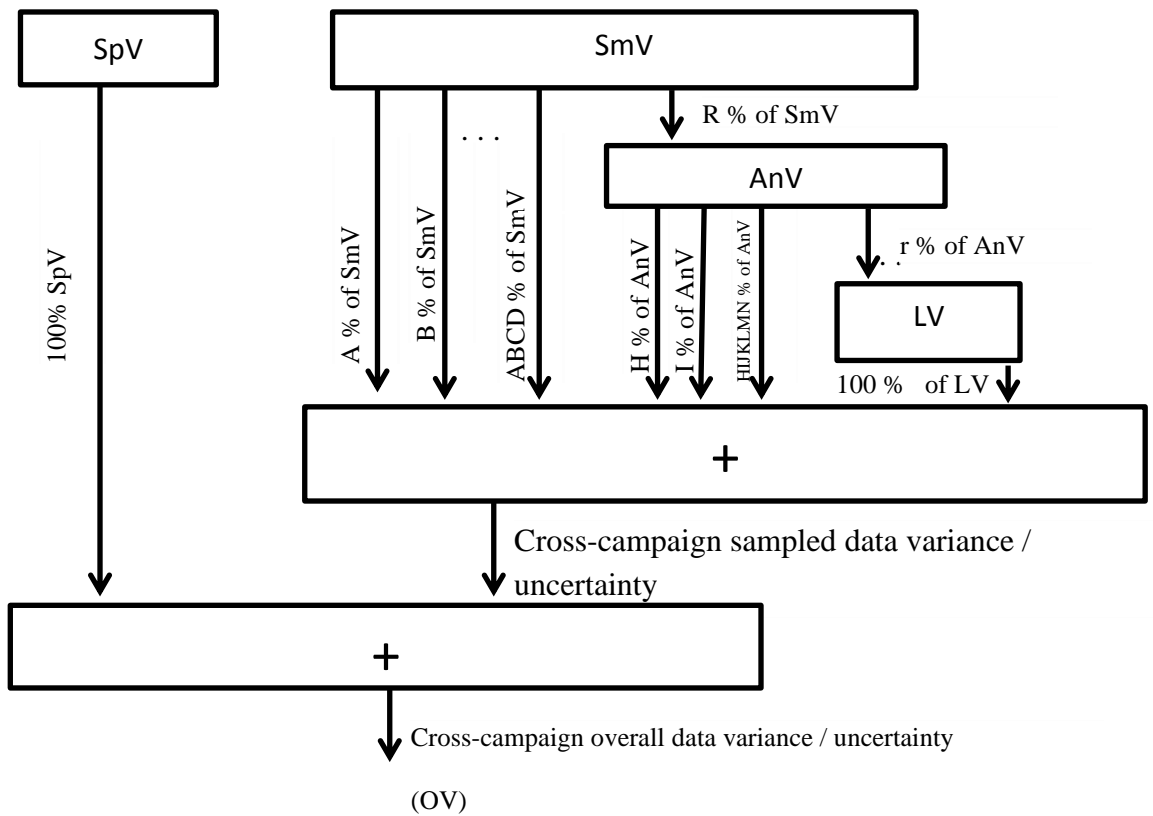
Figure 53: Chart showing variance harmonisation. shows the inter-relationship amongst the various percentage contributions and how this can be used to estimate the overall confidence.

$$LV \; = \; r \; \% \; of \; AnV \tag{18}$$

$$LV \; = \; r \; \% \; of \; (R \; \% \; of \; SmV) \tag{19}$$

$$LV \; = \; \frac{r * R}{10^4} of \; SmV \tag{20}$$

$$SmV \; = \; \frac{LV}{r * R} * 10^4 \tag{21}$$

$$OV \; = \; SpV \; + \; SmV \tag{22}$$

$$OV = SpV + \frac{LV}{r * R} * 10^4 \qquad \textbf{(23)}$$

For example, in applying Equation (23) to the outcome of an experiment, where R and r have values 10.0 and 14.5, respectively;

$$OV = SpV + 69\ LV \qquad \textbf{(24)}$$

<u>Remark</u>

Equation (24) provides a relationship between the variance observed in the laboratory result and the overall variance of the experimental result. This is however a worst-case scenario in which all experimental factors have been made to contribute (according to their eta-squared effect) to the overall variance. This is evident in Equation (19) where the two residual components are only a certain percentage r% and R% of the AnV and SmV respectively.

In cases where the setting of any influential experimental factor is known to have been kept constant across campaigns, then its contribution to overall variance becomes zero, and the residual component increases in percentage. This therefore reduces the overall variance calculated.

In the best-case scenario where the settings of all influential experimental factors are kept constant across campaigns, the two residual components assume values of 100 %. By substituting the new values of r and R into Equation (23), Equation (26) is obtained. This equation indicates that in the best-case scenario, the overall variance at any sampled location is only a function of the laboratory variance observed on sampled data and the spatial variance as obtained from a confidence or variance map discussed in Chapter 4.

$$OV = SpV + LV \qquad (25)$$

Therefore, in an attempt to harmonise the results of sludge characterisation carried out by two or more different teams, the method of variance harmonisation can be

adopted. This provides a tool for laboratory-to-laboratory comparison meetings when held.

6.4   Summary

In this chapter, the need to estimate errors and uncertainty was discussed. The relationship between data variance and uncertainty was also highlighted. In order to identify data variance due to procedural variability in sampling and analytical procedures, and the effect of influence factors on result confidence, the use of statistical tools such as ANOVA and eta-squared effects was discussed. Going forward, sampling simulations and analytical experiments will be conducted to obtain results that will be run on separate ANOVA tests to evaluate the effect of sampling and analytical factors on single-campaign and cross-campaign percentage confidence. However, combining both the sampling and analytical factors in one ANOVA test is unlikely because the sampling will be conducted by computer simulation while the analytical experiments with be conducted in the laboratory.

7 Chapter 7 – The Feasibility of using Ultrasonic Spectroscopy to Measure the Particle Size Distribution of Underwater Radioactive Sludge

7.1 Introduction

The measurement of PSD of the radioactive sludge in a nuclear storage pond may be conducted *ex-situ* or *in-situ*. However, with *ex-situ* methods, the process of sample collection, handling and preparation prior to analysis may introduce uncertainties to the PSD results obtained. Discussions about the influence of certain experimental factors involved in sludge sample collection and laboratory analysis are contained in Chapters 3 to 6.

Furthermore, the challenge of retrieving an adequate amount of radioactive sludge as well as providing adequate storage for them involves a significant amount of time, man-power, logistics, and cost. As an alternative, this chapter considers the feasibility of an *in-situ* measurement of the PSD of radioactive sludge underwater.

In-situ methods generally provide improved safety and accessibility, and the possibility of a reduction in experimental uncertainties. For example, the use of an underwater remote operated vehicle (ROV) to carry a mobile PSD analyser around the pond enables an improvement in the number of sampling locations. According to findings in Chapter 6, this is capable of reducing result variations by 4.4 %.

In addition to increasing the number of sampling locations, an ROV also has the ability to access locations within the pond which may be considered inaccessible to humans. It is therefore expected that by *in-situ* sampling, such as the use of an ROV, there would be improvement in the sampling strategy factor. According to findings in Chapter 6, this factor is responsible for about 8 % of map result variation.

However, in order to improve the penetration depth capability of a sampling device mounted on an ROV, as well as the bias of the sampling device, a number of design considerations need to be made. This includes equipping the ROV with an appropriate sludge penetration and retrieval mechanism such that there is an adequate downward and upward thrust during penetration. The method of sludge collection must also be designed to reduce bias.

Aside the design of an appropriate ROV, there is a major task in the development of an *in-situ* method is the choice of an appropriate PSD analysis technique, suitable for underwater mobility. In Chapter 2, a number of techniques and their limitations have been discussed. A major setback to the deployment some techniques for *in-situ* underwater PSD analysis is their dependence on sample preparation.

For example, LDM requires adequate sample preparation [113] such as the dilution of samples to a volume concentration of about 1 % v/V in de-ionised water. The LDM is also susceptible to mechanical disturbances which distorts the optical alignment of the lenses and by implication, causes downtime.

A PSD measurement technique which could be a prospective choice is the ultrasonic spectroscopy, also referred to as acoustic attenuation spectroscopy [77], or acoustic emission [179]. It is a relatively new technique for measuring particle sizes and other physical properties of a particulate sample [180]. Unlike the laser diffraction method and some other techniques of particle characterisation which strongly require that samples are diluted to as low as 1% in volume concentration [77], ultrasonic spectroscopy has proved to be applicable to samples with volume concentrations as high as 20 % [70]. A comparison of the various techniques is provided in Chapter 2.

7.2 The Principle of Ultrasonic Spectroscopy for PSD Measurement

Ultrasonic spectroscopy involves the transmission of multiple ultrasound waves at high frequency usually in the range of 100 to 100 MHz [87], through a particulate sample of appropriate concentration in water, and studying the speed and attenuation properties of the received wave. The speed and attenuation of the received signals are subsequently analysed and compared to mathematical models based on existing theories to predict the particle characteristics [78] [181] such as particle size distribution and sample concentration. Riebel [70] provides a detailed discussion on the method of data interpretation as will also be addressed later in this chapter.

Figure 54 shows a schematic of an ultrasonic spectroscopy system. An electrical impulse signal kδ(t) of appropriate pulse width τ and amplitude k is generated. This signal is sent to an appropriate transducer which converts it to an acoustic wave of known bandwidth. The wave then travels through the measuring chamber, to the other end and bounces off the reflector.
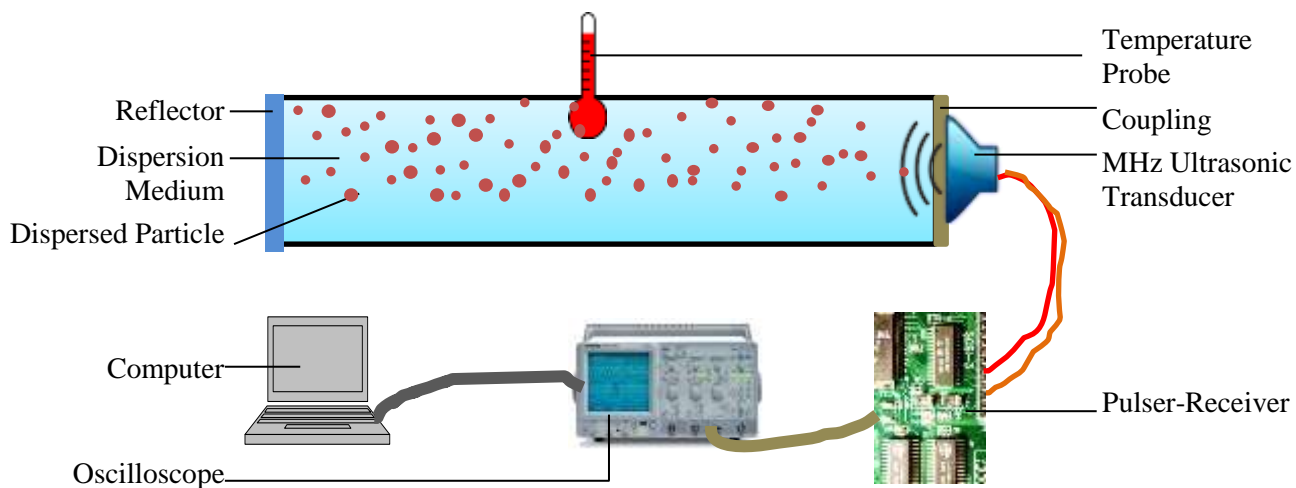
Figure 54: A schematic layout for ultrasonic spectroscopy using the pulse-echo approach. The signals sent and received are analysed by the computer in order to determine the size of particles in the medium.

The backscattered wave returns to the transducer at a time t, having travelled a total distance of 2L (where L is the length of the measurement chamber). Particles in the measuring chamber create resistance to the wave transmission causing power loss (attenuation). This typically involves scattering losses, intrinsic absorption losses, thermal dissipation losses and visco-inertial dissipation losses [44]. These losses are dependent on the physical properties of the particulate sample. The received signal y(t) is subsequently recorded for FFT analysis and for onward interpretation.

Aside being dependent of the particle characteristics, the attenuation coefficient observed is also a function of the sound frequency [182] and thus is measured at multiple frequencies to produce an attenuation spectrum. Wines *et al.* [183] in an experiment to determine droplet size distribution used acoustic spectroscopy with a frequency of 3 MHz to 100 MHz in 18 logarithmic steps. This was applied to droplets of size diameter ranging between 0.0001 μm and 1 μm. The wider the frequency range, the broader the size range for which measurements can be taken. However this must be done with due consideration of the signal-to-noise ratio as transducer sensitivity does have an influence on result validity. In addition to this, attention must also be paid to the transducer alignment as this becomes critical for frequencies over 10 MHz [87]. Unless the particle suspension is stable, it may be necessary to introduce stirrers to the measurement cell to agitate the particles and avoid sedimentation [87]. It has been observed that the stirrer speed does not introduce any additional acoustic attenuation dynamics to the system. [184] [185].

The ultrasonic spectrometer may be setup in a number of ways based on the number of transducers and the type of ultrasonic signal employed and this has been previously discussed extensively [44]. When only one acoustic transducer is used for both transmission and reception, requiring that a reflector is positioned at the other end of the transmission, then either of two techniques could be adopted; one is the pulse-echo technique if the transducer is supplied with a pulse signal, or the resonance technique if the transducer is supplied with a continuous wave [186]. Instead of re-running experiments for individual frequency values, as applicable to

continuous waves, pulse technique provides an opportunity to run multiple frequencies all at once and subsequently conduct a Fast Fourier Transform (FFT) to obtain the required attenuation and velocity spectra [44] [187].

While it is possible to increase the bandwidth of an excitation pulse by decreasing the pulse width [87], the bandwidth capacity of the transducer is limited and thus may require that two or more transducers with complementary bandwidth envelopes are employed to cover a wide broadband [44]. With regards to concentration measurements, a group velocity is required at only one frequency [80].

Also, there is a choice to make with regards to taking measurements at fixed or variable path lengths as this has an effect on data processing speed and result uncertainty. In the case of fixed path lengths, all measurements are done at a fixed distance between the transmitting and receiving transducers or reflector.

The observed signal is then compared with a background signal taken at the same gap but in a reference sample of the continuous phase only. In the case of a variable path length, data collected at two or more distance settings between the transmitter and receiver or moveable reflector are analysed for regression parameters without the need for a background or calibration data [188] [189]. In this regard, Wines *et al.* [183] in an acoustic spectroscopy experiment used a DT-1200 Dispersion Technologies Spectrometer. In this instrument, the path length was made variable in 21 steps from 0.15 mm to 20 mm.

The implementation of the ultrasonic spectroscopy technique involves three stages as highlighted by Alba *et al.* [77]. The first step is to make predictions of expected attenuation spectra for an array of likely sample configurations, such as PSD and dispersion concentrations. The second step is to experimentally obtain the actual attenuation spectra from the sample understudy.

The third step is to perform an appropriate inversion algorithm that produces the best fit particle characteristics from the available attenuation

spectrum and model prediction data. According to Watson [190], based on the concept that a sound wave, upon interaction with a material, is either reflected or absorbed for onward transmission with inherent losses during this interaction, it is possible to model expected interactions.

7.2.1 Mathematical Theories Required for PSD Measurement

There exist a number of theories that guide model predictions. One of such is the one proposed by Epstein and Cahart [191] and Allegra and Hawley [192] known as the ECAH theory which is widely used for samples containing heterogeneous sizes [79]. These theories have identified a relationship between fundamental wave equations and the interaction between sound waves and particles. This relationship enables the calculation of energy losses in the form of viscous, thermal, absorption or scattering losses. It has therefore become possible to predict the expected attenuation of a sound wave based on knowledge of the particulate medium.

This implies that knowledge of the thermodynamic and mechanical properties of the continuous and dispersed phase of a sample may be a crucial component of ultrasonic spectroscopy.

If there is no knowledge about the sample being characterised, there will be no appropriate prediction model to support data interpretation [87]. By simply monitoring changes in the attenuation, time of flight or speed of transmitted ultrasound, relative changes in corresponding sample characteristics such as sample concentration can be estimated and displayed [187] [193].

Another theory is the coupled phase model theory [194] which gives a similar result as the ECAH theory for a less concentrated system. However, as concentration increases, and the effect of multiple scattering can no longer be overlooked, the relationship between particle concentration and observed attenuation becomes nonlinear [80] at which stage, coupled phase model is more reliable. This is so because while the

ECAH theory involves the assumption of independent scattering, the coupled phase model, in calculating total loss, gives less significance to the losses due to intrinsic scattering effect and more to thermal and viscous losses [80].

7.3 Theory Formulation

7.3.1 Translation of Ultrasonic Data to PSD

An ultrasonic impulse kδ(t) is composed of a range of frequencies. This range is dependent on both the width of the impulse and the bandwidth of the transducer in use. For a frequency component w, let the amplitude of the original incident wave be $A(w, 0)$. After travelling to the reflector and back to the transducer, over a total distance of x_i, the new amplitude of that frequency component is represented by $A(w, x_i)$.

$A(w, 0)$ and $A_i(w, x_i)$ can be obtained for all frequency components within the bandwidth by conducting a Fast Fourier Transformation (FFT) on the sent signal kδ(t) and the received signal y(t). Equation (26) is then used to obtain the attenuation coefficient.

$$\alpha_i(w) = \frac{1}{x_i} \, log_e \left| \frac{A(w, 0)}{(A_i(w, x_i))} e^{-\frac{jwx}{c(w)}} \right| \qquad \textbf{(26)}$$

Where, $\alpha(w)$ is the attenuation coefficient, measured in nepers per meter. $c(w)$ is the speed of any sound wave of frequency w.

This experiment is performed a number of times i ∈ {1, 2, 3, …, N}. In each repetition, the distance $0.5x_i$ between the transducer and the moveable reflector is varied. Data collected at two or more transducer-reflector distance settings are analysed for regression parameters. This eliminates the need for background or calibration data.

The mean attenuation coefficient for every frequency component is thereafter obtained using Equation (27). This is known as the *ultrasonic attenuation spectrum* (UAS).

$$\alpha\,(w) = \frac{1}{N} \sum_{0}^{n} \alpha_i(w) \tag{27}$$

The UAS is a function of the properties of the particulate medium contained in the measuring chamber. The properties include an array of particle sizes of radius R_w, the fractional volume φ of the dispersion, and a number of thermo-mechanical parameters A_n. This is defined by the imaginary component of Equation (28) [195].

$$\frac{w}{c(w)} + j\alpha(w) = k_c \left(1 + \frac{3\varphi}{jk_c^3\,R_w{}^3}\right)(A_o + 3A_1 + 5A_2)^{0.5} \tag{28}$$

Where A_2 is negligible at less than 100 MHz. A_1 accounts for visco-inertia effects while A_0 includes other physical quantities. Having obtained the UAS array from Equation (27), the PSD can be obtained using Equation (28), to find R_w.

The A_n parameters are derived by using either of two theories namely: the ECAH theory [191] [192] and the coupled-phase model theory [194]. The ECAH theory is valid at lower sample concentrations [196], while the coupled-phase model is more appropriate at extremely high sample concentrations. This is because of the difference in the power loss models adopted by these theories.

By assuming that particles are isolated in a low concentration medium, where only single-scatterings occur, and by considering sound waves of wavelength $\lambda \ll R_w$ (the Short-Wavelength Region), Equation (28) may be further simplified [197].

$$K_c = \frac{w}{c(w)} \tag{29}$$

$$A_n(R, w) = -j \sin\big(\eta_n(R, w)\big) . e^{-j\eta_n(R,w)} \tag{30}$$

$$K_{i,j}(R_i, w_j) = -\frac{4\pi}{K_c^2}\sum_0^n (2n + 1)|A_n(R_i, w_j)|^2 \qquad \text{(31)}$$

η_n is the phase shift of the partial scattered waves and $A_{n(R,w)}$ is the scattered amplitude coefficient. The relationship between UAS and PSD can therefore be linearised as given by Equation

(32) and referred to as the Lambert-Beer Equation [198].

$$\alpha(w) = C_{p.a}\Delta L \, K(R, w)dQ_2(R) \qquad \text{(32)}$$

$C_{p.a}$ is the projection area concentration, ΔL is the gap width between the transducer and the reflector, $K(R, w)$ is known as *the Matrix of related extinction cross-section* and $dQ_2(R)$ is the PSD of the particulate sample.

From Equation (33), the PSD can be obtained by re-arranging the matrix operation and solving for $dQ_2(R)$. This is a direct method. An indirect method however involves substituting $dQ_2(R)$ with pre-selected mono-modal or bi-modal log-normal distribution models to determine a best-fit PSD model that satisfies the equation, based on a least-square analysis [44].

At low concentrations, parameters such as the density, thermal expansion coefficient, speed of sound in the fluid, sample concentration, density and heat capacity of the particle are of significance influence to the thermo-mechanical properties of the particulate sample [80] [199]. Without adequate knowledge of these relevant thermo-mechanical parameters, neither of A_n nor $K(R, w)$ will be available for Equations (32) and (33).

7.3.2 Challenges involved in the Deployment of Ultrasonic Spectroscopy

Although significant progress has been achieved in the application of ultrasonic to relatively homogenous material mixture, Kress-Rogers [200] identified a problem in that most industrial applications involve inhomogeneous materials with varying acoustic impedance values particularly in the food industry. Any attempt by an acoustic signal to

travel across the boundary layer of two materials with contrasting acoustic impedances creates a high probability of reflection thus decreasing the likelihood of further acoustic penetration and spectroscopy.

Kress-Rogers therefore suggested that in such a situation, it may be necessary to employ an array of acoustic transducers firing and listening from all angles, similar to a work by Schlaberg *et al.* [201] where an array of 36 transducers were mounted around the cross-section of a pipe. The impact of a transducer's sensitivity on particle size analysis has also been queried. Lopez-Sanchez and Schmerr [202] proposed a new model-based approach that includes the determination of both the electric impedance and sensitivity of a single element transducer used in the pulse-echo setup. Similarly, the adverse effect of irradiation on a transducer's characteristics has been observed [203].

There are drawbacks to the proposal of multiple transducer-reflector distance settings. DosRamos [204] remarked that one of these drawbacks is the possible abrasion issues that may arise when moveable reflectors or transducers are exposed to slurries and another drawback may be the requirement of a high resolution motion stepper motor to drive the systematic movements. Therefore, instead of employing moveable reflectors, the author proposed the use of an arrangement of multiple fixed reflectors in a step-wise position known as the AREPA (Acoustic Reflection Particle Analysis).

This development is similar to a recommendation by Kummritz *et al.* [205] wherein it was suggested that in measuring the focal point of transducers as a means to improving material characterisation of multi-layered samples, instead of moving the probe as was proffered in [206], the same could be achieved by implementing delayed excitations of the segments of an annular array.

With regards to reliable model predictions, it was discussed earlier that the ECAH theory assumes that particles are relatively isolated at low concentrations and thus provide single and independent scattering of acoustic signals. Hipp *et al.* [196] sought to investigate the implication of

169

having multiple-particle effect in a concentrated colloidal dispersion. It was observed that while there could be an occurrence of multiple lossless scatterings which have no significant effect on results, the existence of another multiple-particle effect known as the particle-particle effect does have an effect. The particle-particle effect creates the possibility of energy interactions between neighbouring particles thus modifying dissipative energy and absorption characteristics.

Forrester *et al.* [207] identified the challenge inherent in monitoring and interpreting severe attenuations in highly concentrated and dense samples of sizes in the nano scale. The authors recommend that for frequencies in the range 1 MHz to 20 MHz and in samples with concentration below 20 %, a shear-wave reconversion model which recognises the conversion of sound waves from compressional waves to shear waves and back to compressional waves at liquid/particle boundaries would enable a more accurate interpretation of the resulting ultrasonic attenuation spectrum. The authors however noted as frequency and sample concentration increase, the model becomes less accurate. Hence, there is the need to consider the effect of neighbouring interactions on visco-inertial and thermal dissipations in high concentration particulate samples.

Another factor that limits the usability of ultrasonic spectroscopy is its dependence on a number of mechanical and thermodynamic properties of the sample being investigated. For example, in a research by Zozulya *et al.* [208] using pulsed acoustic spectroscopy to determine bubble size distribution, it was remarked that it is necessary to specify the visco-elastic properties of the bubble shell. The authors also identified the difficulty in obtaining such parameters n-situ. For this reason, the authors recommended the use of acoustic spectroscopy only when such parameters are provided. Most often, these properties are not readily available in fact, they could be unknown. In such situations, it is important to know the extent to which parameter assumptions could be made.

Babick *et al.* [80] investigated the stability of particle size results obtained by ultrasonic spectroscopy when incorrect relevant material properties are

used in the model prediction. It was observed that at low concentrations, the density, thermal expansion coefficient and sound speed of the fluid, as well as the concentration, density and heat capacity of the particle were of significance influence. Mougin *et al*. [199] also observed a similar outcome.

Similarly, Zozulya *et al*. [208] in a study on bubble size distribution suggests that visco-elastic properties can be recovered indirectly if the bubble size distribution is first obtained using a different technique. Babick *et al*. [80] suggested the need to investigate the extent to which ultrasonic spectroscopy may also be used to measure these parameters.

There may be some hope in this regard as Holmes *et al*. [184] in an experiment observed the applicability of acoustic spectroscopy in determining temperature dependent bulk viscosity of fluids.

7.3.3   Solving the Challenges

Rather than use theoretical models that require an array of material properties, Babick *et al*. [209] suggests the use of analytical models when faced with the challenge of partly unknown samples. One of the strategies proposed therein was the development of an empirical model using statistical methods of correlating the physical properties of particulate samples with corresponding components of the attenuation spectra. It was observed that this method was successful in determining at least the mean PSD of a sample whose material properties are largely unknown.

The observation by Babick *et al*. [209] is similar to the findings reported in Chapter 5 about the LDM method. In the case of the LDM method, the choice of optical parameters provided was found to have no direct influence on the mean of the particle size distribution observed. However, there was a 5 % influence on the spread of the size distribution observed.

However Babick *et al*. [209] warned that the method of an empirical model to replace knowledge of some thermo-mechanical properties requires a significant amount of training data set, and that the model produced is only applicable to the particular product or process for which

it was designed. In the worst case scenario of a nuclear storage pond however, during *in-situ* analysis, there is no restriction to the variety of unknown materials which may be collected and analysed. The challenge this poses is that either the empirical model becomes significantly inaccurate or there is a need for a continuous increase in the number of training datasets.

To determine the feasibility of ultrasonic spectroscopy as a technique for measuring PSD of radioactive sludge *in-situ*, this chapter examines the success of an empirical model as a replacement of thermo-mechanical properties in an unknown sludge environment.

7.4   Developing an Empirical Model for Converting UAS to PSD

By discretising Equation (30), the term that is dependent on thermo-mechanical parameters can be substituted with an m × m K-Matrix K_m. The UAS and PSD can be discretised into an array of m-elements A_m and Q_m respectively. This results in Equations (34) and (38).

$$A_m = K_m \ Q_m \tag{33}$$

$$\begin{matrix} \alpha_1 \\ \alpha_2 \\ \alpha_m \end{matrix} = \begin{bmatrix} k_{11} & \cdots & k_{1m} \\ \vdots & \ddots & \vdots \\ k_{m1} & \cdots & k_{mm} \end{bmatrix} \begin{matrix} q_1 \\ q_2 \\ q_m \end{matrix} \tag{34}$$

To be able to solve for K_m, the matrices A_m and Q_m can be populated into sizes m × m as in Equation (35). To achieve this, additional samples of the exact same non-homogeneous material need to undergo analyses. The first analysis involves the collection of the UAS raw data from each sample by conducting ultrasonic spectroscopy. This may be performed *in-situ*, after which the material may be taken into a laboratory. The second analysis is the measurement of the PSD data of each of the samples. This involves the

use of the LDM method or any other reliable method of PSD measurement in a laboratory. A total of m samples are required.

$$\begin{bmatrix} \alpha_{11} & \cdots & \alpha_{1m} \\ \vdots & \ddots & \vdots \\ \alpha_{m1} & \cdots & \alpha_{mm} \end{bmatrix} = \begin{bmatrix} k_{11} & \cdots & k_{1m} \\ \vdots & \ddots & \vdots \\ k_{m1} & \cdots & k_{mm} \end{bmatrix} \begin{bmatrix} q_{11} & \cdots & q_{1m} \\ \vdots & \ddots & \vdots \\ q_{m1} & \cdots & q_{mm} \end{bmatrix} \qquad (35)$$

$$AA_m = K_m QQ_m \qquad (36)$$

$$K_m = AA_m QQ_m^{-1} \qquad (37)$$

As the number of unique samples m increases, the resolution and the accuracy of the K-matrix is expected to increase. However, it is possible to have samples which are not entirely unique in their PSD and UAS data. This could cause the matrix operation of Equation (38) to result in non-singularity. For this reason, a pseudo-inverse of QQ_m may be substituted for the inverse matrix QQ_m^{-1}.

The K-matrix obtained by using Equation (38) can be tested on a different set of sludge samples to understand the degree of uncertainty involved in using this for data interpretation.

The series of experiments performed to develop an empirical model as described is best performed on a singular type of sample material. Otherwise, the resulting learning datasets may not agree. However, there is neither an assurance that the sludge material is homogenous across the population nor that the non-homogeneity of sludge material is uniformly distributed across the population. Thus, the material composition of each of the m samples analysed may vary. This underscores the need to use a significant number of samples and the need to have a statistical evaluation of the uncertainty associated with any K-Matrix.

7.5 Laboratory Experiment to Obtain raw UAS data of Soda-lime Glass Microspheres

In order to test the feasibility of empirical models, laboratory experiments were performed to obtain raw UAS data of soda-lime glass microspheres. These soda-lime glass microspheres were the used earlier in the analysis of the LDM method of Chapter 5. Collection of their raw UAS data would therefore provide learning datasets for the development of an empirical relationship between PSD and UAS of soda-lime glass.

This experiment involved the use of soda-lime glass microspheres of two different PSDs. A $170 - 710$ µm size range (Whitehouse Scientific Ltd) and a $465 - 600$ µm size range (produced by Sigma-Aldrich) as obtained from their technical documentation at a sample concentration of 10 % v/V in distilled water. The soda-lime glass microspheres were sampled using an ultrasonic spectroscopy setup at the University of Leeds, UK to obtain UAS raw data. Figure 55 shows the experimental set-up used. Alastair Tonge, PhD student in the acoustics research group, University of Leeds was very helpful in the setup of the acoustic system and in the operation of the data acquisition software.
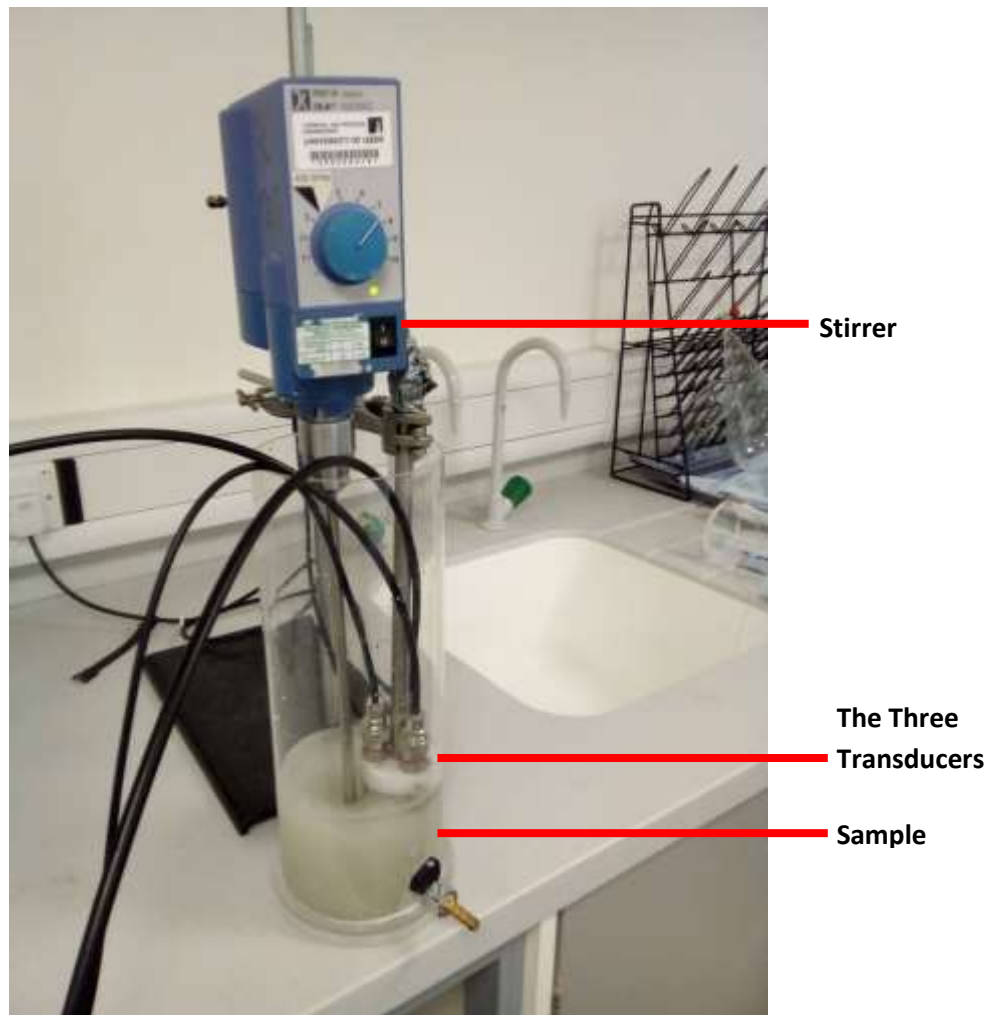
Figure 55: Acoustics Experimental Set-up at Leeds University, UK. The set-up comprises three acoustic transducers, a stirrer, soda-lime glass microspheres, water medium, and a container.

The experimental set-up comprised three acoustic transducers with each operating at three discreet frequencies. They were:

•   Transducer 1: {0.85 MHz, 1 MHz and 1.15 MHz}

•   Transducer 2: {1.75 MHz, 2 MHz and 2.25 MHz}

•   Transducer 3: 3.75 MHz, 5 MHz and 6.25 MHz}

These transducers were used simultaneously so as to provide attenuation readings for a total of nine frequencies. The sample was kept at 10 %v/V in distilled water. A stirrer operating at 400 rpm was used to keep the concentration uniform during measurement.

7.6 The Results of the Ultrasonic Experiment Conducted at Leeds University, UK

The acoustic transducers received voltage signals for each of the nine discrete frequencies. The signals were returned against sample time (which had been converted to travel distances). This result showed significant back reflection even before travelling to the reflector. By collecting voltage signals received at times which correspond to the set distance between the transmitters and the reflector, the attenuation coefficients were calculated and recorded. This was done for each of the four tests run. The results are shown in Figure 56.
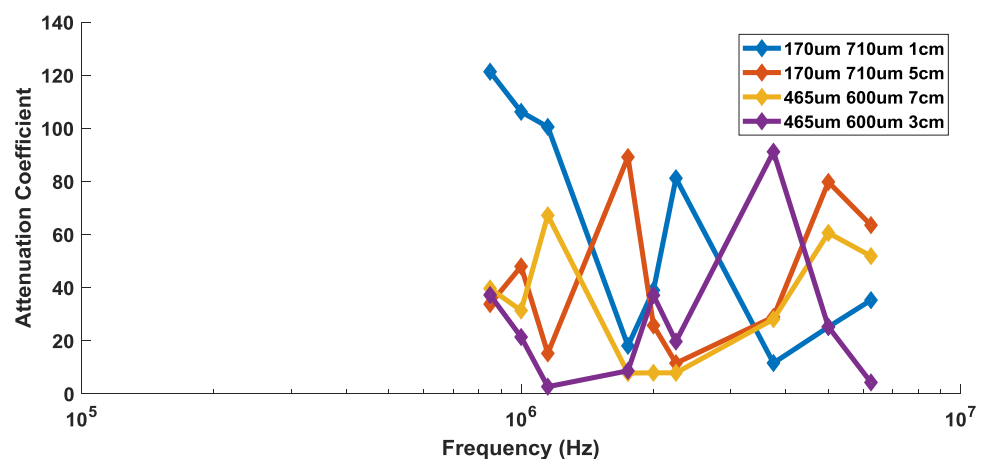
Figure 56: UAS for 4 samples at different gaps between transmitter and reflector. This experiment was carried out for four different sets of soda-lime glass microspheres samples of different mean particle sizes as represented by the different colours.

The received signals were observed to have significant noise levels. This is however understandable considering that the acoustic machine used was not designed to perform PSD analysis. The non-reliability of the UAS

results can be seen in the UAS plots which should typically show a continuous increase in attenuation as frequency increases.

7.6.1 Remark

The experiment to obtain raw UAS datasets and seek to determine an empirical K-Matrix model using PSD results from LDM experiments in Chapter 5 could not achieve meaningful results. One reason for this was the significant noise observed in the device used. Another reason was the available acoustic transducer frequency bandwidth which was inadequate. There were only nine discrete frequencies (between 850 kHz and 6.25 MHz) available as against the required 100 kHz to 150 MHz for ultrasonic spectroscopy. Although this was the only available resource, it was not designed specifically for ultrasonic spectroscopy. Rather it was designed for the determination of settling rates of suspensions.

Due to the failure to obtain raw UAS data, computer simulated PSD and UAS data would be used in developing the required learning datasets.

7.7 Computer Simulation Tests of the Feasibility of an Empirical Model for Unknown Sludge

Given a sludge sample which has a mean PSD of 126 μm and a lognormal distribution variance of 0.09 μm^2, by running a suitable algorithm on MATLAB, the PSD lognormal distribution and cumulative distribution plots can be obtained as shown in Figure 57 and Figure 58, respectively.
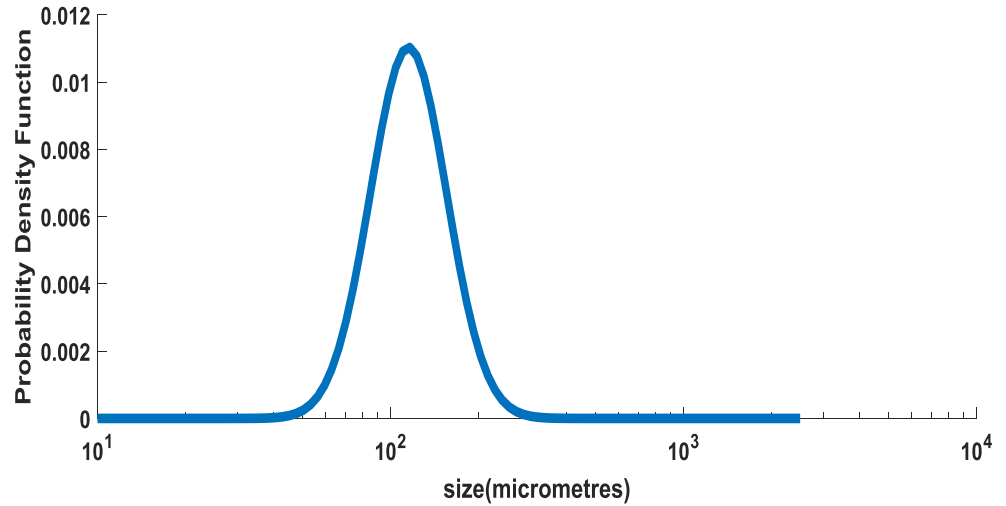
Figure 57: PSD Lognormal Distribution of the given sample. The particle size distribution shown in this figure is a histogram representing the lognormal distribution.
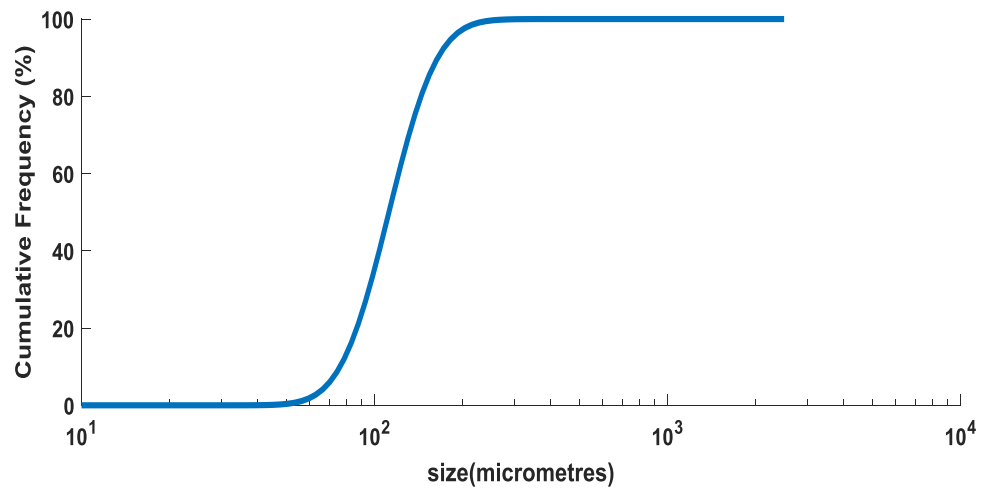
Figure 58: PSD Cumulative Distribution. The particle size distribution shown in this figure is a cumulative frequency curve on a logarithmic scale.

The UAS data which corresponds to this sludge sample can also be obtained by using Equation (32). In implementing this equation, the PSD data already obtained is used, as well as the parameters in Table 12.

Table 12: Parameters used in ultrasonic spectroscopy simulation

Parameter	Value
Distance between transmitter and reflector	0.01 m
Sample concentration	10 %
Frequency Range	100 KHz – 150 MHz

This frequency range was chosen to be able to detect particle sizes across the 10 µm to 2500 µm size range similar to an LDM method. By adopting a generic *Matrix of related extinction cross-section,* the corresponding UAS data is shown in Figure 59. This is the ultrasonic attenuation spectrum expected to be observed on this particular sample in an ultrasonic spectrometer.
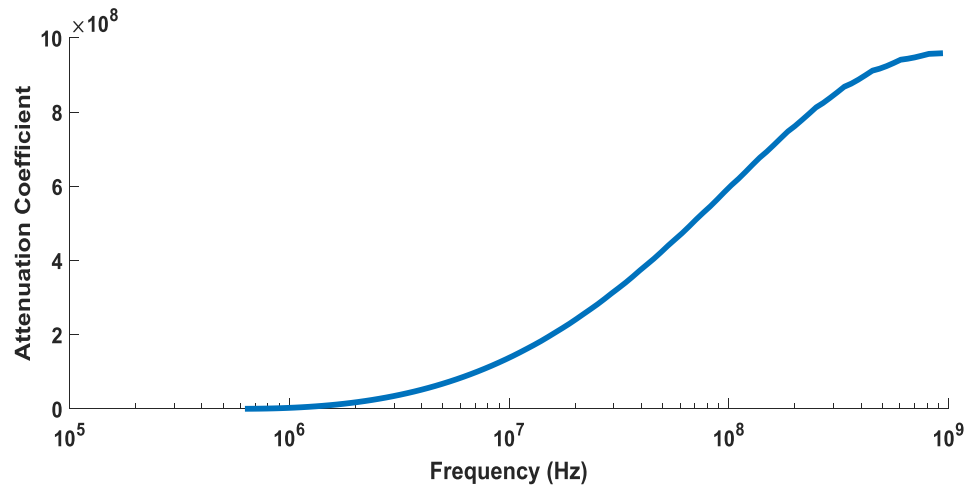
Figure 59: Ultrasonic Attenuation Spectrum (UAS) derived from Simulation. This figure shows UAS against a logarithmic scaled frequency axis.

7.7.1 Collection of Learning Datasets

To develop an empirical model for converting UAS data to PSD for unknown sludge samples, PSD and UAS datasets of ten sludge samples were collected as learning datasets. The PSD data were chosen by a random selection of PSD mean and lognormal distribution variance values. This is shown in Table 13.

Table 13: List of PSD characteristics of ten samples used for learning

Sample S/N	Mean PSD (micrometres)	PSD Variance (Lognormal)
Sample 1	70	0.09
Sample 2	150	0.04
Sample 3	200	0.25
Sample 4	350	0.49
Sample 5	450	0.09
Sample 6	500	0.04
Sample 7	650	0.64
Sample 8	700	1.69
Sample 9	750	0.04
Sample 10	840	2.89

Using the method described for obtaining the PSD cumulative distribution and the UAS plots, Figure 60 and Figure 61 were produced as PSD-UAS learning datasets from ten samples.
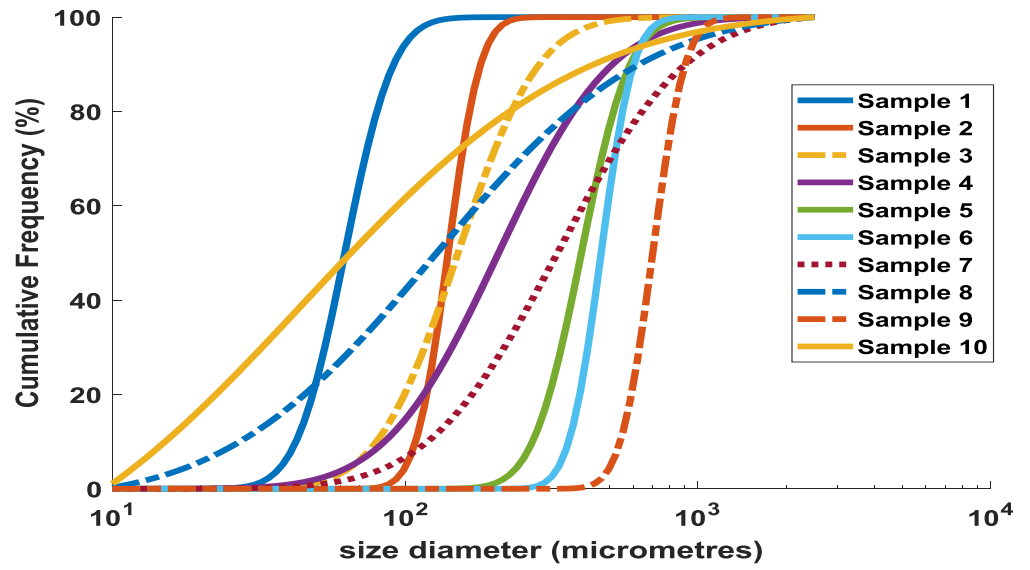
Figure 60: PSD cumulative frequency learning dataset of ten samples. This figure shows the particle size distribution of ten simulated samples with various mean particle sizes. This set of data is to be used for learning an analytical method of interpreting particle sizes from ultrasonic attenuation spectrum.
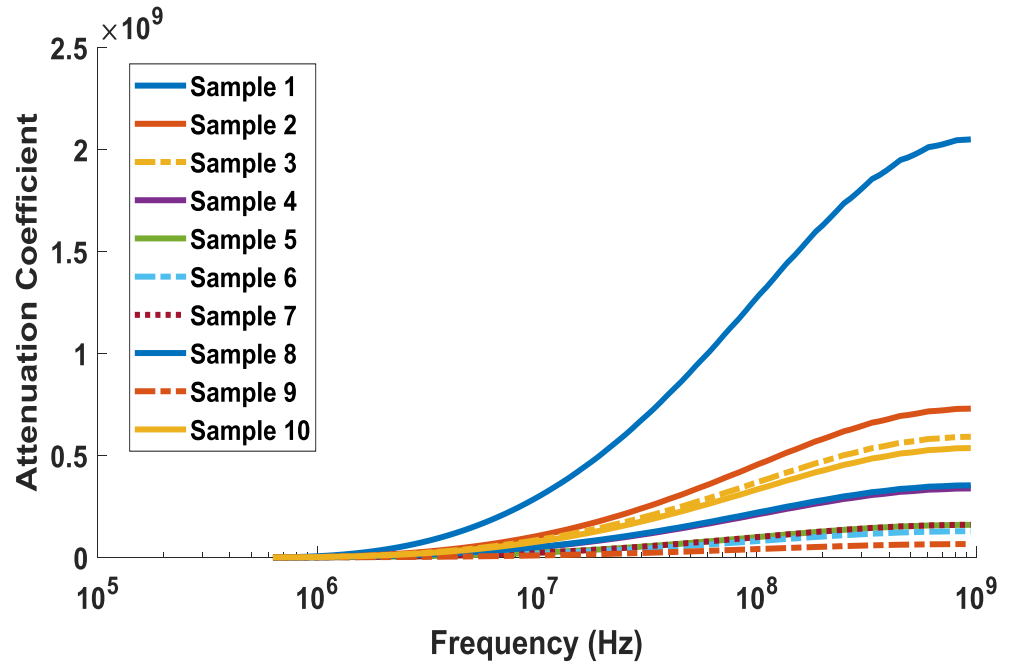
Figure 61: UAS learning dataset of ten samples obtained by simulation. This figure shows the ultrasonic attenuation spectrum (UAS) of ten simulated samples with various mean particle sizes. This set of data is to be used for learning an analytical method of interpreting particle size distributions from a given ultrasonic attenuation spectrum.

7.7.2 Identification of an Empirical Model

The empirical model of the K-matrix which relates UAS and PSD, as given in Equation (37) is then obtained by back substitution of the learning datasets. To do this, the number of data points per dataset had to be equal to the number of datasets used in the learning. This is because the K-matrix can only be a square matrix. Hence, in order to produce a 10×10 K-Matrix, the resolution of the PSD-UAS datasets were reduced to 10 data points per dataset.

7.7.3 Implementation and Analysis of the Empirical Model Obtained

Having obtained a 10×10 K-Matrix, a simulation was carried out to test the empirical model. This involved the collection of PSD test datasets of random test samples and obtaining their corresponding UAS datasets using

already stated procedures. The expectation was that adopting the empirical model of the K-Matrix and the test UAS datasets into Equation (35), the PSD inferred would agree with the test PSD dataset.

Subsequently, by analysing the root mean square error and standard deviation of error of the inferred PSD mean, the suitability of the learned 10-by-10 K-matrix would be ascertained. Where the error margins are significant, the empirical model would be found to be non-suitable and an empirical model with a higher resolution would be suggested. The block diagram on Figure 62 illustrates the test procedure. Table 14 shows the results obtained.
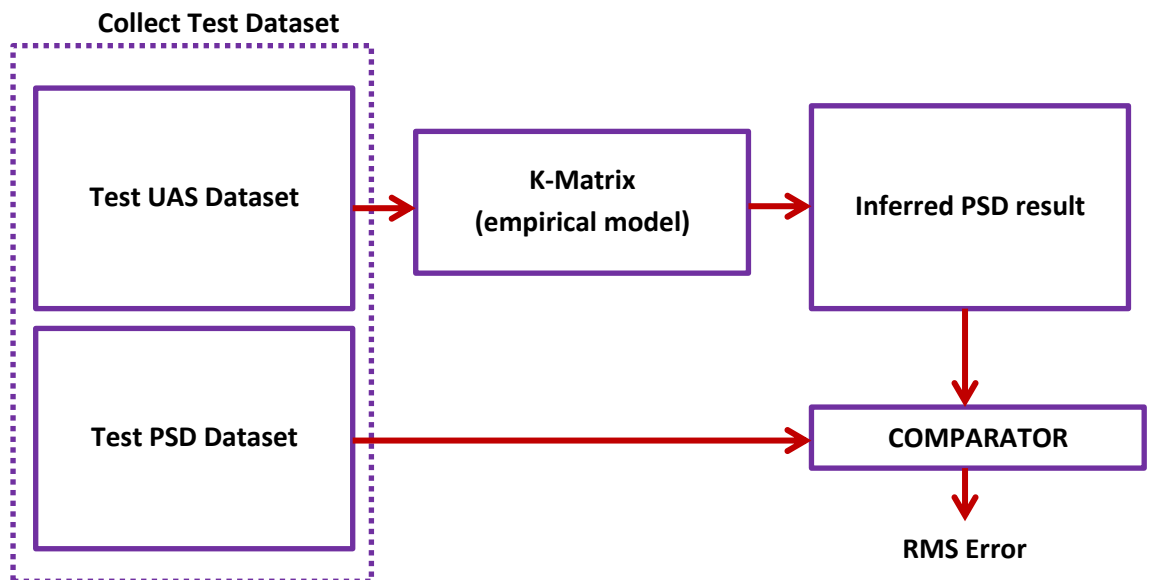
Figure 62: An illustration of a K-Matrix validation test procedure.
This figure describes the method of validating the analytical model.

Table 14: Analysis of the 10×10 K-Matrix

Size of K-Matrix	Root Mean Square of Error	Standard Deviation of Error
10×10	701.9 μm	529.6 μm
20×20	939.5634 μm	298.1556 μm
100×100	1958.3 μm	305.9772 μm

It can be observed on Table 14 that the root mean square of the error of the inferred mean PSD was significantly high when the empirical model relied

on only ten learning datasets. By increasing the number of learning datasets to 20, and subsequently to 100, the resolution of the K matrix also increased up to 100×100. However, against the expectation that such an increase in learning datasets would cause a decrease in the error margin, the results did not provide any such indication.

From the forgoing simulation results, the use of an empirical model obtained from a number of learning datasets to convert raw UAS data into PSD of unknown samples is non-feasible.

7.8 Conclusion

The simulation results showed that while UAS can be derived from PSD in situations where necessary parameters of the material properties are known, the option of inferring PSDs from UAS based on learned K-Matrix empirical models is not feasible.

This confirms the opinion of authors who maintain that there needs to be knowledge of relevant thermo-mechanical properties for ultrasonic spectroscopy method to be employed.

Alternatively, for the purpose of conducting *in-situ* experiments while maintaining the use of the existing method of Laser Diffraction (LDM), a stable robotic platform could be deployed unto the water surface. By mounting a Malvern Mastersizer 3000 instrument of such surface vehicle, sludge samples can be retrieved using a remote operated mobile sampling device and analysed on-board the surface vehicle. This solution however requires further research.

8 Chapter 8 – General Conclusion and Recommendations

8.1 Emphasis on Key Research Findings and their Implications

8.1.1 Quantifying the Influence of Experimental Factors related to Sludge Sampling

This research identified four factors involved in Sludge Sampling. The results confirmed expectations that one of these factors known as the 'depth of penetration of the sampling device has the highest influence on result variability. The choice of depth of penetration in this study was made between a 10 to 100 % penetration of the sludge bed. This factor is responsible for about 48 % (on average) of the overall map result variation in cases where the sludge bed has no spatial autocorrelation.

Similarly, the 'bias of sludge sampling device' and 'number of sampled locations' record significant influence of about 23 % and 4.4 % (on average), respectively. The 'bias of the sludge sampling device' factor was a choice between a sampling device which retains only particles that are less than 400 microns and a sampling device which has no bias, while the 'number of sampled locations' factor was a choice between 8 and 200.

The fourth factor known as the 'strategy of selecting sampling locations' (a choice between simple random sampling and stratified random sampling) recorded the lowest influence (0.3 %) amongst sludge sampling related factors irrespective of the presence or absence of spatial autocorrelation.

It was generally observed that interactions amongst factors were significant. This implied the dependence of the influence of one factor based on the settings of another factor. It was concluded that the use of an *in-situ* sampling mechanism and a determination of an adequate setting for the experimental factors involved would help to improve data quality.

The implication of this result is that it allows field operators seeking to improve the quality of results from sludge characterisation to know what experimental factors to focus on. The number of sampled locations should be a priority. This means there should be concerns on how to improve the number of samplings.

There are also implications for further research. This follows the significant influence of the sampling device's penetration capabilities and bias. Extensive works should be carried out to ensure that appropriate sampling devices are used and that the limitations and bias of the sampling device used is adequately recorded.

The significant influence of the 'number of sampled locations' factor provides a direct implication to this research. It requires a determination of what minimal 'number of sampled locations' will be enough to eliminate result variability amongst field operators. This knowledge will support future sludge sampling standards.

8.1.2 The Recursive Relative Accuracy (RRA) Algorithm

This research found that the challenge of determining the accuracy of characterisation maps in order to assess whether more samples are required or not, can be solved using the RRA algorithm. This is because the RA algorithm does not require ground-truth map of the population. In spite of this, the trend observed in the RRA plot of a computer simulation compared satisfactorily with the plot of actual map accuracy.

In an actual accuracy plot observed on a computer simulated sludge bed model, sludge sampling of 20 locations using a device which penetrated through 30 % of the sludge while collecting samples at 10 % depth intervals was able to generate a map with a PSD inference accuracy of about 60 %. The accuracy plot had a steep rise from 2 to about 200 sampled locations before appearing to converge at about 100 %. The RRA plot on a similar sampling procedure, but using real-life data, and with sampled locations increased from 2 to 20 indicated a similar trend. This

confirms it as a useful tool for improving sludge characterisation accuracy in the absence of ground-truth.

The introduction of the RRA algorithm is of benefit to future research. For example, a recent study on soil exploration [147] identified the importance of the variance map (if OKA is used) or confidence map (if TDA is used) for assessing the quality of the characterisation map produced. The authors' expectation is that by observing the variance or confidence map, the need for further sampling can be determined.

Furthermore, the authors rightly recommend that further sampling is conducted at an appropriate location such that the variance or confidence map is improved. While the authors seek to maximise the benefit of variance or confidence mapping, this research provides a single plot (known as the RRA plot) which indicates the need for any further sampling. This helps to reduce the effect of human error and reduces the cost of excessive sampling and time duration.

8.1.3 Quantifying the Influence of Experimental Factors Related to the use of Laser Diffraction Method for PSD Measurement.

Seven other experimental factors were evaluated. These are factors which relate to the use of Laser Diffraction Method (LDM) for measuring PSD in a laboratory. From the results obtained, it was observed that the choices of LDM instrument model used (a choice between the Malvern Mastersizer 3000 model and the Malvern Mastersizer 2000 model) and the concentration of the sample in water (a choice between 0.5 and 4.0 % V) do contribute about 40 % and 7 % (respectively) to variations observed in the PSD mean value obtained per sample.

However, on their influence on the PSD spread which was represented by the ratio of the upper to lower percentiles, the choice of optical parameters (Refractive Index and Absorption Coefficient) has the most significant influence with about 5 % and 3 % contribution respectively. Interestingly,

factor interactions were predominant in the evaluation of these LDM experimental factors.

This aspect of the research is of immense contribution to knowledge. Although there have been previous studies which identified influential experimental factors in relation to PSD measurements, this research builds on that by quantifying the influence of these factors.

The implication of this result is that field operators using the LDM analytical method for PSD measurement will be required to maintain the same experimental settings across sample analysis in order to minimise result variation. The result also confirms that optical parameters do not have significant influence on the PSD mean observed. They however do influence the PSD spread represented by the ratio of the upper to lower percentiles.

8.1.4 The Feasibility of an *In-Situ* Sludge PSD Characterisation using Ultrasonic Spectroscopy

The research investigated the feasibility of conducting PSD measurements underwater in situ. Ultrasonic Spectroscopy was initially identified as a potential *in-situ* technology due to its scalability. However, there were concerns about its applicability to samples with unknown thermomechanical properties. This was because ultrasonic spectroscopy involves exposing sludge samples to ultrasonic waves and observing the resulting Ultrasonic Attenuation Spectrum (UAS). The UAS is then converted to PSD using a suitable mathematical model. The available mathematical models require knowledge of thermomechanical parameters. The option of using an empirical model was considered.

The expectation was that by obtaining learning data, an empirical model could be developed to provide a "K-Matrix" relationship between UAS and PSD. However, results showed no such relationship, as the average error margin between the true and the inferred PSD mean values was over

600 μm. It was also observed that by increasing the number of learning datasets, the expectation that the error margin would decrease was not met.

The implication of this result is that towards adopting Ultrasonic Spectroscopy, field operators will be required to fully acquire the thermomechanical properties of the sludge in the pond. This will therefore require extensive laboratory experiments with a number of sludge samples. The procedure of characterising sludge for its thermomechanical properties then becomes identical to the procedure of sludge characterisation already discussed in this research.

There could indeed be arguments suggesting that carrying out another ex-situ sludge characterisation in order to determine thermomechanical parameters of sludge before using such parameters for *in-situ* sludge PSD characterisation is pointless. Such arguments would suggest that a more cost effective solution is to continue with ex-situ sludge PSD characterisation.

However, *in-situ* sludge PSD characterisation provides the opportunity for sampling and analysing a higher number of locations unlike ex-situ sludge PSD characterisation. This is because by having a mobile sampler-analyser underwater, the hazards associated with taking out radioactive sludge from ponds into laboratories is eliminated. Hence, continuous PSD measurements can be conducted. This is vital as the 'number of sampled location' has been observed to contribute 4.4% influence on result confidence. For these reasons, there is merit acquiring thermomechanical parameters of sludge by ex-situ means, prior to the use of ultrasonic spectroscopy for *in-situ* sludge PSD characterisation.

8.2 Future Research Works

The findings in Chapter 7 indicate that Ultrasonic Spectroscopy is probably not a feasible *in-situ* analyser for measuring the PSD of radioactive sludge underwater. Going further, the future work is the development of an underwater based ultrasonic spectrometer for monitoring the ultrasonic attenuation spectrum of sludge. Another work is the development of a remote operated laboratory based on the commonly employed LDM technique for analysing sludge samples *in-situ*.

8.2.1 Development of an Underwater Ultrasonic Attenuation Spectrum (UAS) Analyser

To use ultrasonic spectroscopy, it has now been concluded that there is the need to have the thermomechanical parameters of sludge. This has to be obtained via *ex-situ* sludge characterisation methods and by undergoing spatial extrapolation, parameters at non-sampled locations can be inferred.

This investigation can be carried out within a three year research program. This is because it requires the use of laboratory techniques for determining thermomechanical properties of variant sludge simulants. It also involves the construction of a mobile ultrasonic spectroscopy chamber as well as a technique for collecting and disposing sludge samples. The job of the mobile ultrasonic spectroscopy chamber is to continuously collect UAS data which would be converted to PSD data when the required thermomechanical parameters become available.

8.2.2 Development of an LDM Based *In-Situ* Sludge PSD Analyser

An alternative to the use of a mobile ultrasonics based in-situ analyser is the deployment of a Malvern Mastersizer (LDM based) instrument to the pond surface. This involves developing a floating platform on which the LDM instrument can be mounted. A disadvantage of LDM is that it requires a more detailed sample preparation. It is therefore useful to consider the involvement of robotic techniques to cater for the sludge

sample collection and preparation requirements. In the design of a suitable retrieval system, the challenges of collecting sludge samples at different penetration depths, as identified in Chapter 5 should be investigated.

8.2.3 Mobile Laboratory for *In-Situ* Analysis on Land or in Water

Beyond measuring the particle size distribution of radioactive sludge, the nuclear decommissioning programme involves a number of other tasks. For example, developing a mobile laboratory with automated sample retrieval and preparation platform would be useful for regular monitoring and maintenance of legacy ponds. This could be deployed for routine monitoring of water pH levels, radiological dose rate and underwater contamination. This could also be deployed for routine filtration of the pond water.

In order to achieve this, future research should seek to develop on existing projects such as the MallARD [210] and the AVEXIS [211] projects and attempt to develop autonomous coordination between both systems to such an extent that the AVEXIS ROV can serve as the sample collector while MallARD provides the mobile laboratory platfirm.

Similarly, the decommissioning of nuclear waste in dry storage facilities such as Sellafield's Thermal Oxide Reprocessing Plant (THORP) does require *in-situ* sampling and laboratory analysis such as the evaluation of radionuclide distribution (radionuclide speciation).

For the purpose of on-land operation, the future research could build on the progress made in the Continuous Autonomous Radiation-Monitoring Assistance (CARMA) project by the University of Manchester's robotics research group. [212] This could be developed into a mobile laboratory platform with sampling and analysis capabilities.

The mobile laboratory platform should therefore be designed as a remote vehicle operational on water or on any terrain. This mobile laboratory should be equipped with a positioning and communication system to

support the deployment and coordination of multiple mobile sludge sampling vehicles.

The fore-going discussion is not only applicable to the nuclear decommissioning programme. Related projects include the automated clean-up of crude-oil contaminated waterbodies and the routine sampling of ecological parameters across a given region. These projects would also benefit from this development..

8.2.4 Application of the Recursive Relative Accuracy Method for Intelligent Sampling

As a result of findings in this research which indicate that the choice of sampling device has significant influence on the quality of sludge characterisation, appropriate sampling devices for various tasks must be developed. Particular attention must be paid to ensure that the penetration depth is maximised, and the sample bias is minimised.

Future research should take advantage of the Recursive Relative Accuracy (RRA) to determine when to collect further samples. The confidence mapping method can be used in taking decisions regarding which sampling location is most appropriate and to understand the attained percentage confidence.

The procedure adopted in this research for analysing the sampling related experimental factors can be used by operators to further understand and improve their sampling operations and data quality.

Most importantly however, future research should work towards introducing the RRA and other statistical tools to the machine learning algorithm of the mobile robots used for sample collection in order to provide the overall operation with artificial intelligence.

In trying to make this platform multi-functional, and to enable multiple robots coordination, an application software known as Robotics Operating System (ROS) should be installed on it for general robot coordination and communication.

Reference

[1]   W. Koelzer, Glossary of Nuclear Terms, Karlsruhe: Karlsruher Institut für Technologie, 2013.

[2]   Shimadzu Corporation, "Particle Size Distribution Dependent on Principle of Measurement," Lecture on Partical Analysis - Hands-on Course, 2015.

[3]   GRC Data Intelligence, "The Data Quality Glossary," [Online]. Available: http://www.dqglossary.com/data%20quality_.html.   [Accessed   15   12 2015].

[4]   Merriam-Webster Incorporated, "An Encyclopædia Britannica Company," 2015.   [Online].   Available: http://www.merriam-webster.com/dictionary/sludge. [Accessed 3 October 2015].

[5]   Oxford   University   Press,   "Oxford   Dictionaries,"   2015.   [Online]. Available: http://www.oxforddictionaries.com/definition/english/tomography. [Accessed 3 October 2015].

[6]   B. I. 13320:2009(E), Particle Size Analysis - Laser Diffraction Methods, BSI British Standards.

[7]   P. De Zorzi, S. Barbizzi, M. Belli, G. Ciceri, A. Fajgelj, D. Moore, U. Sansone and M. Van Der Perk, "TERMINOLOGY IN SOIL SAMPLING (IUPAC   Recommendations   2005)," INTERNATIONAL   UNION   OF PURE AND APPLIED CHEMISTRY, vol. 77, no. 5, pp. 827-841, 2005.

[8]   D. Griffith, "Spatial Autocorrelation," International Encyclopedia of Human Geography, pp. 308-316, 8 July 2009.

[9]   B. E. Haugan and G. and Mininni, "Characterization of Sewage Sludges," Characterization, Treatment and Use of Sewage Sludge, 1981.

[10]   Nuclear Decommissiong Autority, "Nuclear Provision: Explaining the Cost of Cleaning Up Britain's Nuclear Legacy," 19 July 2017. [Online]. Available: https://www.gov.uk. [Accessed 14 August 2017].

[11] Sellafield Ltd, "Sellafield Sites," [Online]. Available: www.sellafieldsites.com. [Accessed October 2016].

[12] "Leeds 'sludge team' targets nuclear waste," University of Leeds, 21 10 2011. [Online]. Available: https://www.leeds.ac.uk/news/article/2586/leeds_sludge_team_targets_nuclear_waste. [Accessed 20 11 2018].

[13] D Majersky AllDeco, "Removal and Solidification of the High Contaminated Sludges into The Aluminosilicate Matrix Sial During Decommissioning Activities," May 2004. [Online]. Available: https://www.iaea.org/OurWork/ST/NE/NEFW/CEG/documents/ws052004 _Majersky-eng.pdf. [Accessed 26 November 2015].

[14] A. Schmidt and A. Zacher, "Composition and Technical Basis for K Basin Settler Sludge Simulant for Inspection, Retrieval and Pump Testing," PNNL, United States, 2007.

[15] Office for Nuclear Regulation, "Basic Principles of Radioactive Waste Management," February 2015. [Online]. Available: http://www.onr.org.uk/wastemanage/basic-principles.pdf. [Accessed 12 June 2019].

[16] Nuclear Decommissioning Authority, "Integrated Waste Management. Radioactive Waste Strategy," July 2018. [Online]. Available: https://assets.publishing.service.gov.uk. [Accessed 12 06 2019].

[17] Sellafield Ltd, "HAL Workstream," 12 July 2017. [Online]. Available: https://webarchive.nationalarchives.gov.uk/20170712123647/http://www.sellafieldsites.com/solution/risk-hazard-reduction/hal-workstream/. [Accessed 12 June 2019].

[18] Sellafield Ltd, "The Magnox Swarf Storage Silo: Making our most harzadous facility a safer place," Youtube, 2017.

[19] Sellafield Sites, "Hole cutting work starts on the Pile Fuel Cladding Silo," Youtube, 2017.

[20]   Cavendish Nuclear, "Pile Fuel Cladding Silo," 2018. [Online]. Available: http://www.cavendishnuclear.com/news/pile-fuel-cladding-silo. [Accessed 5 July 2018].

[21]   World Nuclear News Org, "First Sellafield Fuel Pond Sludge Encapsulated," [Online]. Available: http://www.world-nuclear-news.org/WR-First-Sellafield-fuel-pond-sludge-encapsulated-2002174.html . [Accessed 5 July 2018].

[22]   D. Gradden, "Decommissioning at Sellafield," in n-eboc15 - Nuclear Energy Business Opportunities Conference 13 & 14 October 2015, 2015.

[23]   P. Reeve, The Sellafield Sludge and Slurry Challenge [PowerPoint slides], Sellafield: Technical and Strategy Decommissioning Directorate, Sellafield Ltd, 2012.

[24]   T. Calvin, "Decommissioning Sellafield's First Fuel Storage Pond - 11125," in WM2011 Conference, February 27 – March 3 2011, Phoenix, AZ, 2011.

[25]   M. Gunther, "Stuck in the sludge," Chemistry World, 2015.

[26]   R. Baker and D. Trimble, "Characterization Program Management Plan for Hanford K Basin Spent Nuclear Fuel (SNF) (OCRWM) (HNF-SD-SNF-PLN--010/Rev3)," IAEA, United States, 2000.

[27]   E. Erpenbeck, G. Leshikar and G. Hofferber, "Sludge Retrieval from Hanford K-West Basin Settler Tanks -11449," in WM2011 Conference, Phoenix, AZ, 2011.

[28]   NNL, "Design, Manufacture and Validation of Waste Samplers," [Online]. Available: http://www.nnl.co.uk/media/1873/12-ac-cs-re-design-manufacture-and-validation-of-waste-samplers.pdf. [Accessed 5 July 2018].

[29]   Legislation.gov.au, "National Environment Protection (Assessment of Site Contamination) Measure 1999," 1999. [Online]. Available:

https://www.legislation.gov.au/Details/F2013C00288. [Accessed 5 July 2018].

[30]   C. Draghici, C. Jelescu, C. Dima, M. Sica, E. Chirila, S. Dobrinas and A. Socean, "Method validation and uncertainty estimation for total phosphorus determination in wastewater sludge samples. Studia Universitatis Babeș-Bolyai," Chemia, vol. 57, pp. 93-102, 2012.

[31]   P. Wright and P. McMahon, "Sampling and Analysis Plan for the Characterization of Groundwater Quality in Two Monitoring Wells near Pavillion, Wyoming," U.S. Geological Survey Open-File Report 2012–1197, 2012.

[32]   "Technical Report - Sampling," Sellafield Ltd Technical Directorate.

[33]   N. Leyva and M. P. Mullarney, "Modeling Pharmaceutical Powder- Flow Performance Using Particle - Size Distribution data," Pharmaceutical Technology, vol. 33, no. 3, 2009.

[34]   C. Servais, R. Jones and I. Roberts, "The Influence of Particle Size Distribution on the processing of Food," Journal of Food Engineering, vol. 51, pp. 201-208, 2002.

[35]   J. P. Hecht, J. A. Stamper and D. K. Giles, "Pneumatic Atomization of Laundry Detergent Slurries as affected by Solid Particle Size and Concentration," in 20th Annual Conference on Liquid Atomization and Spray Systems, Chicago, 2007.

[36]   J. Gracia-Mesa, F. Delgado-Ramos, M. Munio, E. Hontoria and J. Poyatos, "Comparison of Activated Sludge Technologies by Particle Size Analysis," Water Air Soil Pollution, vol. 223, pp. 4319-4331, 2012.

[37]   D. C. Montgomery, Introduction to Statistical Quality Control, 6th ed., NJ: John Wiley & Sons, Inc, 2009.

[38]   A. J. Hansen, J. J. Rotella, M. P. V. Kraska and D. Brown, "Spatial Patterns of Primary Produtivity in the Greater Yellowstone Ecosystem," Landscape Ecology, vol. 15, pp. 505-522, 2000.

[39] J. Abrefah, T.A. Thornton, L.E. Thomas, F.M. Berting and S.C. Marschman, "Characterization plan for Hanford spent nuclear fuel," Pacific Northwest Laboratory, Richland, Washington, 1994.

[40] A.P. Simpson, M.J. Clapham, and B. Swinson, "In-Situ Characterization of Underwater Radioactive Sludge," in Waste Management (WM)'08, Phoenix, AZ, 2008.

[41] M. Ryzak, A. Bieganowski and R. Walczak, "Application of Laser Diffraction Method for Determination of Particle Size Distribution of Grey-rown Podzolic Soil," RES. AGR. ENG., vol. 53, no. 1, pp. 34-38, 2007.

[42] Z. Gu, Y. Wang, Y. Wang and Y. Li, "Analysis on Influencing Factors of the Particle Size Measurement of Superfine Polishing Powders via Malvern nano-ZS90," in Remote Sensing, Environment and Transportation Engineering (RSETE), 2011 International Conference on, Nanjing, 2011.

[43] A. Virden, "Method Development for Laser-Diffraction Particle-Size Analysis," Pharmaceutical Technology, vol. 34, no. 11, pp. 100-106, November 2010.

[44] D. McClements, "Ultrasonic Measurements in Particle Size Analysis," Encyclopedia of analytical Chemistry, 2006.

[45] Dispersion Technology Inc, "Particle Size and Particle Size Distribution, Short Tutorial," 2013. [Online]. Available: http://www.dispersion.com/particle-size-measurement-short-tutorial. [Accessed 3 October 2015].

[46] British Standards, "Measurement and characterization of particles by acoustic methods — Part 1: Concepts and procedures in ultrasonic attenuation spectroscopy," BS ISO, United Kingdom, 2006.

[47] D. J. McClements, "Ultrasonic Measurements in Particle Size Analysis," in Encyclopedia of Analytical Chemistry: Applications, Theory and Instrumentation, Chichester, John Wiley & Sons Ltd, 2001.

[48] US PHARMACOPEIA, "Particle Size Distribution Estimation by Analytical Sieving," [Online]. Available: http://www.pharmacopeia.cn/v29240/usp29nf24s0_c786.html. [Accessed 3 October 2015].

[49] Horiba Instrument, Inc, "Horiba Scientific: A Guidebook to Particle Size Analysis," Horiba Instrument, Inc, Irvine, 2014.

[50] ASTM, "ASTM C1751-11 Standard Guide for Sampling Radioactive Tank Waste," ASTM International, West Conshohocken, PA, 2011.

[51] C. Grinand, D. Arrouays, B. Laroche and M. P. Martin, "Extrapolating Regional Soil Landscapes from an Existing Soil Map: Sampling Intensity, Validation Procedures and Integraton of Spatial Context," Geoderma, vol. 143, pp. 180-190, 2008.

[52] S. Thompson, Sampling, 3rd ed., New jersey: John Wiley & Sons, Inc., 2012.

[53] J. Aldworth and N. Cressie, "Sampling design and prediction methods for Gaussian spatial processes," in Multivariate analysis, design of experiments, and survey sampling, S. Ghosh, Ed., New York, Marcel Dekker, Inc., 1999.

[54] R.S. Solanki and H.P. Singh, "An Improved Estimation in Stratified Random Sampling.," Communications in Statistics - Theory and Methods, vol. 45, no. 7, pp. 2056-2070, 2016.

[55] Marine and Sediment Assessment Group, "2006 Sediment Sampling Event: Marine Outfall Baseline Sediment Characterization - Final Sampling and analysis Plan," King County Department of Natural Resources and Parks, King, 2006.

[56] D. Nielsen and G. L. Yeates, "A Comparison of Sampling Mechanisms Available for Small-Diameter Ground Water Monitoring Wells," Ground water Monitoring & Remediation, vol. 5, no. 2, pp. 83-99, June 1985.

[57] A. Ballesteros-Gomez and S. Rubio, "Recent Advances in Environmental Analysis," Analytical Chemistry, vol. 83, pp. 4579-4613, 2011.

[58] Central Pollution Control Board, "Manual On Sampling, Analysis and Characterisation of Hazardous Wastes," Ministry of Environment & Forests, Govt. of India, New Delhi, 2001.

[59] New jersey Department of Environmental Protection, "New Jersey Sludge Sampling and Analytical Guidance Document," Bureau of Pretreatment and Residuals, New Jersey, 2012.

[60] E. M. S. Laboratory, "Characterization of Hazardous Waste Sites - A Methods Manual: Volume II. Available Sampling Methods, Second Edition," United States Environmental Protection Agency, Las Vegas, 1984.

[61] S. Wu, "Sampling Guidelines and Protocols - Technological Background and Quality Control/Quality Assurance for NYS DEC Spill Response Program," New York State Department of Environmental Conservation, New York, 1991.

[62] A. Zele, "A Sludge Sampler," Water Environment Federation, vol. 17, no. 1, pp. 142-143, January 1945.

[63] L. Seuront, "Marine Biology: A Sub-Sample of a Vast Topic," Open Journal of Marine Science, vol. 3, pp. 1-8, 2013.

[64] G. Blacquiere, "3D Wave Field Extrapolation in Seismic Depth Migration; PhD Thesis," Delft University of Technology, Delft, 1989.

[65] K. Heaney, "A Modelling Approach to Spatial Extrapolation of Ocean Ambient Noise Measurements," in Inter-Noise, Melbourne, 2014.

[66] A. Contreras, C. Torres-Verdin, W. Chesters, K. Kvien and T. Fasnacht, "Extrapolation of Flow Units away from Wells with 3D Pre-Stack Seismic Amplitude Data: Field Example," Petrophysics, vol. 47, no. 3, pp. 223-238, June 2006.

[67]   Y. Zhu and Y. Zhao, "Stabilization process within a sewage sludgelandfill determined through both particle size distribution and content of humic substances as well as by FT-IR analysis," Waste Management & Research, vol. 29, no. 4, pp. 379 - 385, 2010.

[68]   J. I. Houghton, J. E. Burgess and T. Stephenson, "Off-line particle size analysis of digested sludge," Water Research, vol. 36, pp. 4643-4647, 2002.

[69]   P. F. Luckham and M. A. Ukeje, "Effect of Particle Size Distribution on the Rheology of Dispersed Systems," Journal of Colloidal and Interface Science, vol. 220, pp. 347-356, 1999.

[70]   U. Riebel, "Ultrasonic Spectrometry: On-Line Particle Size Analysis at Extremely High Particle Concentrations," in Particle Size Analysis, N. Stanley-Wood and R. Lines, Eds., Royal Society of Chemistry, 1992, pp. 488-497.

[71]   G. Rideal, "Absolute Precision in Particle Size Analysis," Whitehouse Scientific Ltd, Chester, 2015.

[72]   M. Kane, Errors Of Measurement, Theory, and Public Policy, New Jersey: Educational Testing Service, 2010.

[73]   R. Jones, "Particle Size Analysis by Laser Diffrcation: ISO 13320, Standard Operating procedures, and Mie theory," American Laboratory, no. January, pp. 44-47, 2003.

[74]   Malvern, "Mastersizer 3000 smarter particle sizing," [Online]. Available: http://www.malvern.com. [Accessed 18 04 2017].

[75]   Escubed Ltd , "Particle Size Analysis by Laser Diffraction," [Online]. Available: www.escubed.co.uk . [Accessed 3 October 2015].

[76]   M. Sperazza, J. N. Moore and M. S. Hendrix, "High-Resolution Particle Size Analysis of Naturally Occuring Very Fine-Grained Sediment Through laser Diffractometry," Journal of Sedimentary Research, vol. 74, no. 5, pp. 736-743, 2004.

[77] F. Alba, "Acoustic Spectroscopy as a technique for the Particle Sizing of High Concentration Colloids, Emulsions and Suspensions," Colloids and Surfaces A: Physiochemical and Engineering Aspects, vol. 153, pp. 495-502, 1999.

[78] O. Harlen, M. Holmes, M. Povey, Y. Qiu and B. Sleeman, "A Low Frequency Potential Scattering Description of Acoustic Propagation in Dispersions," SIAM Journal on Applied Mathematics, vol. 61, no. 6, pp. 1906-1931, 2001.

[79] A. Dukhin and P. Goetz, "Acoustic and Electroacoustic Spectroscopy for Characterizing Concentrated Dispersions and Emulsions," Advances in Colloids and Interface Science, vol. 92, pp. 73-132, 2001.

[80] F. Babick, F. Hinze and S. Ripperger, "Dependence of Ultrasonic Attenuation on the Material Properties," Colloids and Surfaces A: Physicochemical and Engineering Aspects, vol. 172, pp. 33-46, 2000.

[81] H. P. Rice, M. Fairweather, t. N. Hunter, B. Mahmoud, S. Biggs and J. Peakall, "Measuring Particle Concentration in Multiphase Pipe Flow using Acoustic backscatter: generalization of the Dual-Frequency Inversion Method," The Journal of the Acoustical Society of America, Vols. 136, No. 1, no. July, pp. 156 - 169, 2014.

[82] M. Inam, S. Ouattara and C. Frances, "Effects of Concentration of Dispersions on Particle Sizing During Production of Fine Particles in Wet Grinding Process," Powder Technology, vol. 208, no. 2, pp. 329-336, 2011.

[83] Y. Hu, X. Huang, X. Qian, L. Gao and Y. Yan, "Online Particle Size Measurement through Acoustic Emission Detection and Signal Analysis," in 2014 IEEE International Instrumentation and Measurement Technology Conference (I2MTC), Montevideo, 2014.

[84] J. Pierre, F. Elias and V. Leroy, "A Technique for Measuring Velocity and Attenuation of Ultrasound in Liquid Foams," Ultrasonics, vol. 53, pp. 622-629, 2013.

[85]   L. Anson and R. Chivers, "Thermal Effects in the Attenuation of Ultrasound in Dilute Suspensions for Low Values of Acoustic Radius," Ultrasonics, vol. 28, pp. 16-25, 1990.

[86]   T. Goodenough, V. Rajendram, S. Meyer and D. Pretre, "Detection and Quantification of Insoluble Particles by Ultrasound Spectroscopy," Ultrasonics, vol. 43, pp. 231-235, 2005.

[87]   B. I. 20998-1:2006, Measurement and Characterization of Particles by Acoustic Methods — Part 1: Concepts and Procedures in Ultrasonic Attenuation Spectroscopy, British Standard, 2006.

[88]   Retsch GmbH & Co. , "The Basic Principles of Sieve Analysis," [Online]. Available: http://www.ninolab.se/fileadmin/Ninolab/pdf/retsch/documents/af_sieving _basics_2004_en.pdf. [Accessed 3 October 2015].

[89]   Malvern Instruments Ltd, "Dynamic Light Scattering (DLS)," Malvern Instruments Ltd, [Online]. Available: http://www.malvern.com/en/products/technology/dynamic-light-scattering/. [Accessed 3 Octoberr 2015].

[90]   LS Instruments, "Dynamic Light Scattering: Measuring the Particle Size Distribution," LS Instruments, 2015. [Online]. Available: http://www.lsinstruments.ch/technology/dynamic_light_scattering_dls. [Accessed 3 October 2015].

[91]   Particle Analytical, "Microscopy and Digital Image Analysis," Particle Analytical, 2015. [Online]. Available: http://particle.dk/methods-analytical-laboratory/optical-microscopy-particle-size/. [Accessed 3 October 2015].

[92]   H. Cole, "A Special-Purpose Computer for Particle Size Analysis," The Radio and Electronic Engineer, vol. 33, no. 5, pp. 325-335, May 1967.

[93]   R. Berg, "Rapid Volumetric Particle Size Analysis Via Electronics," IRE Transactions on Industrial Electronics, Vols. PGIE-6,, pp. 46-52, May 1958.

[94] G. Lei, Y. Li, J. Zhao and K. Shao, "Statistical Sequential Analysis for Particle Size Distribution of Magnetic Nanoparticles," in 2008 World Automation Congress, Hawaii, 2008.

[95] X. Zhai and J. Liu, "Characterization of Particle Size Distribution (PSD) Evolution During Flocculation by an Image Acquisition and Analysis System," in 2009 International Conference of Environmental Science and Information Application technology, Wuhan, 2009.

[96] T. Koh, N. Miles, S. Morgan and B. Hayes-Gill, "Image Segmentation of Overlapping Particles in Automatic Size Analysis Using Multi-Flash Imaging," in IEEE Workshop on Applications of Computer Vision (WACV'07), Austin, 2007.

[97] R. May, M. Evans, S. Zhong, R. Clarkson, Y. Shen, L. Gladden and J. Zeitler, "Real Time In Situ Measurement of Particle Size in Flowing Powders by Terahertz Time-Domain Spectroscopy," in 2009 34th International Conference on Infrared, Millimeter, and Terahertz Waves, Busan, 2009.

[98] T. Tschudi, G. Herziger and A. Engel, "Particle Size Analysis Using Computer-Synthesized Holograms," Applied Optics, vol. 13, no. 2, pp. 245-248, 1974.

[99] G. Hancke and R. Malan, "A Modal Analysis technique for the On-Line Particle Size measurement of Pneumatically Conveyed Pulverized Coal," IEEE Transactions of Instrumentation and Measurement, vol. 47, no. 1, pp. 114-122, 1998.

[100] W. Divito, M. Mazumder, J. Wilson, R. Sims, L. P, A. Ojha, N. Grabe and S. Chapman, "Simultaneous Analysis of Particle Size and Electrostatic Charge Distribution of Powder with High Accuracy and Precision, and its Applicataion to Electrostatic Processes," in Industry Applications Conference, 1998. Thirty-Third IAS Annual Meeting, St. Louis, 1998.

[101] P. Barrett and B. Glennon, "In-Line FBRM Monitoring of Particle Size in Dilute Agitated Suspensions," Particle and Particle Systems Characterization, vol. 16, pp. 207-211, 1999.

[102] M. Li and D. Wilkinson, "Determination of Non-Spherical Particle Size Distribution from Chord length measurements. Part 1: Theoretical Analysis," Chemical Engineering Science, vol. 60, pp. 3251-3265, 2005.

[103] E. Daymo, T. Hylton and T. May, "Acceptance testing of the Lasentec Focused Beam Reflectance Measurement (FBRM) Monitor for Slurry Transfer Applications at Hanford and Oak Ridge," in Part of the SPIE Conference on Nuclear Waste Instrumentation Engineering, Boston, 1998.

[104] P. Dowding, J. Goodwin and B. Vincent, "Factors Governing Emulsion Droplet and Solid Particle Size measurements Performed Using the Focused Beam Reflectance Technique," Colloids and Surfaces A: Physicochemcal and Engineering Aspects , vol. 192, pp. 5-13, 2001.

[105] B. De Clercq, P. Lant and P. Vanrolleghem, "Focused beam reflectance technique for In Situ Particle Sizing in Wastewater Treatment Settling Tanks," Journal of Chemical Technology and Biotechnology, vol. 79, pp. 610-618, 2004.

[106] D. Law, A. Bale and S. Jones, "Adaptation of Focused beam reflectance Measurement to In Situ Particle Sizing in Estuaries and Coastal Waters," Marine Geology, vol. 140, no. 1-2, pp. 147-59, 1997.

[107] J. d. L. Dijkstra and A. Pot, "In-Line Measurement of Crystal Size - Campaign Experience with Lasentec M200 System," International Sugar Journal, vol. 98, no. 1174, pp. 521-523, 1996.

[108] O. Monnier, J. Klein, B. Ratsimba and C. Hoff, "Particle Size Distribution by Laser Reflection: Methodology and Problems," Particle & Particle Systems Characterization, vol. 13, no. 1, pp. 10-17, 1996.

[109] W. Richmond, R. Jones and P. Fawell, "The Relationship Between Particle Aggregation and Rheology in Mixed Silica-Titania Suspensions," Chemical Engineering Journal, vol. 71, no. 1, pp. 67-75, 1998.

[110] M. Li, D. Wilkinson and K. Patchigolla, "Determination of Non-Spherical Particle Size Distribution from Chord length Measurements. Part 2: Experimental Validation," Chemical Engineering Science, vol. 60, pp. 4992-5003, 2005.

[111] L. Beaubien and A. J. Vanderwielen, "Particle-Size Analysis of Pharmaceutical Powders," Journal of Pharmaceutical Sciences, vol. 69, no. 6, pp. 651-655, 1980.

[112] H. G. Brittain, "Characterization of Pharmaceutical Compounds in the Solid State," in Handbook of Modern Pharmaceutical Analysis, Second ed., vol. 10, S. Ahuja and S. Scypinski, Eds., NewYork, Elsevier Inc, 2011, pp. 11-49.

[113] M. Ryzak and A. Bieganowski, "Methodological Aspects of Determining Soil Particle-Size Distribution Using the Laser Diffraction Method," J. Plant Nutr. Soil Sci, vol. 174, pp. 624-633, 2011.

[114] U. Riebel, "Ultrasonic Spectrometry: On-line Particle Size Analysis at Extremely High Particle Concentrations," in Particle Size Analysis, Cambridge, Royal Society of Chemistry, 1992, pp. 488-497.

[115] A. Abbas, J. Romgnoli and D. Widenski, "Modelling of Crystallization Processes," in Process Systems Engineering: Dynamic Process Modelling, vol. 7, M. Georgiadis, J. Banga and E. Pistikopoulos, Eds., Weinheim, WILEY-VCH, 2011.

[116] H. Raiffa and R. Schlaifer, "Applied Statistical Decision Theory," Division of Research, Havard Business School, 1961.

[117] P. Webb, "Interpretation of Particle Size Reported by Different Analytical techniques," Micrometritics Instrument Corp, 2002.

[118] R. Zhang, X. Z. S. Song, J. Hu and W. Tan, "Investigation of influence factors on particle size measurement with pMDI," Biomedical Research, vol. 28, no. 21, pp. 9582-9588, 2017.

[119] F. Storti and F. Balsamo, "Particle Size Distribution by Laser Diffraction: Sensitivity of Granular Mater Strength to Analytical Operating Procedures," Solid Earth, vol. 1, pp. 25-48, 2010.

[120] Z. Stojanovic and S. Markovic, "Determination of Particle Size Distribution by Laser Diffraction," Technics-New Materials, vol. 21, pp. 11-20, 2012.

[121] C. M. Keck, "Cyclosporine nanosuspensions: optimised size characterisation & oral formulations," Berlin, 2006.

[122] K. Dias, "High-Resolution Methodology for Particle Size Analysis of Naturally Occuring Sand Size Sediment Through Laser Diffractometry With Application to Sediment Cores: Kismet, Fire Island, New York," Stony Brook University; Masters Thesis, New York, 2014.

[123] R. Tantra, A. Sikora, N. B. Hartmann and J. R. Sintes, "Comparison of the Effects of Different Protocols on the Particle Size Distribution of TiO2 Dispersions," Particuology, vol. 19, pp. 35-44, 2015.

[124] A. Sochan, C. Polakowski and G. Lagod, "Impact of Optical Indices on Particle Size Distribution of Activated Sludge Measured by Laser Diffraction Method," ECOL CHEM ENG, vol. 21, no. 1, pp. 137-145, 2014.

[125] R. G. Knollenberg and R. C. Gallant, "Refractive Index Effects on Particle Size Measurement in Liquid Media by Opticl Extinction," in Int'l Conf. on Parlicle Detection, Metrology and Control, Arlington, 1990.

[126] G. Currell, Analytical Instrumentation: Performance Characteristics and Quality, Chichester: John Wiley & sons, Ltd, 2000.

[127] W. French, "Computer Migration of Oblique Seismic Reflection Profiles," Geophysics, vol. 40, pp. 961-980, 1975.

[128] W. Mousa, M. Van Der Baan, S. Boussakta and D. Mclernon, "Designing Stable Extrapolators for Explicit depth Extrapolation of 2D and 3D

Wavefields Using Projections onto Convex Sets," Geophysics, vol. 74, no. 2, pp. S33-S45, March-April 2009.

[129] J. Miller, M. Turner, A. Erica, C. Smithwick, L. Dent and E. Stanley, "Spatial Extrapolation: The Science of predicting Ecological Patterns and Processes," BioScience, vol. 54, no. 4, pp. 310-320, April 2004.

[130] Unit Geo Software Development, ILWIS 3.0 Academic user's guide, Enschede: International Institute for Geo-Information Science and Earth Observation (ITC), 2001, p. 530.

[131] D. Muller and A. McBratney, "Soil Spatial Variability," in Handbook of soil Science, M. Sumner, Ed., FL, CRC Press, 2000, pp. A321-A352.

[132] R. Webster and M. Oliver, "Geostatistics for Environmental Scientists," Technometrics, vol. 43, no. 4, November 2001.

[133] P. De Dorzi, S. Barbizzi, M. Belli, M. Barbina, A. Fajgelj, R. Jacimovic, Z. Jeran, S. Menegon, A. Pati, G. Petruzzelli, U. Sansone and M. Van der Perk, "Estimation of Uncertainty arising from Different Soil Sampling Devices: the Use of Variogram Parameters," Chemosphere, vol. 70, pp. 745-752, 2008.

[134] M. Franklin, "Solution to Ordinary and Universal Kriging Equations," Division of Biostatistics, USC Keck School of Medicine, Los Angeles, 2014.

[135] ArcGis, "How Kriging Works," Environmental Systems Research Institute, Inc, 2016.

[136] P. Bolestad, W. Swank and J. Vode, "Predicting Southern Appalachian Over-Story vegetation with Digital Terrain Data," Landscape Ecology, vol. 13, pp. 271-283, 1998.

[137] G. Bohling, "Kriging," Resources for C&PE940, Data Analysis in Engineering and Natural Science, Lawrence, 2005.

[138] E. Isaaks and R. Srivastava, Applied Geostatistics, New York: Oxford University Press, Inc, 1989.

[139] H. Karl, "Sediment of the Sea Floor," in Beyond the Golden Gate—Oceanography, Geology, Biology, and Environmental Issues in the Gulf of the Farallones, H. Karl, J. Chin, E. Ueber, P. Stauffer and J. Hendley II, Eds., Virginia, U.S. Geological Survey, 2001.

[140] M. Ledbetter and A. Klaus, "Influence of bottom currents on sediment texture and sea-floor morphology in the Argentine Basin," Geological Society, vol. 31, pp. 23-31, 01 01 1987.

[141] S. Xiao, R. Li and M. Chen, "Detecting Sedimentary Cycles using Autocorrelation of Grain size," Scientific Reports, 11 04 2013.

[142] S. Ly, C. Charles and A. Degre, "Geostatistical Interpolation of Daily Rainfall at Catchment Scale: the Use of Several Variogram Models in the Ourthe and Ambleve Catchments, Belgium," Hydrology and Earth System Sciences, vol. 15, pp. 2259-2011, 2011.

[143] "4 key aspects to Variography," Snowden, 29 08 2017. [Online]. Available: https://snowdengroup.com/news/4-key-aspects-variography/. [Accessed 01 12 2018].

[144] X. Yao, B. Fu, Y. Lu, F. Sun and S. L. M. Wang, "Comparison of Four Spatial Interpolation Methods for Estimating Soil Moisture in a Complex Terrain Catchment," PLoS One, vol. 189, no. 10, p. 525, 2013.

[145] Z. Jia, S. Zhou, Q. Su, H. Yi and J. Wang, "Comparison Study on the Estimation of the Spatial Distribution of Regional Soil Metal(loid)s Pollution Based on Kriging Interpolation and BP Neural Network," Int J Environ Res Public Health, vol. 15, no. 1, p. 34, 2018.

[146] D. Panday, B. Maharjan, D. Chalise, R. Shrestha and B. Twanabasu, "Digital soil mapping in the Bara district of Nepal using kriging tool in ArcGIS," PLoS One, vol. 13, no. 10, 2018.

[147] J. Fentanes, I. D. T. Gould, S. Pearson and G. Cielniak, "3D Soil Compaction Mapping through Kriging-based Exploration with a Mobile Robot," IEEE Robotics and Automation Letters, vol. 3, no. 4, 2018.

[148] J. Batista-Foguet, G. Coenders and M. Ferragud, "Using Structural Equation Models to Evaluate the Magnitude of Measurement Error in Blood Pressure," Statistics in Medicine, vol. 20, no. 15, pp. 2351-2368, 2001.

[149] E. Harris and R. Smith, "Accounting for Measurement Error: A Critical But Often Overlooked Process," Archives of Oral Biology, vol. 54s, pp. s107-s117, 2009.

[150] A. Banerjee, U. Chitnis, S. Jadhav, .. J Bhawalkar and S. Chaudhury, "Hypothesis testing, type I and type II errors," Industrial Psychiatry Journal, vol. 18, no. 2, pp. 127-131, 2009.

[151] M. Anderson and P. Whitcomb, DOE Simplified: Practical Tools for Effective Experimentation, 3rd ed., FL: CRC Press, 2016.

[152] G. A. D. Granato, Ed., Mathematical and Statistical Methods in Food Science and Technology, NJ: John Wiley & Sons, 2014.

[153] NIST/SEMATECH, "e-Handbook of Statistical Methods "Engineering Statistics Handbook," 30 October 2013. [Online]. Available: http://www.itl.nist.gov/div898/handbook/pri/section5/pri598.htm. [Accessed 23 November 2017].

[154] M. R.W., "Analysis of Full Factorial Experiments," in A Comprehensive Guide to Factorial Two-Level Experimentation, New York, Springer, 2009.

[155] G. Blom, Statistical Estimates and Transformed Beta Variates, New York: Wiley, 1958.

[156] S. COLEMAN and J. NICHOLLS, "Designing experiments for maximum information from cyclic oxidation tests and their statistical analysis using half normal plots (COTEST)," in Novel Approaches to Improving High Temperature Corrosion Resistance, W. Q. M Schütze, Ed., Elsevier, 2008, pp. 312-333.

[157] W. Taam, Half-Normal Plot. Encyclopedia of Statistics in Quality and Reliability. II., 2008.

[158] T. Levine and C. Hullett, "Eta Squared, Partial Eta Squared, and Misreporting of Effect Size n Communication Research," Human Communication Research, vol. 28, no. 4, pp. 612-625, 2002.

[159] Z. Sun, N. Ya, R. C. Adams and F. S. Fang, "Particle Size Specifications for Solid Oral Dosage Forms: A Regulatory Perspective," American Pharmaceutical Review, vol. 13, no. 4, 2010.

[160] C. Daly, M. Halbleib, J. Smith, W. Gibson, M. Doggett, G. Taylor, J. Curtis and P. Pasteris, "Physiographically Sensitive Mapping of Climatological temperature and Precipitation across the Conterminous United States," International Journal of Climatology, vol. 28, pp. 2031-2064, 2008.

[161] N. Oreskes, K. Shrader-Frechette and K. Beitz, "Verification, Validation and Confirmation of Numerical Models in the Earth Sciences," Science, vol. 263, pp. 641-646, 1994.

[162] A. Guisan and N. Zimmermann, "Predictive Habitat Distribution Models in Ecology," Ecological Modelling, vol. 135, pp. 147-186, 2000.

[163] A. Hart, "Effect of Particle Size on Detergent Powders Flowability and Tabletability," J Chem Eng Process Technol, vol. 6, no. 1, 2015.

[164] G. V. Barbosa-Canovas, F. Harte and H. H. Yan, "Particle Size Distribution in Food Powders," Food Engineering: Encyclopedia of Life Support Systems, vol. 1, pp. 119-130, 2005.

[165] I. Kaminski, N. Vescan and A. Adin, "Particle size distribution and wastewater filter performance," Water Science and Technology, vol. 36, pp. 217-224, 1997.

[166] A. Tiehm, V. Herwig and U. Neis, "Particle size analysis for improved sedimentation and filtration in waste water treatment," Water Science and Technology, vol. 39, no. 8, pp. 99-106, 1999.

[167] E. Hirleman, "Modeling of Multiple Scattering Effects in Fraunhofer Diffraction Particle Size Analysis," in International Symposium on Optical Particle Sizing: Theory and Practice, Rouen, 1987.

[168] S. Dubin, S. Zietz, K. Gabriel and D. Gabriel, "The Mahalanobis Distance as a Metric in Dynamic Light Scattering Particle Size Analysis: Model Studies," in IEEE 27th Annual Northeast Bioengineering Conference, Storrs, 2001.

[169] N. Pandis and T. Walsh, "Argy Polychronopoulou, Christos Katsaros, Theodore Eliades; Factorial designs: an overview with applications to orthodontic clinical trials," European Journal of Orthodontics, vol. 36, no. 3, pp. 314-320, 2014.

[170] J. Richardson, "Eta squared and partial eta squared as measures of effect size in educational research," Educational Research Review, vol. 6, no. 2, pp. 135-147, 2011.

[171] R. Littell, G. Milliken, W. Stroup, R. Wolginger and O. Schabenberger, Eds., SAS for Mixed Models, 2nd ed., Cary: SAS Institute, 2006.

[172] W. Houston, "The Analysis of errors in Orthodontic Measurements," Americal Journal of Orthodontics, vol. 83, no. 5, pp. 382-390, 1983.

[173] J. Taylor, An Introduction to Error analysis: The Study of Uncertainties in Physical Measurements, 2nd ed., Sausalito: University Science Books, 1997.

[174] P. Bevington and D. Robinson, Data Reduction and Error Analysis for the Physical Sciences, 2nd ed., Singapore: McGraw-Hill, Inc., 1969.

[175] N. Cameron, The Measurement of Human growth, vol. 68, London: Taylor & Francis, 1984, pp. 560-561.

[176] S. Bell, Measurement Good Practise Guide: A Beginner's Guide to Uncertainty of Measurement, 2 ed., vol. 11, Teddington: Crown Copyright, 1999.

[177] L. Blackwood and Y. Harker, "Uncertainty Analysis of Nondestructive Assay Measurements of Nuclear Waste," in Part of the SPIE Conference on Nuclear Waste Instrumentation Engineering, Boston, 1998.

[178] Y. Amemiya, "Instrumental Variable Estimation of the Nonlinear Measurement Error Model," in Contemporary Mathematics - Statistical Analysis of measurement Error Models and Applications: Proceedings of the AMS-IMS-SIAM Joint Summer Research Conference, 1989, P. Brown and W. Fuller, Eds., Providence, American Mathematical Society, 1990.

[179] M. Uher and P. Benes, "Measurement of Particle Size Distribution by the Use of Acoustic Emission Method," in Instrumentation and Measurement Technology Conference (I2MTC), 2012 IEEE International, Graz, 2012.

[180] U. Riebel and F. Loffler, "The Fundamentals of Particle Size Analysis by Means of Ultrasonic Spectroscopy," Particle & Particle System Characterisation, vol. 6, pp. 135-143, 1989.

[181] A. Dukhin, P. Goetz and V. Hackley, "Modified Log-Normal Particle Size Distribution in Acoustic Spectroscopy," Colloids and Surfaces A: Physicochemical and Engineering Aspects, vol. 138, pp. 1-9, 1998.

[182] H. Djelouah, N. Bouaoua and A. Alia, "A Pulsed Technique for Measurement of the Ultrasonic Attenuation," in International Congress on Acoustics (ICA) 2001, Rome, 2001.

[183] T. Wines, A. Dukhin and P. Somasundaran, "Acoustic Spectroscopy for Characterizing Heptane/H2O/AOT Reverse Microemulsions," Journal of Colloid and Interface Science, vol. 216, pp. 303-308, 1999.

[184] M. Holmes, N. Parker and M. Povey, "Temperature Dependence of Bulk Viscosity in Water Using Acoustic Spectroscopy," Journal of Physics: Conference Series, vol. 269, no. 1, 2011.

[185] T. Hazlehurst, "Acoustic Solutions to the Particle Mixing Problem in Aqeous Dispersions," University of Leeds; PhD Thesis, Leeds, 2015.

[186] V. Keppens, "Pesonance methods: Principles and Applications," in Ultrasonics International 2001, Lecture Notes, 2001.

[187] P. Nelson, M. Povey and Y. Wang, "An Ultrasound Velocity and Attenuation Scanner for Viewing the temporal Evolution of a Dispersed Phase in Fluids," Review of Scientific Instruments, vol. 72, no. 11, pp. 4234-4241, 2001.

[188] F. Peters and L. Petit, "A Broad Band Spectroscopy Method for Ultrasound Wave velocity and attenuation measurement in Dispersive Media," Ultrasonics, vol. 41, pp. 357-363, 2003.

[189] T. Goodenough, V. Rajendram, S. Meyer and D. Pretre, "Development of a Multi Frequency Pulse Diagnostic Ultrasound Device," Ultrasonics, vol. 43, pp. 165-171, 2005.

[190] F. Watson, "The Absorption of Sound by Materials," University of Illinois Bulletin, vol. XXV, no. 13, 1927.

[191] P. S. Epstein and R. R. Carhart, "The Absorption of Sound in Suspensions and. Emulsions I. Water Fog in Air," The Journal of the Acoustical Society of America, vol. 25, no. 3, pp. 553-565, 1953.

[192] J. Allegra and S. Hawley, "Attenuation of sound in Suspensions and Emulsions: Theory and Experiments," The Journal of the Acoustical Society of America, vol. 51, p. 1545, 1972.

[193] D. Scott, "Industrial Applications of In-Line Ultrasonic Spectroscopy," in Ultrasonic and Dielectric Characterization Techniques for Suspended Particulates, V. Hackley and J. Texter, Eds., Westerville, American Ceramic Society, 1998, pp. 155-165.

[194] A. Dukhin and P. Goetz, "Acoustic Spectroscopy for concentrated Polydisperse Colloids with High Density Contrast," Langmuir, vol. 12, no. 21, pp. 4987-4997, 1996.

[195] R. Challis, A. Holmes and A. Kalashnikov, "Ultrasonic Monitoring of Particulate Suspensions In-Process: Physics, Technology and

Applications," WCNDT e-Journal of Nondestructive Testing, vol. 9, no. 11, 2004.

[196] A. Hipp, G. Storti and M. Morbidelli, "On Multiple-Particle Effects in the Acoustic Characterisation of Colloidal Dispersions," Journal of Physics D: Applied Physics, vol. 32, no. 5, pp. 568-576, 1999.

[197] A. E. HAY and D. G. MERCER, "On the theory of sound scattering and viscous absorption in aqueous suspensions at medium and short wavelengths," Journal of Acoustical Society of America, vol. 78, no. 5, pp. 1761-1771, 1985.

[198] J. Jordan, H. Geers and W. Witt, "Novel Evaluation Algorith for In-Line Droplet Size Analysis of Emulsions with Ultrasonic Extinction," in PARTEC 2007, 2007.

[199] P. Mougin, D. Wilkinson, K. Roberts, R. Jack and P. Kippax, "Sensitivity of Particle Sizing by Ultrasonic Attenuation Spectroscopy to Material Properties," Powder Technology, vol. 134, pp. 243-248, 2003.

[200] E. Kress-Rogers, "Ultrasound Propagation in Foods and Ambient Gases: Principles and Applications," in Instrumentation and Sensors for the Food Industry, 2nd ed., E. Kress-Rogers and C. Brimelow, Eds., Cambridge, Woodhead Publishing Limited, 2001, p. 836.

[201] H. Schlaberg, M. Yang and B. Hoyle, "Ultrasound Reflection Tomography for Industrial Processes," Ultrasonics, vol. 36, no. 1-5, pp. 297-303, 1998.

[202] A. Lopez-Sanchez and L. Schmerr, "Determination of an Ultrasonic Transducer's Sensitivity and Impedance in a Pulse-Echo Setup," IEEE Transactions on Ultrasonics, Ferroelectrics, and Frequency Control, vol. 53, no. 11, pp. 2101-2112, 2006.

[203] M. Coeck and C. Laermans, "Tunneling States in Neutro-Disorderedbulk Silicon," Physical Review B, vol. 58, p. 6708, 1998.

[204] J. DosRamos, "Acoustic Attenuation Spectroscopy for Process Control of Dispersed Systems," IOP Conference Series: Materials Science and Engineering, vol. 42, no. 012023, pp. 1-4, 2012.

[205] S. Kummritz, M. Wolf and E. Kuhnicke, "Simultaneous Determination of Thickness and Sound velocity in Layered Structures," in 11th European Conference on Non-Destructive Testing (ECNDT 2014), Prague, 2014.

[206] N. Gust, "Improvement of Signal Analysis Ultrasonic Microscopy," Technische Universität Dresden, Dissertation, Dresden, 2011.

[207] D. Forrester, J. Huang and V. Pinfield, "Characterisation of Colloidal Dispersions Using Ultrasound Spectroscopy and Multiple-Scattering Theory Inclusive of Shear-Wave Effects," Chemical Engineering research and Design, 2016.

[208] O. Zozulya, G. Maximov and I. Pelivanov, "Comparison of Microbubble Size Distributions Obtained by Pulse Acoustic Spectroscopy and Dynamic Light Scattering," in 2012 IEEE International Ultrasonics Symposium, Dresden, 2012.

[209] F. Babick, M. Stintz and A. Richter, "Ultrasonic Particle Sizing of Disperse Systems with Partly Unknown Properties," Particle & Particle Systems Characterization, vol. 23, pp. 175-183, 2006.

[210] K. Groves, A. West, K. Gornicki, S. Watson, J. Carrasco and B. Lennox, "MallARD: An Autonomous Aquatic Surface Vehicle for Inspection and Monitoring of Wet Nuclear Storage Facilities," Robotics, vol. 8, no. 2, p. 47, 2019.

[211] M. Nancekievill, A. Jones, A. Joyce, B. Lennox, S. Watson, J. Katakura, K. Okumura, S. Kamada, M. Katoh and K. Nishimura, "Development of a Radiological Characterization Submersible ROV for Use at Fukushima Daiichi," IEEE Transactions on Nuclear Science, vol. 65, no. 9, pp. 2565 - 2572, 2018.

[212] B. Bird, A. Griffiths, H. Martin, E. Codres, J. Jones, A. Stancu, B. Lennox, S. Watson and X. Poteau, "A Robot to Monitor Nuclear Facilities: Using

Autonomous Radiation-Monitoring Assistance to Reduce Risk and Cost," IEEE Robotics & Automation Magazine, no. March 2019, pp. 35 - 43, 2019.

[213] J. Stoklosa, C. Daly, S. Foster, M. Ashcroft and D. Warton, "A Climate of Uncertainty: Accounting for Error in Climate Variables for Species Distribution Models," Methods in Ecology and Evolution, vol. 6, pp. 412-423, 2015.

[214] H. Devon, M. Block, P. Moyle-Wright, D. Ernst, S. Hayden, J. Deborah, S. Savoy and E. Kostas-Polston, "A Psychometric Toolbox for Testing Validity and Reliability," Journal of Nursing Scholarship, vol. 39, no. 2, pp. 155-164, 2007.

APPENDIX

APPENDIX A : Additional data on Sludge Sampling Related Factors

Table A1: A summary of the ANOVA test showing F-Statistic and Probability (P) results

	Factor	Bed 1 $\overline{HSAC}$ $VSAC$		Bed 2 $HSAC$ $VSAC$		Bed 3 $\overline{HSAC}$ $\overline{VSAC}$		Bed 4 $HSAC$ $\overline{VSAC}$	
		F	**P**	**F**	**P**	**F**	**P**	**F**	**P**
Main Factors	A	1054.1	0	3666.9	0	1284.5	0	3199.4	0
	B	40.1	0	18.1	0	28.9	0	46.1	0
	C	3502.9	0	7257.9	0	693.2	0	1396.5	0
	D	1277.9	0	6710.1	0	371.3	0	3857.3	0
Factor Interactions	AB	4.5	0.03	43.5	0	4.7	0.03	41.4	0
	AC	290.8	0	1343.2	0	35.3	0	267.1	0
	AD	163.6	0	547.5	0	226.2	0	1026.6	0
	BC	26.2	0	22.0	0	15.7	0	19.5	0
	BD	3.9	0.05	3.6	0.06	6.6	0.01	4.1	0.04
	CD	1313.4	0	6712.2	0	48.35	0	143.5	0
	ABC	6.0	0.02	21.0	0	4.1	0.04	14.6	0
	ABD	14.0	0	2.0	0.16	5.4	0.02	4.0	0.05
	ACD	153.1	0	545.4	0	11.8	0	73.9	0
	BCD	7.4	0.01	4.9	0.03	8.1	0	9.8	0
	ABCD	9.3	0	1.3	0.26	6.9	0.01	12.0	0

Table A2: Eta Squared Effect of Sampling Factors and their Interactions

	Factor	Eta-Squared Effect (%)			
		Bed 1 $\overline{HSAC}$ $VSAC$	Bed 2 $HSAC$ $VSAC$	Bed 3 $\overline{HSAC}$ $\overline{VSAC}$	Bed 4 $HSAC$ $\overline{VSAC}$
Main Factors	A	12.9	13.5	42.0	30.7
	B	0.5	0.1	0.9	0.4
	C	42.9	26.7	22.7	13.4
	D	15.6	24.7	12.2	37.0
Factor Interactions	AB	0.1	0.2	0.2	0.4
	AC	3.6	4.9	1.2	2.6
	AD	2.0	2.0	7.4	9.9
	BC	0.3	0.1	0.5	0.2
	BD	0.0	0.0	0.2	0.0
	CD	16.1	24.7	1.6	1.4
	ABC	0.1	0.1	0.1	0.1
	ABD	0.2	0.0	0.2	0.0
	ACD	1.9	2.0	0.4	0.7
	BCD	0.1	0.0	0.3	0.1
	ABCD	0.1	0.0	0.2	0.1
	Residual R	3.7	1.1	10.0	2.9
	TOTAL	**100**	**100**	**100**	**100**
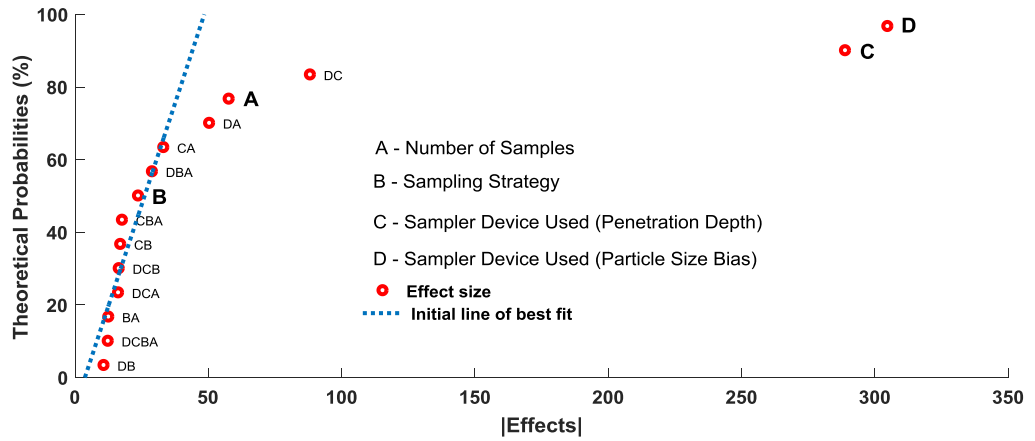
Figure A1: Half normal plot of effects - Bed 5. This is a pictorial representation of the significance of each experimental factor.
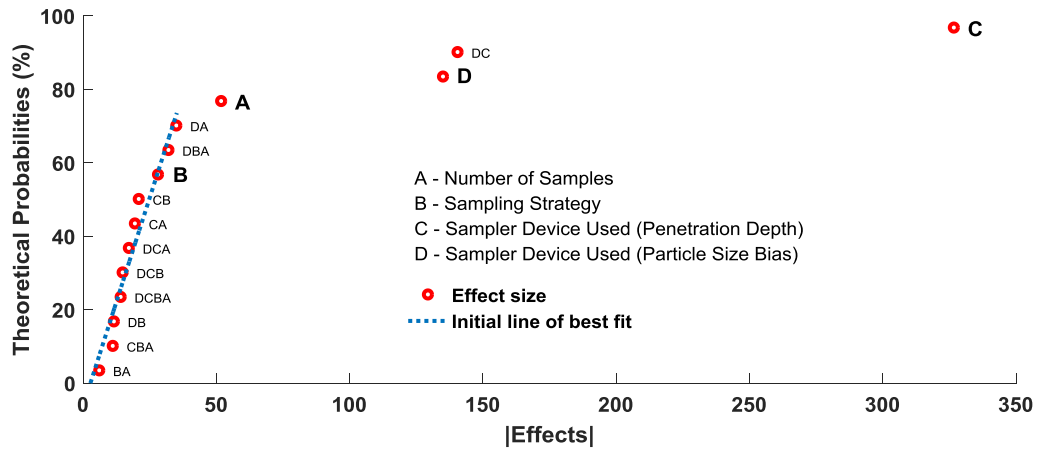

Figure A2: Half normal plot of effects - Bed 6. This is a pictorial representation of the significance of each experimental factor.
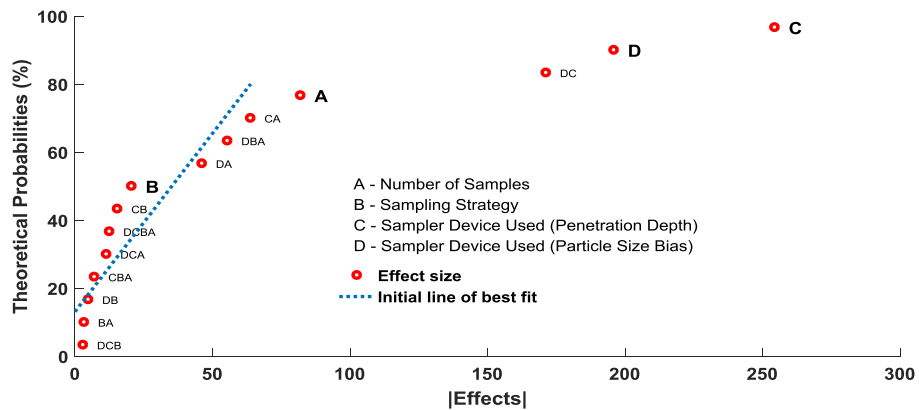

Figure A3: Half normal plot of effects - Bed 7. This is a pictorial representation of the significance of each experimental factor.
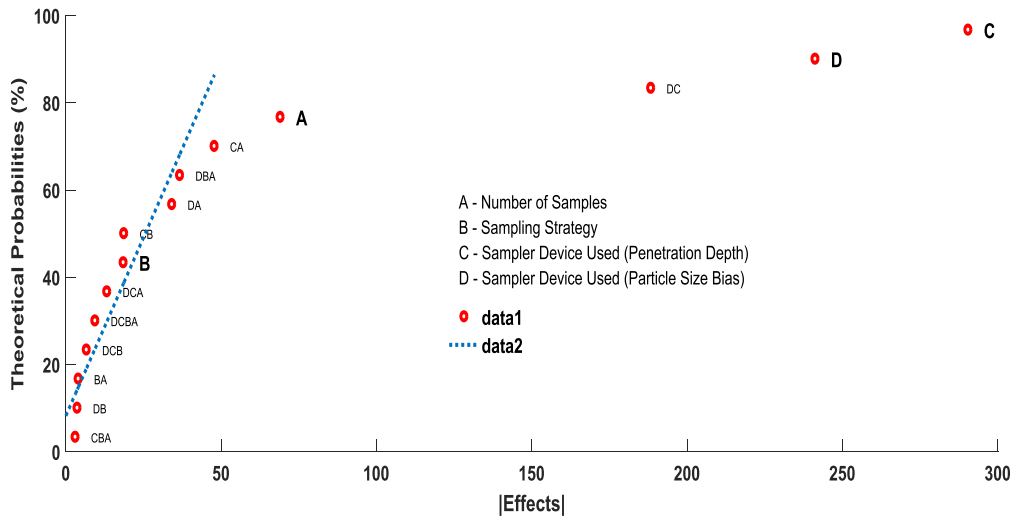
Figure A4: Half normal plot of effects - Bed 8. This is a pictorial representation of the significance of each experimental factor.
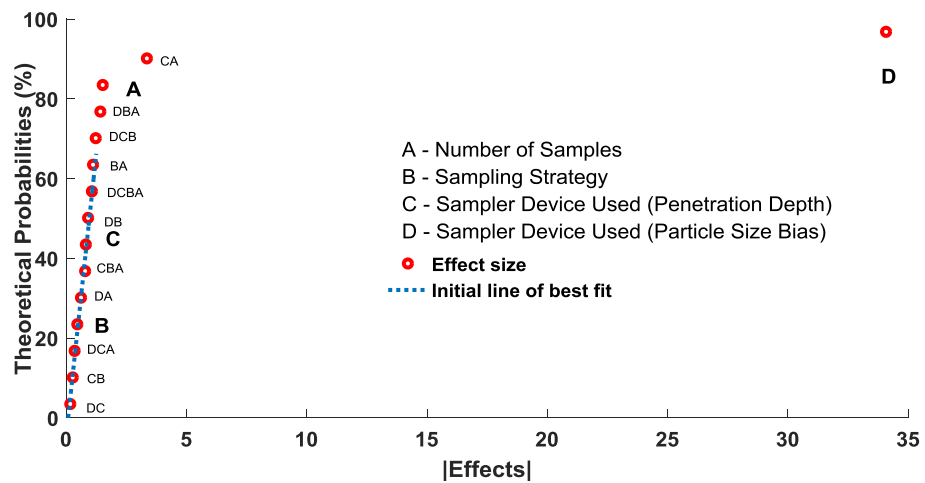

Figure A5: Half normal plot of effects - Bed 9. This is a pictorial representation of the significance of each experimental factor.

APPENDIX B: Matlab Code for $\overline{HSAC}\ \overline{VSAC}$ Bed Generation

```
clc
clear

layer_set=[1 2 4 5 6;1 2 2 3 4;1 2 4 5 6;1 2 3 3 4;1 2 3 4 5 ;1 2
3 5 6;1 3 4 5 6;1 3 3 5 6;1 2 4 3 5;2 3 4 6 6 ];
%could be anywhere really, it just describes the PSD class
contained in
%each layer, it increases with depth

for ico=1:2
    %that means run for sludge bed 1 and bed 2
    aprop=1;
for layercount = 1:10
    %that means run for sludge layer 1 to 10
Bedlayer = zeros(100,200);
count = 0;
storelayer=zeros(100,20000);
for r = 1:100
    for c = 1:200
        count = count+1;


        A = 30*randn(100,1) + 100;
        B = 40*randn(100,1) + 200;
        C = 48*randn(100,1) + 350;
        D = 50*randn(100,1) + 585;
        E = 68*randn(100,1) + 800;
        F = 85*randn(100,1) + 1250;


        roam=[A,B,C,D,E,F];
        layerchoice=layer_set(layercount,:);

    if ico==2

        CVqq=sqrt((r-50)^2+(c-100)^2);
        if CVqq>=100 & CVqq<120

                Bedlayer(r,c) = layerchoice(1);storelayer(:,count)
= roam(:,Bedlayer(r,c));
        end
        if CVqq>=90 & CVqq<100

                Bedlayer(r,c) = layerchoice(2);storelayer(:,count)
= roam(:,Bedlayer(r,c));
        end
        if CVqq>=80 & CVqq<90

                Bedlayer(r,c) = layerchoice(3);storelayer(:,count)
= roam(:,Bedlayer(r,c));
        end
        if CVqq>=70 & CVqq<80

                Bedlayer(r,c) = layerchoice(4);storelayer(:,count)
= roam(:,Bedlayer(r,c));
        end
```

```matlab
        if CVqq>=60 & CVqq<70

                Bedlayer(r,c) = layerchoice(5);
storelayer(:,count) = roam(:,Bedlayer(r,c));
        end
        if CVqq>=50 & CVqq<60

                Bedlayer(r,c) = layerchoice(5);storelayer(:,count)
= roam(:,Bedlayer(r,c));
        end
        if CVqq>=40 & CVqq<50

                Bedlayer(r,c) = layerchoice(4);
storelayer(:,count) = roam(:,Bedlayer(r,c));
        end
        if CVqq>=30 & CVqq<40

                Bedlayer(r,c) = layerchoice(3);
storelayer(:,count) = roam(:,Bedlayer(r,c));
        end
        if CVqq>=20 & CVqq<30

                Bedlayer(r,c) = layerchoice(2);
storelayer(:,count) = roam(:,Bedlayer(r,c));
        end
        if CVqq<20

                Bedlayer(r,c) = layerchoice(1);
storelayer(:,count) = roam(:,Bedlayer(r,c));
        end

   elseif ico==1
        if r>=1 && c<=60

            Bedlayer(r,c) = layerchoice(1);storelayer(:,count) =
roam(:,Bedlayer(r,c));

        elseif c>60 && c<=130
            if r<50

             Bedlayer(r,c) = layerchoice(2); storelayer(:,count) =
roam(:,Bedlayer(r,c));

            else

                Bedlayer(r,c) = layerchoice(3);storelayer(:,count)
= roam(:,Bedlayer(r,c));

            end
        else
            if r<40

                Bedlayer(r,c) = layerchoice(4);
storelayer(:,count) = roam(:,Bedlayer(r,c));

            else
```

```
                Bedlayer(r,c) = layerchoice(5);
storelayer(:,count) = roam(:,Bedlayer(r,c));
                asa=round(1+ 40*rand);



        end
    end


    CVX=sqrt((r-aprop*70)^2+(c-aprop*160)^2);
    if CVX<=10*aprop

            Bedlayer(r,c) = layerchoice(1);
storelayer(:,count) = roam(:,Bedlayer(r,c));
    end
    CVY=sqrt((r-aprop*60)^2+(c-aprop*100)^2);
    if CVY<=10
        Bedlayer(r,c) = layerchoice(1);storelayer(:,count) =
roam(:,Bedlayer(r,c));

    end
    CVZ=sqrt((r-aprop*20)^2+(c-aprop^2*100)^2);
    if CVZ<=10*aprop

            Bedlayer(r,c) = layerchoice(1);storelayer(:,count)
= roam(:,Bedlayer(r,c));
    end
    CVW=sqrt((r-aprop*35)^2+(c-aprop*160)^2);
    if CVW<=10*aprop

            Bedlayer(r,c) = layerchoice(1);storelayer(:,count)
= roam(:,Bedlayer(r,c));
    end
    CVV=sqrt((r-aprop*70)^2+(c-aprop*90)^2);
    if CVV<=10*aprop

            Bedlayer(r,c) = layerchoice(1);storelayer(:,count)
= roam(:,Bedlayer(r,c));
    end
    CVA=sqrt((r-aprop*30)^2+(c-aprop*30)^2);
    if CVA<=15*aprop

            Bedlayer(r,c) = layerchoice(2);storelayer(:,count)
= roam(:,Bedlayer(r,c));
    end
    CVB=sqrt((r-aprop*100)^2+(c-aprop*60)^2);
    if CVB<=40*aprop

            Bedlayer(r,c) = layerchoice(3);storelayer(:,count)
= roam(:,Bedlayer(r,c));
    end
    CVCC=sqrt((r-aprop*57)^2+(c-aprop*150)^2);
    if CVCC<=30*aprop

            Bedlayer(r,c) = layerchoice(1);storelayer(:,count)
= roam(:,Bedlayer(r,c));
    end
    CVD=sqrt((r-aprop*90)^2+(c-aprop*200)^2);
    if CVD<=23*aprop
```

```matlab
                    Bedlayer(r,c) = layerchoice(2);
storelayer(:,count) = roam(:,Bedlayer(r,c));
        end
        CVE=sqrt((r-aprop*15)^2+(c-aprop*15)^2);
        if CVE<=30*aprop

                    Bedlayer(r,c) = layerchoice(4);storelayer(:,count)
= roam(:,Bedlayer(r,c));
        end

        CVG=sqrt((r-aprop*73)^2+(c-aprop*100)^2);
        if CVG<=25*aprop

                    Bedlayer(r,c) = layerchoice(2);
storelayer(:,count) = roam(:,Bedlayer(r,c));
        end
        CVt=sqrt((r-aprop*20)^2+(c-aprop*150)^2);
        if CVt<=20*aprop

                    Bedlayer(r,c) = layerchoice(1);storelayer(:,count)
= roam(:,Bedlayer(r,c));
        end




    end

    end

    end


storelayer=abs(storelayer);

storagename=['SCA_storeANDbed' num2str(ico) 'layer'
num2str(layercount)];
save([storagename '.mat'],'storelayer','Bedlayer')


end
end
```